MIT Libraries
Document Services

Room 14-0551
77 Massachusetts Avenue
Cambridge, MA 02139
Ph: 617.253.5668 Fax: 617.253.1690
Email: docs@mit.edu
http://libraries.mit.edu/docs

DISCLAIMER OF QUALITY

Due to the condition of the original material, there are unavoidable flaws in this reproduction. We have made every effort possible to provide you with the best copy available. If you are dissatisfied with this product and find it unusable, please contact Document Services as soon as possible.

Thank you.

Some pages in the original document contain color pictures or graphics that will not scan or reproduce well.

Cellular Responses to Mechanical Stresses Applied via Magnetic Manipulators

By

Hayden Huang

S.M. Mechanical Engineering
MIT, 1997

Submitted to the Harvard-MIT Division of Health Sciences and Technology
in partial fulfillment of the requirements for the degree of

Doctor of Philosophy in Medical Engineering
at the
MASSACHUSETTS INSTITUTE OF TECHNOLOGY

September, 2001
[February 2002]

© 2001 Massachusetts Institute of Technology.
All Rights Reserved.

Signature of Author: _____
Harvard-MIT Division of Health Sciences and Technology, MEMP Program
Sept., 2001

Certified by: _____
Richard T. Lee
Associate Professor of Health Sciences and Technology
Thesis Supervisor

Certified by: _____
Peter T. C. So
Associate Professor of Mechanical Engineering
Thesis Supervisor

Accepted by: _____
Martha L. Gray, Ph.D.
Edward Hood Taplin Professor of Medical and Electrical Engineering
Co-director, Harvard-MIT Division of Health Sciences and Technology

MASSACHUSETTS INSTITUTE OF TECHNOLOGY
MAY 0 9 2002
LIBRARIES

ARCHIVES

Acknowledgements

I'd like to thank my family for their caring support, and dedicate this thesis to them.

I would also like to thank my committee, Dr. Roger Kamm, my committee chair and academic advisor, Dr. Rich Lee and Dr. Peter So, my thesis supervisors, for their time and expertise.

Thanks go to all the people in the labs I worked at, especially Mr. William Briggs for his tutelage in cell culture, Ms. Quynh Dang for her help in Northern blotting, Anna and Marysia of the Libby Lab for their generous donations of endothelial cells, Mr. Jan Lammerding for his MATLAB programs, Toshi for his help in viral creation (including his 293A cell and BJ5183 bacterial donations), Dr. Chen Dong for his help in setting up the two-photon system, Ki-Hean for helping with the fast-scan system, Hyuk-Sang and Jason Sutin for their help with the magnetic trap, and Mohammed and Helene for their FEM work.

Table of Contents

Abstract 11

1 Introduction 13

1.1 Background 13

1.1.1 Ion Channels 13

1.1.2 Cell Morphology 14

1.1.3 Gene Induction 15

1.1.4 Techniques for Single Cell Studies 16

1.2 Cell Models 16

1.2.1 Tensegrity 18

1.2.2 Open-Foam 18

1.2.3 Other Cell Models 19

1.3 Thesis Goals 20

2 Cell Culture and Bead Techniques 23

2.1 Methods for Cell Culture 23

2.1.1 Cell Types 23

2.1.2 Cell Plating 23

2.2 Beads 24

2.2.1 Bead Target 24

2.2.2 Bead Preparation Methods 24

3 Molecular Biology at the Single Cell Level 26

3.1 Initial Studies 26

3.1.1 Northern Analysis With a Cam-Piston Device 26

3.1.2 Limitations With Using Northerns 28

3.2 Magnetic Trap: Octopolar Design 29

3.2.1 Theory and Design Parameters 29

3.2.2 Maxwell Simulations 30

3.2.3 Magnetic Trap Construction 35

3.2.4 Operation and Calibration of the Magnetic Trap 35

3.2.5 Magnetic Trap Characterization 37

3.3 Molecular Assay of the Cell 41

3.3.1 Reporter Beta-Lactamase and CCF-2/AM 41

3.3.2 Beta-Lactamase Plasmid Construction 42

3.3.3 Beta-Lactamase Plasmid Transfection 43

3.3.4 Adenoviral Construction 44

3.4 Two-Photon Microscope 47

3.4.1 Motivation for Using the Two-Photon Microscope 47

3.4.2 Instrumentation of the Two-Photon Microscope 49

3.4.3 The "Fast-Scan" Two-Photon Microscope 50

3.5 Octopolar Magnetic Trap Results: Molecular Assay 51
3.5.1 Control Response 51
3.5.2 PAI-1 Response 52
3.5.3 EGR-1 Response 52
3.6 Octopolar Magnetic Trap Results: Cell Deformation Assay 58
3.6.1 Methods for Cell Deformation 58
3.6.2 Post-Processing Cell Deformation Data 59
3.6.3 Controls for Remodeling and Vibrations 61
3.6.4 Reconstruction of Data in a Different Plane 63
3.6.5 Discussion of Octopolar Cell Deformation 64
4 Single Pole Experiments: Cell Moduli Determination 66
4.1 Introduction: Techniques to Probe Single Cells 66
4.1.1 Magnetic Twisting Cytometry 66
4.1.2 Other Techniques 67
4.1.3 Single Pole Magnetic Trap 68
4.2 The Single Pole Magnetic Trap 68
4.3 Single Pole Magnetic Trap Characterization 70
4.4 Single Pole Trap Cell Studies 71
4.4.1 Experimental Methods 71
4.4.2 Cell Model and Analysis 73
4.4.3 Comparison of Theory and Experiments 75
4.5 Discussion of Cell Strain Experiments 81
4.5.1 Results from Other Techniques 81
4.5.2 Actin Gel Study 84
4.6 Limitations and Uncertainties of Analysis 84
4.6.1 Range of Moduli 84
4.6.2 Other Factors, and the Influence of Cell Height 85
4.6.3 Zero-Displacement Beads 88
4.6.4 Lack of Viscous Contributions 89
4.7 Preliminary Finite Element Model Comparison 90
5 General Discussion 93
6 Future Work 97
7 References 99
Appendix A: Cell Culture Techniques 105
Appendix B: Beta-Lactamase System 108
Appendix C: Matlab Programs 112
Appendix D: Viral Construction Protocol 155
Appendix E: Magnetic Trap Design Drawings 164

List of Figures

Figure 1: Depictions of tensegrity models 17

Figure 2: Schematic of the open foam model 19

Figure 3: Conceptualization of the fluid mosaic model 20

Figure 4: Variation in cell modulus across different techniques 21

Figure 5: Photograph of the piston-cam strain device 27

Figure 6: Northern blots of the EGR-1 and PAI-1 promoter 28

Figure 7: Maxwell drawing of the octopolar magnetic trap design 32

Figure 8: Maxwell field results of magnetic traps with and without backirons 33

Figure 9: Maxwell drawing showing details of the tip regions for the octopolar trap design 34

Figure 10: Photographs of the constructed octopolar magnetic trap 36

Figure 11: Maxwell field results of the final octopolar trap design in the sample region 38

Figure 12: Maxwell field vector results of the final octopolar trap design in the sample region 38

Figure 13: Field results from a Hall probe measurement of the octopolar trap design 39

Figure 14: Calibration plots of the octopolar magnetic traps, with paramagnetic and ferromagnetic beads 40

Figure 15: Schematic of the action of beta-lactamase on the cell permeant dye CCF-2/AM 42

Figure 16: Smooth muscle cells transfected with beta-lactamase showing some blue cells 44

Figure 17: Schematic of the protocol used for creating replication-deficient adenovirus 46

Figure 18: Northern blot of the PAI-1 response to adenoviral infection 47

Figure 19: Schematic of the theory behind two-photon microscopy 48

Figure 20: Photograph showing the effects of the two-photon microscope as compared to laser widefield fluorescence. 48

Figure 21: Schematic of the instrumentation setup for using the octopolar magnetic trap with two-photon microscopy 50

Figure 22: Two-photon images of control and CMV-beta-lactamase infected cells 54

Figure 23: Time plot of the blue-green ratio for control and CMV 55

Figure 24: Time plot of the blue-green ratio for smooth muscle cells infected with a promoterless beta-lactamase adenovirus 55

Figure 25: Time plot of the response of PAI-1 to serum induction 56

Figure 26: Two-photon images of smooth muscle cells infected with EGR-1 beta-lactamase adenovirus 56

Figure 27: Time plot of the response of EGR-1 to PMA, magnetic trapping, and controls 57

Figure 28: Northern blot for EGR-1 activity under different temperatures. 57

Figure 29: Northern blot for COX-1 activity, under different strain amplitudes. 58

Figure 30: Two-photon images of a smooth muscle cell deforming under 50 pN 59

Figure 31: Two-photon images of a smooth muscle cell deforming under 120 pN 60

Figure 32: Vector plot of displacements in a smooth muscle cell from cross-correlation analysis under 50 pN 61

Figure 33: Vector plot of displacements in a smooth muscle cell with no applied stress 62

Figure 34: Plot of y-displacements for two cells under 120 pN magnetic forces, one with and the other without magnetic beads 63

Figure 35: Reconstruction of two-photon images into a vertical plane 64

Figure 36: Photograph of the single-pole magnetic trap setup. 69

Figure 37: Sample displacement curve of a free-floating paramagnetic bead with the single-pole magnetic trap activated; used for calibration 70

Figure 38: Force calibration curves for the single-pole magnetic trap 71

Figure 39: Sample image from a movie showing the arrangement of the single-pole magnetic trap, the cells and beads 73

Figure 40: Experimental and theoretical displacement vector fields for three cell types 77-80

Figure 41: Experimental and theoretical displacements, normalized against exerted force, for three cell types 80

Figure 42: Images showing magnetic bead rolling 82

Figure 43: Displacement, normalized by applied force, of the magnetic beads showing a wide variation in data 83

Figure 44: High and low estimates for moduli that correspond to the experimental data 85

Figure 45: Sample graph of data used to measure cell height 87

Figure 46: Effects of sustained forces on magnetic beads on cells; intended to show viscous effects and limitations thereof 89

Figure 47: Limitations in gene induction by cell confluence, using fast-scan two-photon microscopy. 92

List of Tables

Table 1: Modulus and Parameters of Cells from Analysis 75

Table 2: Modulus and Parameters of Cells from Analysis without Zero-Displacement Points 75

Table 3: Cell Heights 87

Table 4: Modulus of Cells with Height Variation 88

Abstract

A mechanotransduction model aims to explain how a cell senses mechanical forces and translates them into molecular events, such as changes in intracellular ion concentrations, gene expression, post-translational protein modification, or cytoskeletal redistribution. Many studies of mechanotransduction explore the responses of cell populations to large and, occasionally, poorly characterized deformation. More recent techniques provide the means for characterizing the physical properties of the cell, with the potential for uniting the molecular responses with the material properties and deformation characteristics of the cell. These recent techniques have an additional advantage – they can be used to probe cells at the single cell level. Single cell studies have the potential to elucidate more precisely the specific mechanisms by which a cell senses and transmits signals, because the information gathered from each cell is not averaged over thousands or millions of cells.

Over the past decade, several approaches to studying mechanical properties at the single cell level were developed. Atomic force microscopy, optical and magnetic tweezers, micropipette aspiration and other techniques have been used to explore and develop physical models of the cell. By using these techniques, the basic physical response of a cell to mechanical forces has been analyzed, yet the reported cell moduli in the literature, when taken in aggregate, span up to 6 orders of magnitude. It is not clear whether this wide distribution is due to the disparity in different cell types being examined, the methods being used to stress the cell, or the models used to analyze the responses. No study to date has addressed this variability, nor have many studies used the same physical model to test the variability of cellular mechanical properties across different cell types.

To help clarify this broad variability in cellular mechanical properties, and to understand factors that may influence the responses of cells, two magnetic traps were designed to study the mechanical and molecular responses of different cell types. It was found that different cells may in fact have different mechanical properties, but the shear moduli are distributed over only one or two orders of magnitude, and not the five or six reported in the literature. Thus, the remaining variance in results is likely due to differences in modeling or technique. It is likely that differences in technique contribute substantially to the remaining variance, since molecular studies indicate that cellular responses are sensitive to environmental conditions such as temperature and to cellular conditions such as confluency.

1.0 Introduction

1.1 Background

How cells respond to mechanical stresses is relevant in many physiological systems, including bone remodeling and cardiovascular disease, and is relevant for tissue engineering (Fung 1990; Mow VC 1994). For example, one aspect of Wolff's Law states that bone will remodel in response to dynamic loads (Park 1992). A study by Kim et al found that when using appropriate scaffolds, applying cyclic strain on smooth muscle cells increases both the Young's modulus and ultimate tensile stresses of the cells, and could improve the organization of the cells, which is important for tissue engineering purposes (Kim and others 1999a). Despite the importance of mechanical effects on living tissues and cells, little is known about the general nature of the responses to a specified stress. In cardiovascular studies, most research has focused on biochemical mediators of the vascular remodeling process such as cytokines and growth factors, while the critical influence of mechanical stimuli has only recently been recognized.

1.1.1 Ion Channels and Other Molecules

Recent studies have characterized some of the responses of cells to mechanical stimuli. Various molecules are thought to participate in these responses. In this review, some of the more commonly studied ones are presented.

Some ion channels have been shown to be responsive to mechanical stresses, particularly calcium channels. Endothelial cells show increased cytosolic calcium levels when exposed to shear stress in the presence of ATP or ADP (Shen and others 1994), or when exposed to cyclic strain (Rosales and others 1997). Other cell types also show calcium response, for example Pommerenke et al showed that applying forces on integrin receptors on the osteogenic cell line U-2 OS resulted in increased intracellular calcium, whereas applying the same forces on transferrin receptors has significantly less effect on intracellular calcium levels (Pommerenke and others 1996). Other ion channels have been studied in some detail, such as the Shaker potassium channels (Gu and others 2001; Koh and Sanders 2001).

Ion channel activation has been studied in detail using patch clamp techniques (Gu and others 2001; Yao and others 2001). Recently, the structure of a bacterial mechanosensitive ion

channel, the MscL homolog from Mycobacterium tuberculosis, has been determined using x-ray crystallography (Chang and others 1998).

Other proteins are thought to participate in the mechanical response pathways. For example, G-proteins are implicated in the osteoblast nitric-oxide-mediated response to shear stress. G-proteins are also thought to be responsible for extracellular signal-regulated kinases 1 and 2 (ERK1/2) resonse to shear flow in endothelial cells (Bao and others 2001; McAllister and Frangos 1999).

Ingber's laboratory has demonstrated that when cells bind to microbeads, mRNA and ribosomes rapidly localize to focal adhesion complexes, indicating that mechanical signals may regulate translation of proteins near sites of signal reception (Chicurel and others 1998). These studies and others indicate that the cell responds to mechanical stimuli as an integrated structure, with focal adhesion complexes as important transducing regions. Since focal adhesion complex proteins interact with both the cell cytoskeleton and the integrins (heterodimeric cell surface receptors), it is likely that integrins directly participate in transducing mechanical signals of the extracellular environment into the cell (Wang and others 1993). The integrin family includes at least 16 α subunits and 8 β subunits that can form at least 21 different heterodimers. Integrins govern cell-matrix interactions by functioning as receptors for extracellular matrix constituents by recognizing specific amino acid sequences in different ligands.

1.1.2 Cell Morphology

Changes in cell geometry in response to mechanical stimuli, especially for endothelial cells, are also well characterized. One of the best known cell-geometry responses is the endothelial cell's tendency to elongate in the direction of shear flow, with an internal rearrangement of the cytoskeleton to match the elongation. This response depends partially on the matrix that the cells adhere to and partially on the presence of additional forces acting upon the cells (i.e., shear forces in combination with stretched membranes) (Ookawa and others 1993; Zhao and others 1995). In addition, there are purely geometric considerations that affect the nature of the stresses acting on the cell. For example, endothelial cells are not simple cylinders with smooth, flat surfaces; instead, they have a complex topology, making the shear stresses vary across different parts of the cells (Davies and others 1997). Chen et al showed that the geometry of the cellular enironment has a direct effect on cellular development. Endothelial cells that were

not allowed to spread underwent apoptosis, a cellular suicide (Chen and others 1997). These studies indicate that the effects of mechanical forces, whether external to the cell, or internal for cell spreading, are important for modeling cellular responses in many biomedical systems.

1.1.3 Gene Induction

Gene induction via mechanical stresses has been established by several studies on numerous cell types, usually by Northern analysis and more recently, the use of DNA microarrays. Although Leung et al reported that mechanical stretch increased matrix synthesis by vascular smooth muscle cells over two decades ago, only recently have studies more clearly demonstrated the mechanical influence on molecular signals (Leung and others 1976). For example, endothelial cells respond to shear flow with the upregulation of several genes such as platelet-derived growth factor B (PDGF-B), and the downregulation of endothelin-1, reviewed by Malek et al (Malek and Izumo 1995). The finding that many endothelial cell functions are affected by physical stresses demonstrates the importance of understanding not only biochemical regulators of vascular remodeling, but biomechanical factors as well.

Although vascular smooth muscle cells are critical structural cells in the normal and diseased artery, less is known about the effects of biomechanical forces on these cells. The results from one cell type cannot be applied to another, because different cells can respond in different ways to the same stimulus, or they can have the same response to different stimuli. For example, EGR-1 is upregulated by shear stress in endothelial cells and by stretch in aortic smooth muscle cells (Khachigian and others 1997; Khachigian and Collins 1997; Khachigian and others 1996; Morawietz and others 1999). While less is known about the smooth muscle cell mechano-response, certain chemical signaling pathways, most notably the kinase pathways, have been shown to be affected by mechanical stresses (Reusch and others 1997). DNA microarray experiments show that several genes (e.g., tenascin-C, cyclooxygenase-1) are affected by stretching smooth muscle cells, and that the changes in regulation appear to generate a protective response against overstressing the cells (Feng and others 1999). While the changes in gene expressions are often upregulations, downregulation of genes can also contribute to the protective response, such as by the decreased expression of metalloproteinases that degrade cellular matrix (Yang and others 1998).

1.1.4 Techniques for Single Cell Studies

In most of the studies discussed, stresses were applied globally over a large number of cells, either by fluid shear stress or by some form of membrane stretching (Brown and others 1998). These techniques are not well suited, however, for studying individual cells or probing local cell membrane and cytoskeletal mechanics. Individual cell studies are vital for identifying variations in responses and increasing the sensitivity of assays to distinguish between different types of responses. For example, a Northern analysis combines the responses of several thousands or millions of cells to obtain a single readout. Individual cell assays, however, can provide a clearer idea of the nature of the response, differentiating between small global changes and drastic local changes (Brown and others 1998; Davies 1995; Davies and others 1999). Studying individual cells has some inherent difficulties, however, which may explain the relative dearth of such studies until recently. For example, more expensive equipment and time-consuming experiments are required, making it difficult to study the number of cells needed for statistical significance under uniform conditions. Despite these and other difficulties, several new techniques for studying individual cells have been developed.

Of the various techniques recently developed to examine single cells, most are used to probe the mechanical properties of cells. Pipetting technologies are used to deform cells locally, typically on blood cells, in order to probe the membrane stiffness (Mow VC 1994). Atomic Force Microscopy (AFM) and optical traps are used to probe cellular and subcellular forces, such as those generated by kinesin motors (Sleep and others 1999). Magnetic traps with one pole (single pole) can generate more force (~one nN) on beads attached to cells, and have been used to probe the properties of cell membranes (Bausch and others 1998). Similar to the single pole trap is the magnetic twisting cytometer, developed primarily by Ingber et al (Ingber and others 1995; Wang and others 1993; Wang and Ingber 1994). Instead of a force, this cytometer generates a torque on magnetic beads attached to cells. The use of these techniques for characterizing the mechanical properties of cells is discussed in section 4.1.

1.2 Cell Models

With the introduction of many diverse techniques to study the mechanics of single cells, it became important to create a model that would help interpret the data acquired from the experiments without requiring an onerous amount of data. The model would ideally help link the

data from individual cell studies to the established molecular results from the more global studies already done (e.g., gene induction via Northern analysis). The ultimate goal of such a model would be to incorporate a mechanism by which mechanical forces are sensed and transmitted throughout the cell, transduced to molecular messengers, and ultimately converted to a change in cellular state. This model could then be used to make predictions about the cellular and tissue response to perturbations, and to help determine the course of therapy, e.g., for atherosclerotic prevention, or to help make tissue engineering more robust, e.g., by increasing the mechanical integrity of replacement tissue.

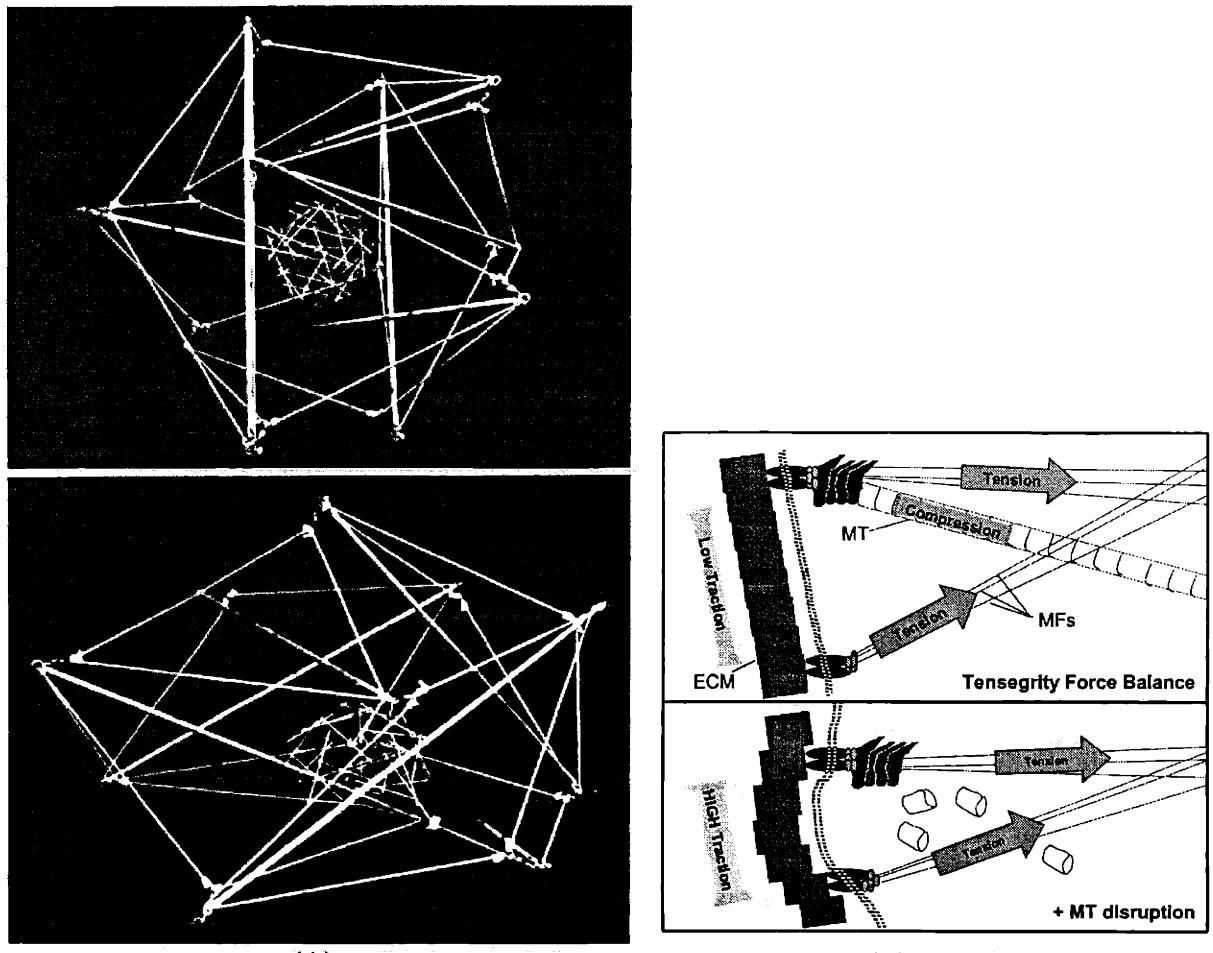

(A) (B)

Figure 1. Visualization of concept of tensegrity. The figures represent (A) a cell model showing the global changes in cell shape and nuclear motion when the cell is placed under stress (from (Ingber 1997)), and (B) the theoretical prediction of increased cellular surface traction on the extracellular matrix (ECM) when the compressive elements (MT = microtubules) inside the cell are disrupted, leaving only the tension elements (MF = actin microfilaments) behind (from (Wang and others 2001)).

1.2.1 Tensegrity Model

The tensegrity-based model developed and characterized by Ingber (Ingber 1997) considers the cell as a three-dimensional structure with individual tension and compression elements distributed throughout the cytoskeleton (see Figure 1, from (Wang and others 2001)). Ingber and colleagues have demonstrated that pre-existing tension within the cytoskeleton is a major determinant of cell deformability (Pourati and others 1998). More recently, Wang et al demonstrated that the microtubules are a good candidate for the compressive element, just as actin filaments are the tensile elements (Wang and others 2001). The tensegrity model has been developed to the point where mathematical formulations of simplified cell models could be performed. One of the consequences of the model is that the shear modulus should increase linearly with increasing prestress of the tensegrity network (Stamenovic and Coughlin 1999; Stamenovic and Coughlin 2000; Wang and others 2001). Mathematical considerations of the model have been performed on simplified tensegrity structures with few struts (Stamenovic and Coughlin 2000).

1.2.2 Open-Foam Model

Another cell model is the open-foam, or cellular solids model (Figure 2, from (Satcher and Dewey 1996; Stamenovic and Coughlin 1999)). This model treats a cell as a unit with fully interconnected internal support structures. These structures are similar to those found in wood and bread. By treating the cytoskeleton as a lattice of elastic beams, it is possible to derive certain relationships between the various material properties, such as elastic and shear moduli as a function of the cellular foam density (Satcher and Dewey 1996). While this model does not give a definitive link between the more passive material properties of the cell and the internal molecular response, the model is quantitative and accommodates a large variance in cell properties by taking into account the inherent cytoskeletal densities and other physical parameters. In contrast, the tensegrity model yields quantitative information only upon deciding the number of struts, and the nature of the connection between the tension and compression bearing elements.

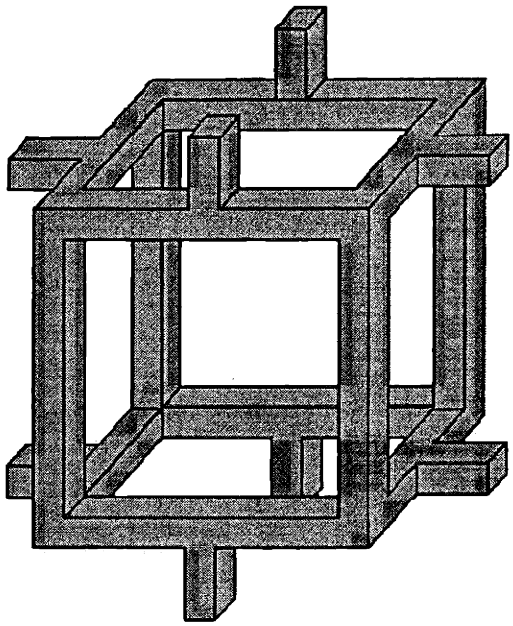

Figure 2. A schematic of the cellular solids model. This is a basic unit of the open-foam, consisting of elastic beams representing the cross-linked cytoskeleton (from (Satcher and Dewey 1996; Stamenovic and Coughlin 1999)).

1.2.3 Other Models

There are other models as well, such as the fluid mosaic (or membrane fluidity) model. This model treats the membrane as a fluid, where some proteins are free to float around, and has no main structural role by itself (Singer 1972; Singer 1982; Singer and Nicolson 1972). While the original formulations of this model from Singer did not specifically relate the membrane model to mechanotransduction, he did propose that "physical or chemical perturbations can affect or alter a particular membrane component or set of components; a redistribution of membrane components can then occur...thereby allowing new thermodynamic interactions ... to take effect." More recently, compartmentalization of the membrane into floating rafts has been proposed to explain apparent binning behavior, where free-floating proteins can diffuse only in certain confined areas (Figure 3) (Jacobson and others 1995).

An extension of the fluid mosaic model considers the entire cell membrane to be a sensor for mechanical forces. The relevant hypothesis here is that cellular regulation can be explained, at least in part, by biomechanical changes manifesting in the form of altered membrane permeability or fluidity. Shear stresses, for example, can cause the membrane permeability of calcium to increase, leading to increased intracellular calcium concentrations, which in turn

causes a downstream cascade of other signals. The effects of mechanical forces on the fluid properties of membranes was tested using dyes that are sensitive to membrane viscosity, for example, and it was found that cells change their membrane fluidity in a spatially and temporally regulated fashion (Butler and others 2001; Haidekker and others 2000).

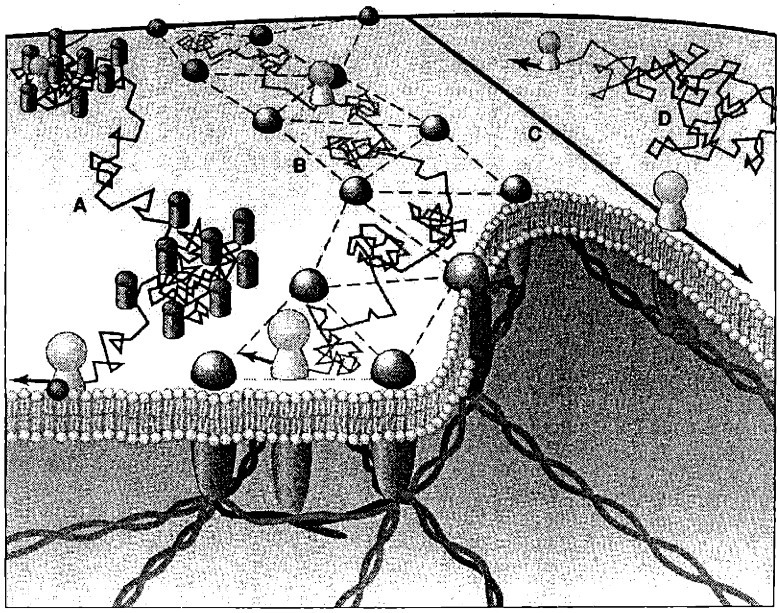

Figure 3. Conceptualization of the fluid mosaic model. The dashed triangles in the region near the letter "B" represent regions of "transient confinement" by the cytoskeleton, inside which a molecule can freely diffuse, from (Jacobson and others 1995; Stamenovic and Coughlin 2000) .

For the most part, regardless of which model is used, numerical models are generated based on simplifying assumptions about the cell and mechanisms used for probing, and are often customized for that particular study (e.g., (Boulbitch 1999; Satcher and Dewey 1996)). Thus, to interpret physical responses, the exact nature of the model used is not as important as the specific assumptions made for performing the analysis.

1.3 Thesis Goals

One of the problems in cell mechanics is that with the development of these different techniques and models, a large variation in the measured material properties has become apparent. The elastic modulus (or sometimes, shear modulus) is often calculated to quantify the cell stiffness, or the cell's resistance to deformation. There is a reported variation of six orders

of magnitude for the elastic modulus alone, from 10^0 to almost 10^6 Pa (see Figure 4, taken from (Stamenovic and Coughlin 2000)). This poses a complication for trying to develop a general cell model. Since it is not known why there is such a large variance in measured cell properties, different models cannot be as easily distinguished. In Figure 4, the open-foam and tensegrity models predict moduli different by one to two orders of magnitude, yet experimental data spans throughout, and even outside of the predicted ranges. It is possible to explain the disparity in moduli of the cell models by considering the assumptions made (such as the assumption of

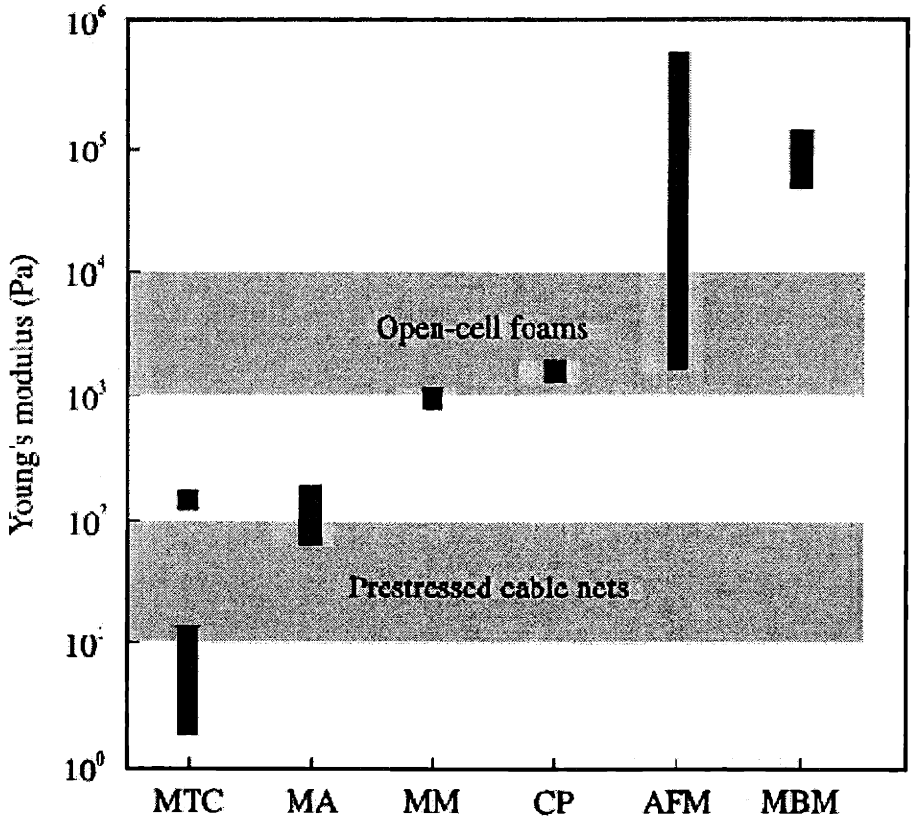

Figure 4. Graph of the theoretically predicted ranges of cellular modulus ("stiffness") are represented by the shaded grey areas, and the solid black bars indicate the range of moduli experimentally obtained through the various techniques of mechanically probing cells. MTC = magnetic twisting cytometry, MA = micropipette aspiration, MM = microplate manipulation, CP = cell poking, AFM = atomic force microscopy, and MBM = magnetic bead rheometry. From (Stamenovic and Coughlin 1999).

maximal cross-linking between actin filaments in the open-cell foam model). However, such a large range of measured cell properties makes it tedious to improve existing models, because refining analytical parameters is unlikely to produce a better fit to all the data.

Thus it is important to try to understand what the source of variation is. Possible candidates include:

(1) instrumentation variances, meaning that different techniques probe difference aspects of cells, and thus result in different stiffnesses,

(2) cellular variances, meaning that studies are performed on different types of cells, and each cell type may exhibit vastly different mechanical behaviors, and

(3) model variances, meaning that the conversion of experimental data into a modulus relies on different assumptions, which may not be compatible with the experimental system used.

The aim of this thesis is to study the response of cells to mechanical stresses at the single cell level. An octopolar magnetic trap was designed in order to exert up to 200 pN of force on several hundreds to thousands of cells. This trap could be used in conjunction with a two-photon microscope in order to assay molecular responses using a recently developed FRET assay consisting of CCF-2 and beta-lactamase. This trap is also capable of examining the medium to long term physical response of cells. Finally, this study will use a single pole magnetic trap to gather deformation data on three different cell types. The deformation data will be used to generate shear moduli for these different cell types, in order to see if there is a substantial variance among different cell types. These results will be discussed in the context of different reported instrumentation and different cell models to help develop a working hypothesis about the major sources of variation in shear moduli. Furthermore, the molecular responses of cell, as probed by the octopolar magnetic trap will be discussed in its relation to deformation data and to the future directions of study that are suggested by the results.

2.0 Cell Culture and Bead Techniques

2.1 Methods: Cell Culture

2.1.1 Cell Types

Basic cell culture techniques were used in this study. These techniques are described in the literature and only the general methods are discussed here. Appendix A contains more detailed information about the maintenance of cell lines.

Three cell types were used in this study. Human aortic smooth muscle cells (SMC), human saphenous vein endothelial cells (EC), and human kidney embryonic epithelial cells (293A) were used since they are subjected to different types of mechanical loading. Smooth muscle cells form the supporting structure of the major arteries and sustain periodic stretch, endothelial cells line the interior of blood vessels and experience periodic or nearly static shear stress caused by blood flow, and kidney epithelial cells serve little if any supporting function.

SMCs were derived by explant outgrowth of human donor aorta obtained as normally discarded tissue from orthotopic cardiac transplantation surgery. Vascular smooth muscle cells modulate phenotype in culture; therefore, only cells between passages 2 and 5 following isolation were used. The 293A cells were graciously donated from the Experimental Medicine Division (Brigham and Women's Hospital, Boston, MA). They were cultured in the same medium as the SMCs, and being transformed, do not have passage-use limitations. Human aorta smooth muscle cells and 293 cells were cultured in Dulbecco's Modified Eagle Medium (DMEM, 1 gm glucose/liter, BioWhittaker, Walkersville, MD) supplemented with 10% heat-inactivated fetal calf serum (Hyclone, Logan, Utah), 25 mM Hepes, penicillin, streptomycin, and 2 mM L-glutamine. All tissue culture reagents were selected for low endotoxin levels (<40 pg/ml) by Limulus amoebocyte lysate assay. The ECs were graciously donated by Dr. Libby's Cell Culture laboratory (Longwood Medical Research Center, Boston, MA), and were kept in M-199 with 1-10% fetal calf serum and supplemented with penicillin and fungizide (Biowhittaker).

2.1.2 Cell Plating

The cells were plated on glass coverslips or the glass Bioptechs coverslip gaskets, with human plasma fibronectin (FN, GibcoBRL/LifeTechnologies, Gaithersburg, MD) coating.

Fibronectin stock at 1 mg/ml was diluted to 2 μg/ml of Hanks Balanced Salt Solution with calcium and magnesium supplement (Hanks, GibcoBRL/LifeTechnologies) and placed on the coverslips. Glass coverslips (18 mm, VWR, West Chester, PA) were placed in 6-well plates, one coverslip per plate, for the purposes of retaining the solution. The FN was then allowed to coat the glass for 1 to 3 days at 4°C. Immediately prior to use, the FN solution was aspirated and the glass was washed twice with Hanks.

Cells were plated to achieve high confluency for most studies. SMCs were typically plated at 8,000 to 20,000 cells/cm^2, with 8,000 yielding 50% confluency the next day. The 293A cells were plated at 30,000 to 50,000 cells/cm^2 to get 60-100% confluency, and the ECs were plated at 20,000 cells/cm^2 to achieve about 80% confluency. Full confluency was not used to avoid the problem of cell crowding, which is especially a concern with the fast growing 293 cells. Cells were detached using Hanks w/o calcium and magnesium together with trypsin, centrifuged to pellet the cells and resuspended in media. A sample was taken from the resuspension and placed into a hemocytometer, which was used to determine cell number. There were some variations from sample to sample, since cells grew at different rates (even different lines of the same type of cell could grow at vastly different rates) and since there were differences in viabilities of the resuspended cells. One to three days post plating, the cells were used for the experiments.

2.2 Beads

2.2.1 Bead Target

In order to study the effects of mechanical forces on cells, it is important that the same receptor is used so that the results are consistent. The integrins, described in the introduction, are a possible link between the extracellular cell environment probed with single cell studies and the intracellular signaling cascades that constitute one step in the process of mechanotransduction. Thus, the integrins serve as a suitable target for the beads to attach to, in order to study both the structural and molecular responses of cells.

2.2.2 Bead Methods

Both polystyrene and paramagnetic beads were used for cell studies in the magnetic traps. The paramagnetic beads were acquired from Dynal (Oslo, Norway). These beads lose most of

their magnetization when the field is removed (the paramagnetic property). This is useful for studies where stresses are intermittently applied – if the beads acquire significant magnetization, they may retain some residual stresses and strains when the field is turned off. These beads are also among the most uniform magnetic beads to be produced – according to the manufacturer, the beads' variance is about 20% in magnetizable content. The tosylactivation protocol for fibronectin coating the magnetic beads was performed according to manufacturer's instructions. Approximately 0.5-1 microliters of the magnetic beads were used per coverslip or gasket, corresponding to about quarter million beads. This averages 1-2 beads/cell. Fibronectin was chosen because it forms strong bonds to cells, specifically binding integrin units, predominantly the $\alpha_5\beta^1$ subunit .

Polystyrene beads were coated with fibronectin using passive adsorption (Duke Scientific beads, Palo Alto, CA) or the carbodiimide covalent binding protocol (Polysciences, Warrington, PA and Bangs Laboratories, Fishers, IN) for carbodiimide activated beads. For passive adsorption, all centrifugations were at 14,000 RPM for 5 minutes at 4°C. The beads were supplied at 1% (v/v). One ml of the beads was pelleted by centrifugation, then resuspended in 1 ml sodium phosphate buffer, pH 7.3, and pelleted again. The beads were again resuspended in 950 μl of sodium phosphate buffer (Gibco BRL/LifeTechnologies) and then added to a microcentrifuge tube containing 50 μl of human plasma fibronectin (stock at 1 mg/ml) and incubated at room temperature for 3 hours while agitated. The beads were pelleted again, washed once with PBS, and then resuspended in one ml PBS for the final solution. This suspension was stored at 4°C until needed, at which time it was sonicated in a bath sonicator for 10 to 30 seconds. The carbodiimide protocol was followed according to manufacturer's instructions (Polysciences) with all centrifugations and incubations at maximum.

Paramagnetic beads were coated with various antibodies using the tosylactivated bead coating protocol according to manufacturer's instructions. However, these beads did not adhere to the cells in numbers greater than beads that were left uncoated (non-specific binding); thus for this study only FN coated beads were used. Polystyrene beads had much less non-specific binding and thus occasionally TS2/16 coated polystyrene beads were used. TS2/16 is a mouse monoclonal antibody that is highly specific for the human β^1 subunit of the integrins.

3.0 Molecular Biology at the Single Cell Level

3.1 Initial Studies

3.1.1 Northern Analysis with Cam-Piston Device

The molecular responses of cells to mechanical stresses have been explored by using methods on large numbers of cells. One common way to examine molecular responses is to perform a Northern blot, which compares relative levels of a specific mRNA from cells under control conditions to cells under some applied stimulus. Since the mRNA level is an indicator of promoter activity leading to gene transcription (as well as the rate of mRNA degradation), the changes in levels of mRNA with the application of some stimulus is indicative of the molecular direction of a group of cells.

Initial studies were performed on two well characterized promoters, EGR-1 (early growth response factor one) and PAI-1 (plasminogen activator inhibitor number one), which are known to be responsive to cellular strain in smooth muscle cells by previous studies (Feng and others 1999). Mechanical strain was exerted on cells plated on silicone membranes to determine the time course of promoters' responses and to test the sensitivity of the promoter to transfection. The mechanical strain device provides a nearly homogeneous biaxial strain profile; that is, strains that are equal at all locations on the membrane in all directions by use of a cam-driven platen (described in (Cheng and others 1997) and shown in Figure 5). For the silicone membrane, 2 μg FN per ml of Hanks was used to allow for cell adhesion. After the cells were stretched with the strain device, the cells were harvested using a guanidium thiocyanate solution. The mRNA was isolated using Qiagen's RNA isolation kit and a Northern blot was performed as described in a previous publication (Feng and others 1999).

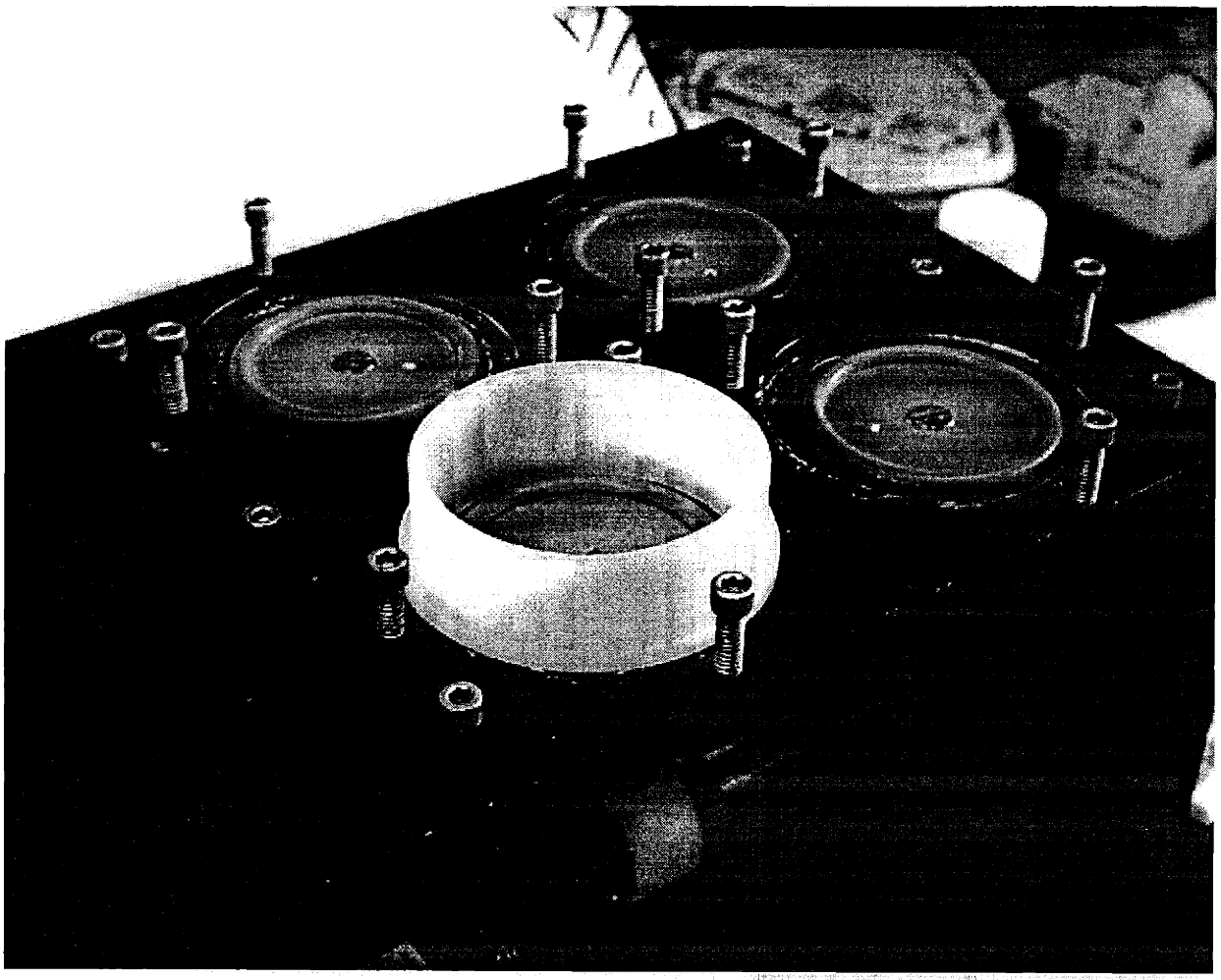

Figure 5. A cam-piston device for applying nearly uniform biaxial strain on cells. The cells are cultivated on silicone membranes (not shown) attached to the bottom of the white dishes (such as the one shown on the closest platen). The up and down motion of the platens due to the cam-piston motion results in a strain on the membrane that is transmitted to the cells.

By using the membrane strain device, one can plot the time-course of the upregulation of the promoters by performing Northern blots (Figure 6).

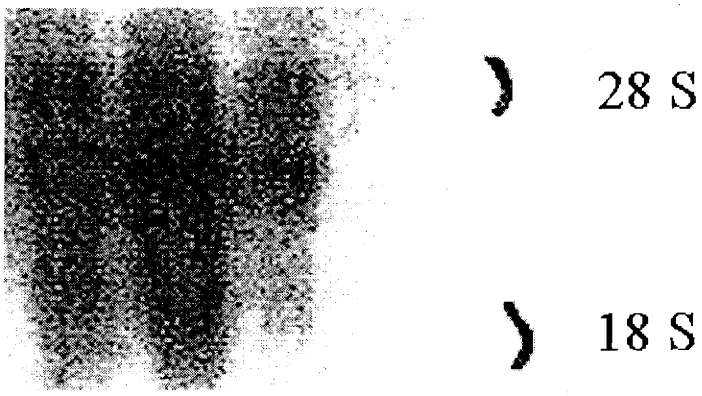

(A)

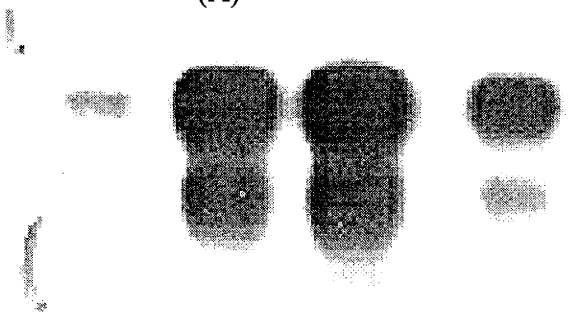

(B)

Figure 6. Northern blots of the time-course of the (A) EGR-1 promoter and the (B) PAI-1 promoter in HASMCs. In both cases, H stands for hours of stimulus at 5% strain. For PAI-1, the 1/6 and 1/24 indicate that strain was applied for one hour, then the cells were left quiescent for 5 and 23 hours, respectively, before harvesting the cells and performing the Northern. C is control, indicating a specimen that was plated in the same dishes as the strained cells, but without having had a stimulus applied. The 18s and 28s markers for ribosomes from the gel for (B) are on the left, with 28S on the top and 18S on the bottom.

3.1.2 Limitations of Northerns

The limitation of using Northern analysis is that the results invariably combine the responses of all the cells together (typically over one million per condition). Thus, the upregulation of the PAI-1 promoter after six hours can be explained by several possibilities, including increased promoter activity within all the cells, greatly increased promoter activity within only a small percentage of the cells, decreased mRNA degradation activity in all or some of the cells, or a combination of these. Understanding the actual distribution of cellular response

is an important step in the study of mechanotransduction, since information about the distribution of signals within cell populations can reveal more about the signaling pathways than just the average of all the cells. For example, if only a small fraction of the cells is responsible for upregulation of certain genes, then one possibility suggested by this is that not all cells are equipped to respond to mechanical forces (possibly by their phenotype or by some sort of cell-cell inhibition). On the other hand, if all cells respond to a stimulus in a similar fashion, then it is likely that this response is regulated in the same fashion across all the cells. Clearly the two results would lead to different methods of study, and quite possibly different models to explore. The two results would have implications for drug design and tissue engineering as well, since the targets would need to be refined to match the actual activity expressed by the cells.

Therefore, it is more useful to be able to examine the responses of a group of cells on a single cell basis. In order to do this, a new method of exerting a precisely controlled mechanical stimulus on cells needs to be developed, since most current techniques for single cell studies are limited to very few cells at a time (e.g., micropipette aspiration, AFM), or do not control the actual forces exerted on cells (e.g., magnetic twisting cytometry). Magnetic trapping, because of its large range of forces it can apply on magnetic beads, the precision in control of the magnitude and waveform of the stimulus, the potential for tagging specific receptors by coating the magnetic beads with the appropriate ligands, and the relative non-invasiveness of the technique, is well suited for studying individual cell response. However, a single-pole magnetic trap exerts a force that varies with the distance to the trap tip, and the only uniform-field magnetic trap (Amblard and others 1996) exerts only a few tens of piconewtons (10^{-12} N), which may not be enough to result in a detectable response. In fact, a magnetic trap similar to Amblard's was built and tested, and neither a molecular signal, nor consistent cell deformation was detected. As a result, a new magnetic trap was designed in order to eliminate or circumvent most of these limitations.

3.2 Magnetic Trap:Octopolar Design

3.2.1 Theory and Design Parameters

The design of the magnetic trap had to satisfy many requirements. Geometrically, the trap has to fit on the stage of the two-photon microscope (described later), while allowing the objective to move to within the working distance of the sample. The field exerted by the trap

should result in a uniform field gradient in a sample region large enough to contain many tens of cells. The magnitude and direction of the force needs to be controllable, and the trap could not get so hot that cells die with a few hours of exposure to the operationing trap. The design was developed to satisfy these requirements while maximizing the force that would be generated on a given micromagnetic bead.

Magnetic transducers exert forces on paramagnetic or ferromagnetic objects. Ferromagnetic materials have a permanent magnetic dipole moment and will experience a force in the presence of an external magnetic field gradient according to the following:

$$\mathbf{F} = \frac{1}{2}\mu_0 \nabla(\mathbf{m} \cdot \mathbf{H}),$$

where μ_0 is the permeability constant, **m** is the magnetization of the particle which is assumed to be uniform and **H** is the external magnetic field strength. Although higher forces are typically generated with ferromagnetic particles due to their higher magnetization volume, they are more difficult to manipulate because these particles aggregate once magnetized. For some applications, super-paramagnetic beads can be applied more conveniently. By definition, super-paramagnetic systems lose their magnetization once the external field is removed. The typical magnetic susceptibility of these particles is on the order of unity in SI units. The force exerted on a super-paramagnetic particle is:

$$\mathbf{F} = \mu_0 \chi V \nabla(\mathbf{H} \cdot \mathbf{H}),$$

where χ is the volume susceptibility and V is the bead volume. The applied force increases with increasing field strength and increasing field gradient, up to the saturation of the transducer material in the ferromagnetic case and both the transducer and magnetic beads in the paramagnetic case.

3.2.2 *Maxwell* Simulations

The basic octopolar trap design follows the work of Amblard (Amblard and others 1996). The configuration of the poles and the use of four sets of poles pointing towards the center of the trap are designed to yield a high field gradient in almost any direction.

Enhancements to the design were guided in part by the electromagnetic simulation program *Maxwell* from Ansoft (Pittsburgh, PA). The main material for the trap was chosen to be CMI-C rod, which has a relatively high permeability and saturation. While it is possible to use

materials of higher permeability and saturation (e.g., Hiperco 50), simulations indicated that for the intended current levels of a few amperes, there is no significant difference in field strength or gradient. Materials with higher saturation levels can exert increased forces at large currents, but at those currents the magnetic trap will heat to temperatures detrimental to cell function quickly (within an hour). Permanent magnets have not been used since they offer no easy way of precisely controlling or producing time-dependent variations in the force.

The magnetic poles are directed to the center of the trap, where the specimen will be placed. This location is denoted the sample region. Each pole is wrapped 550 times with a #24 gauge copper wire, turning the pole into an electromagnet when current is passed through the wire. By altering the currents through these coils, the magnetic field can be changed, giving control of the force levels and directions in the sample region. Instead of using four linked poles (Amblard's design), the new design consists of eight individual poles (the "octopolar" configuration). This permits vertical force generation (force perpendicular to the microscope stage) as well as horizontal. By directing the current away from the center of the trap along one pair of poles, and towards the center along the other three pairs, a field gradient is generated, resulting in a magnetic force on beads in the sample region.

The main optimizations of the trap obtained with the simulations are the addition of a backiron, the spacings used in the trap, and the shape of the pole tips. In order to use the field as efficiently as possible, a backiron made from CMI-C rod was used to connect a set of four poles to complete the magnetic flux circuit (Figure 7). Each set forms a magnetic quadropole. The complete trap consists of two quadropoles placed in a mirror-image configuration (Figure 7). The magnetic field in the sample region was compared for three possibilities: a magnetic trap with no backiron, with a backiron, and finally with triple-length poles and no backiron (to test the contribution of the extra material in the backiron). The mean field strength was significantly higher for the trap with a backiron arrangement (for strength, 50-100% higher than the triple length polar trap and >300% higher than the no backiron configuration, see Figure 8). Since we are aiming for a uniform field gradient, the mean field strength is sufficient to gauge the net force generated.

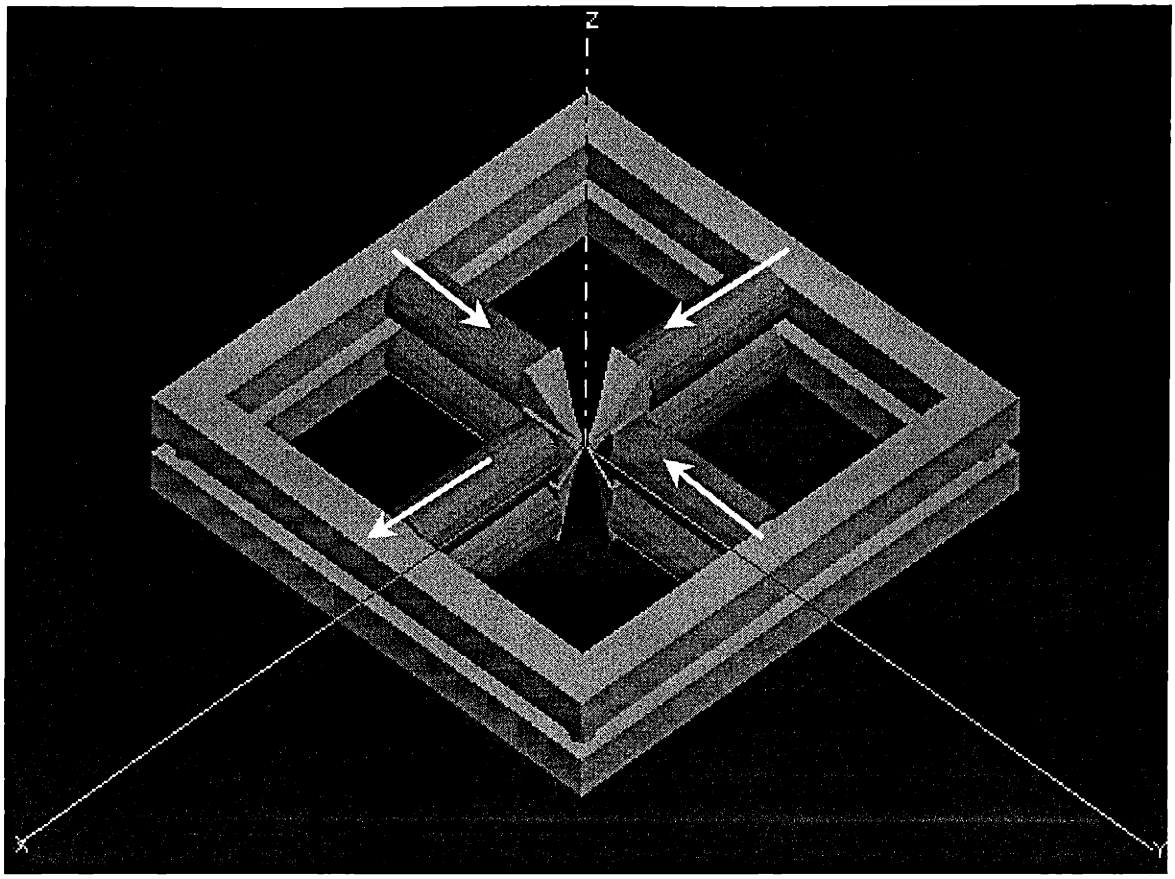

Figure 7. The basic structure of the octopolar magnetic trap. The arrows indicate the direction of current, in order to generate a uniform field gradient along the x-axis (axis that runs from the upper right to lower left of the image).

The spacing between the tips of the poles in both the vertical and horizontal directions was chosen to be the smallest possible in order to prevent field deterioration. The horizontal spacing was set at minimal distance of 5 mm, which still accommodates water immersion objectives with long working distances (Achro-plan 63x, 0.9 NA, 1.5 mm working distance or Achro-plan 100x, 1.0 NA, 1.0 mm working distance, Zeiss, Thornwood, New York). The distance between the two quadropoles was set to bring the tips 2.5mm apart vertically.

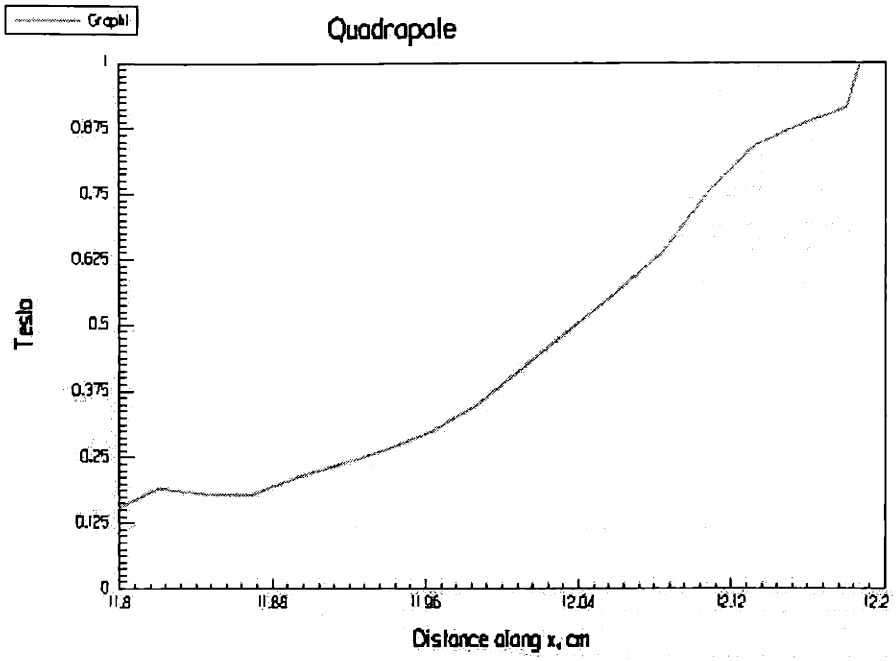

(A)

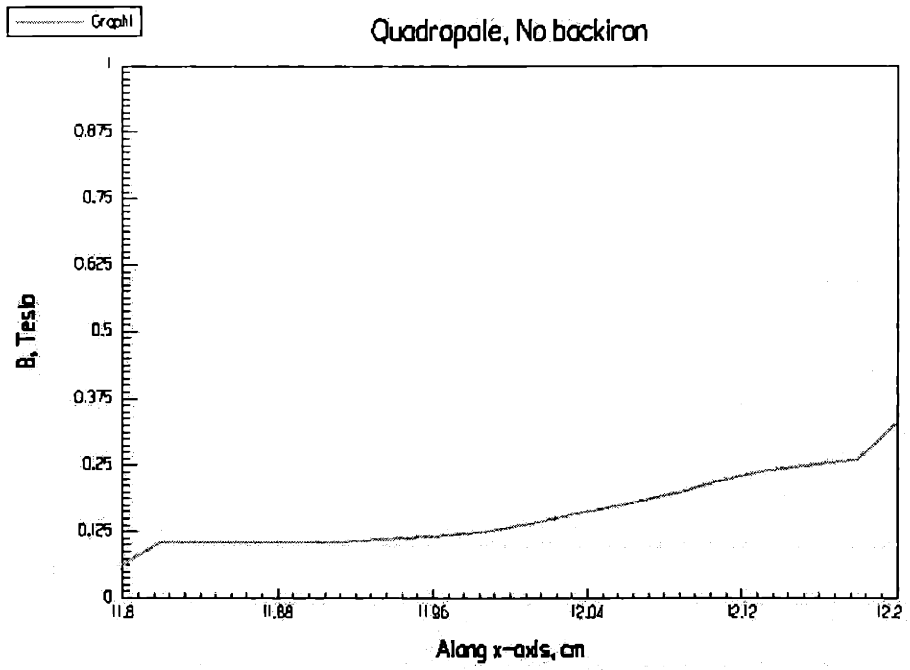

(B)

Figure 8. Comparison of the field strength in Tesla between (A) a single quadropole with a backiron, and (B) four isolated poles. In both cases, the poles are the same size, wrapped with the same number of wire turns, and have the same current running through the poles. The field strength and field gradient are substantially lower for the isolated pole case. The case for triple-length poles is not shown, but also has lower field strength and gradient when compared to the case with backiron.

This distance was chosen partially to permit the insertion of the sample, and partially based on finite-element analysis of a simplified model that indicated that a ratio of 1:2 of vertical-separation:pole-tip-separation would result in losses of field strength of about 15% (from the maximum at the tip), but that a separation of 1:1 would result in more severe losses, of up to 35%, and a separation of 1:1.5 would result in losses of 55%. The tip's vertical geometry was designed in order to fit the objective body, while the lateral angle was designed for stability (Figure 9). Two lateral angles were tested, 50° and 90°, and the field strength did not change between these two angles when the tip-to-tip separation was kept constant. However, a 90° tip would be extremely short and thin, so the 50° tip was used in the design.

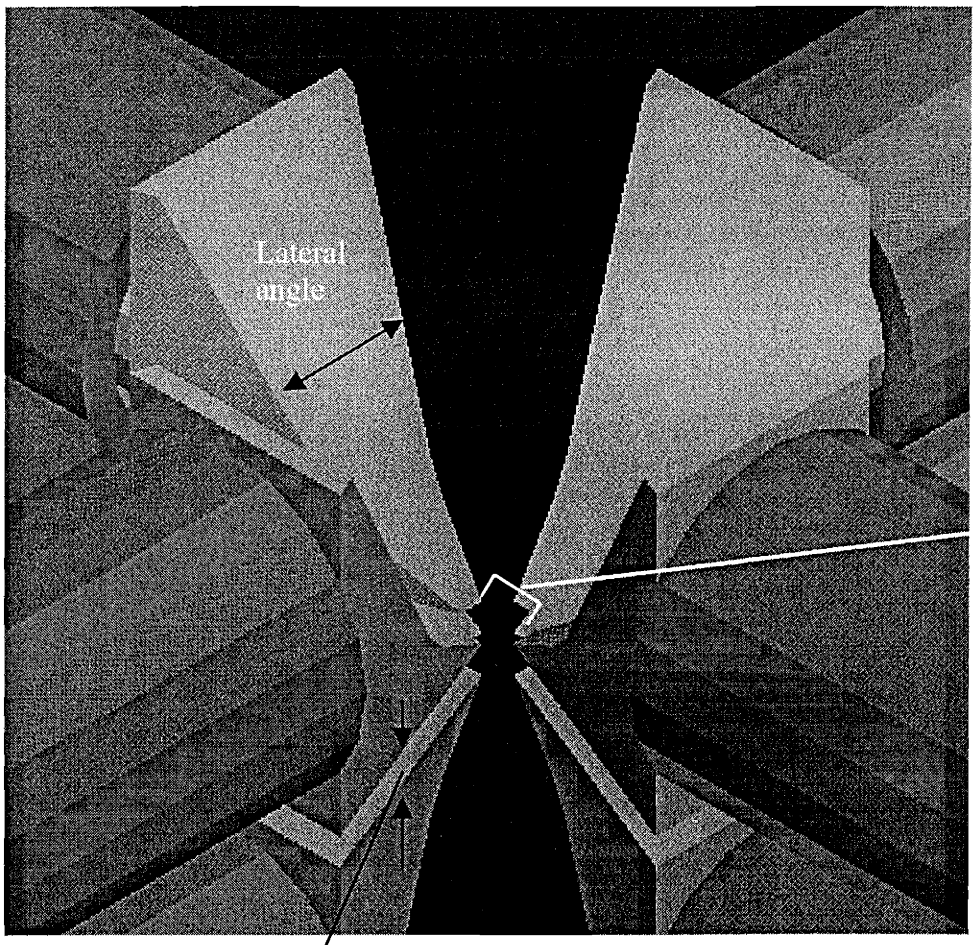

Figure 9. A close-up of the octopolar magnetic trap, in the tip region.

Finally, the trap was designed to be large, about 24 cm on a side, to maximize the magnetic field strength that could be generated. While a significantly larger trap may produce a slightly higher field, and may be able to generate more force, the loss of stability resulting from being larger than the microscope stage would be undesirable. Additionally, the simulations show that the trap poles are saturated in the tip and mid-pole regions, and thus increasing the size will lead to diminishing returns in increased force.

3.2.3 Trap Construction

The trap was machined from stock CMI-C rod, wrapped with copper wire manually, and then assembled with bolts and set screws held with loctite. A brace was attached to each of the quadropole tips and the corners of the trap to minimize deformation of the transducer components when the trap was toggled (Figure 10).

3.2.4 Operation and Calibration of the Octopolar Trap

In order to gauge the ability of the trap to produce a horizontal linear force, a calibration was performed at various current levels. Each pole is driven by current of the same amplitude, but the directions of the currents are different as specified in figure 7. This creates the necessary field gradient to generate a force. By changing the direction and amplitudes of the currents, it is possible to generate torques on beads as well as forces in the vertical direction.

Paramagnetic microspheres, 4.5 μm diameter from Dynal (Oslo, Norway), were used to perform the calibration. A bead is placed into a chambered gasket (Incubation Chambers, Grace Biolabs, Bend OR) with an aqueous solution of 70-80% sucrose, with viscosity 100 centiStokes (the lower than predicted viscosity is due in part to repeated autoclaving to dissolve the sucrose). The trap was turned on, and the steady state velocity of the bead was measured using a custom particle-tracking program. Using Stokes' formula for low Reynolds numbers flow, it is possible

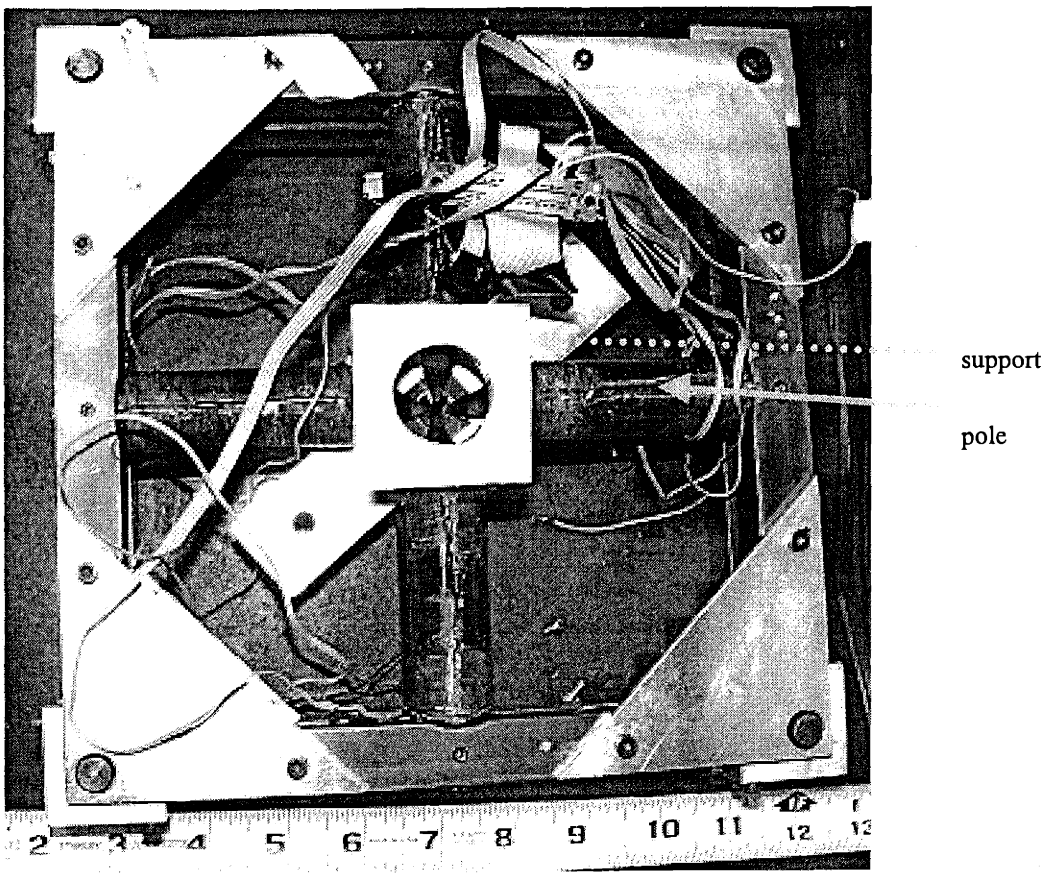

(A)

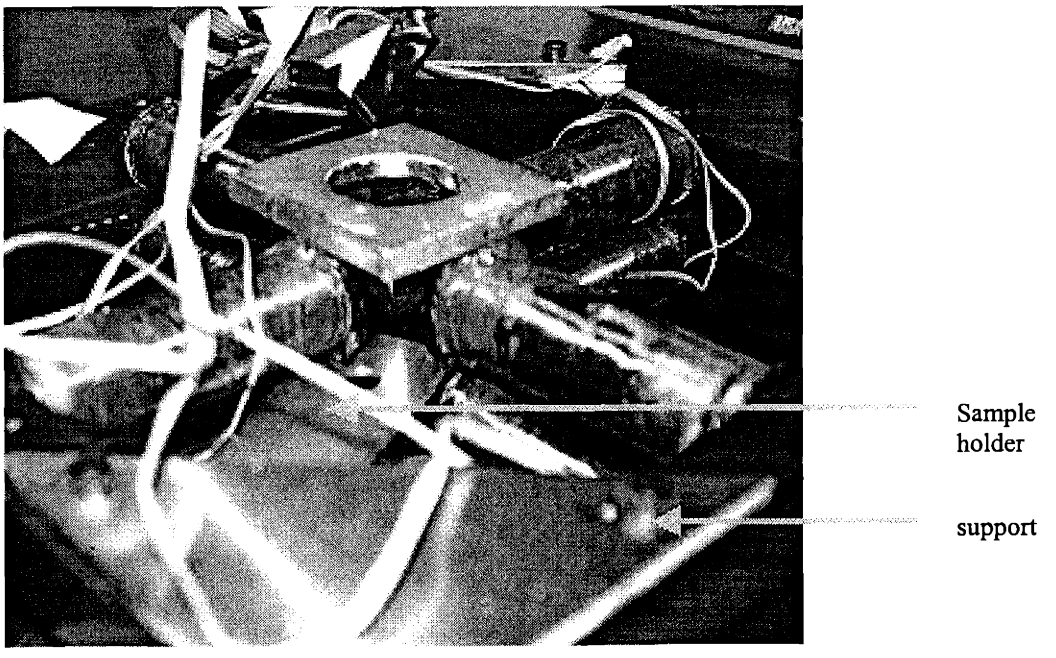

(B)

Figure 10. The octopolar magnetic trap, from (A) the top, and (B) an angle from a corner.

to calculate the corresponding force on the beads. Briefly, Stokes' formula states that

$$F = 3\pi\mu VD,$$

where μ is the viscosity of the fluid, V is the velocity of the bead at steady state, and D is the diameter of the bead. Reynolds number is given by

$$\mathrm{Re} = \frac{VD}{\upsilon},$$

where ν is the kinematic viscosity. For our calibrations, the maximum velocity is 0.01 m/s, with a bead diameter of 4.5 μm and a kinematic viscosity of 10^{-4} m^2/s. Thus, the maximum Reynolds number for our experiment is $4.5*10^{-4} << 1$ so Stokes' formula applies. Similar experiments were performed using ferromagnetic microspheres (graciously donated by Dr. Ben Fabry, Harvard University, Boston MA).

To measure magnetic field uniformity, the magnetic field distribution in the trap was measured using a DC magnetometer (Alpha Lab Inc., Salt Lake City, UT) with a miniaturized Hall probe. The active area of the Hall probe has dimensions of 3 mm by 2.5 mm and a thickness of 0.7mm. Since the sample space in the trap is only about 5 mm × 5mm × 2.5 mm, the small size of the probe is critical. The measured field distribution is the actual field distribution convoluted by the probe active area. These measurements should be a reasonable representation of the actual field distribution, since the field distribution inside the sample space of the trap varies gradually (as observed in scaled models of the current trap and in the results of the *Maxwell* simulation).

Experiments were performed using either a step increase and decrease in force, or by the use of a rectified sinusoidal wave of frequency 1 Hz. The magnetic trap is controlled by a PC workstation via a custom program, where the user controls the voltage driving the current through the coils.

3.2.5 Octopolar Magnetic transducer characterization

According to the *Maxwell* simulations, when the trap is configured to generate a force along the x-direction with pole currents set at 1A, the B field strength in the center of the trap is

0.17 T and has a gradient of 0.5 T/cm. The field gradient along the x-axis is fairly uniform and the magnitude of the field varies by less than 10% over a distance of 100 μm (Figures 11, 12).

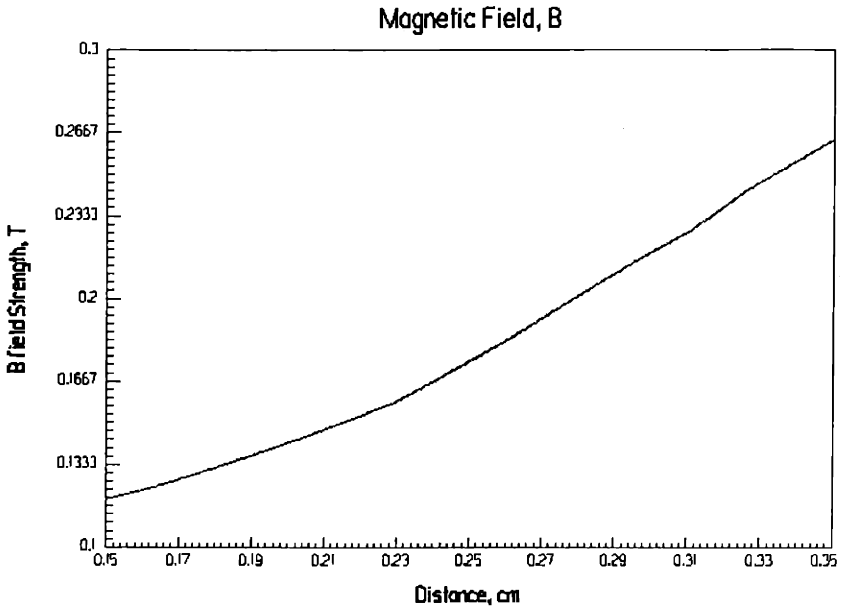

Figure 11. Maxwell simulation of the variation in magnetic field strength in the gap. The distance along the x-axis shown here is in the direction of the magnetic current, the x-axis of Figure 7. The center of the gap is at 0.25 cm.

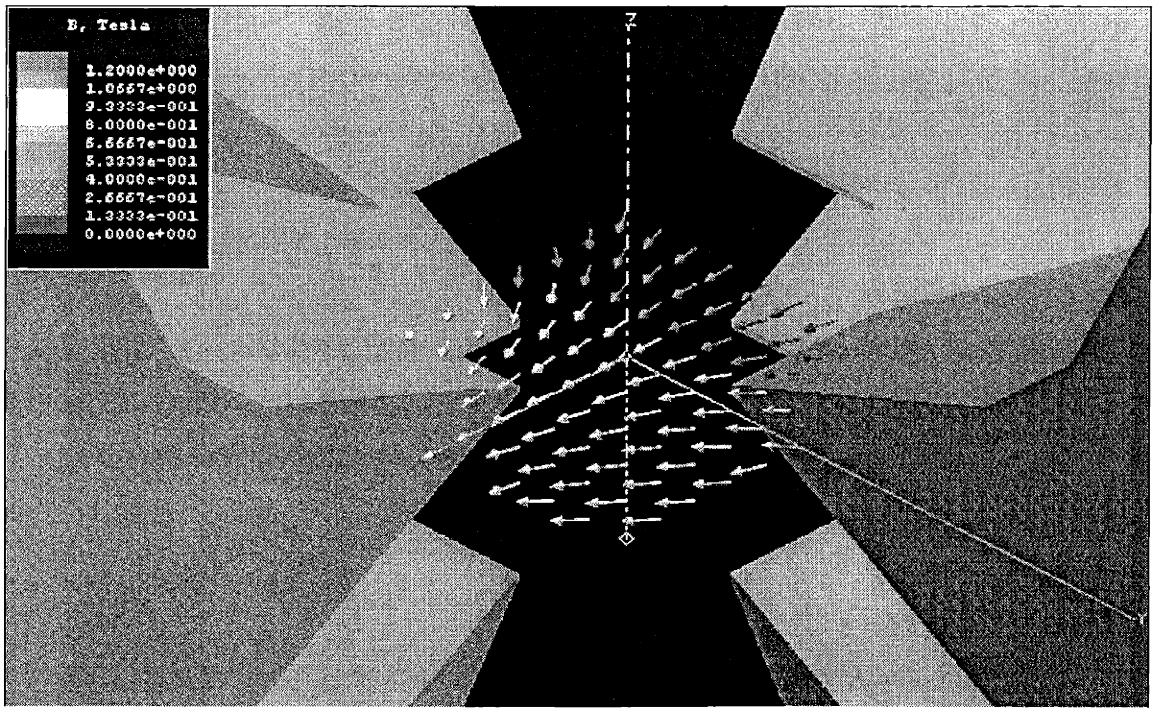

Figure 12. The magnetic field near the tip region. Note that the field is very uniform near the origin, where the cells will be placed.

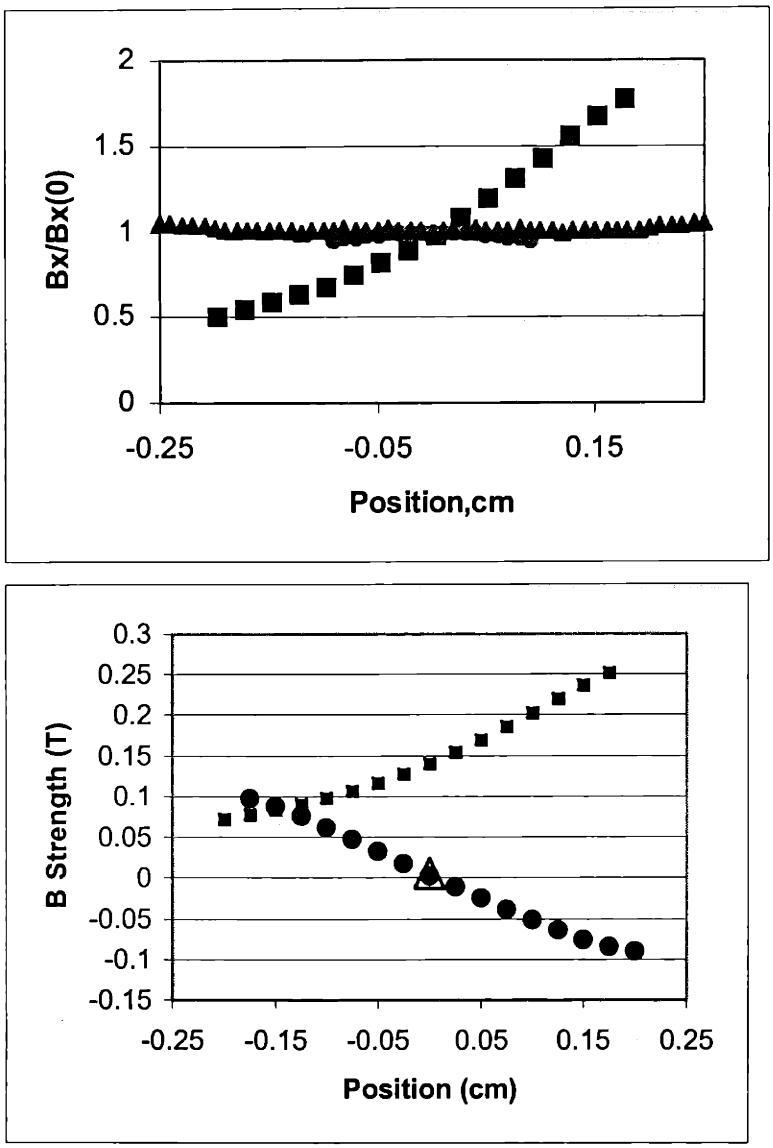

Figure 13. Hall probe measurements of the B-field of the octopolar magnetic trap in the sample region. (A) The x-components of the magnetic field strength (B_x) is plotted as a function of distances from the trap center along x- (square), y- (circle), and z- (triangle) directions. The plotted field strength is normalized to the maximum value at the trap center. (B) The x-components of the magnetic field strength (B_x) are measured along x-direction (square); the y-components of the magnetic field strength (B_y) are measured along y-direction (circle); the z-components of the magnetic field strength (B_z) at the trap center is plotted (cross hair). Due to geometric constraints of the trap, B_z can only be measured at trap center.

The simulation is in excellent agreement with the actual field measurements. Driving the magnet with 1A of current, the x-component of the magnetic field at the center of the trap is 0.15 T at the gap center with a gradient of 0.4 T/cm. These values agree with the *Maxwell* simulation

to within 25%. The variation of in x-component of the magnetic field along y- and z- axis are less than 1% within ±500μm from the trap center and less than 10% to within ±1 mm. This degree of variation is also in agreement with the *Maxwell* simulations.

The field strengths at the gap center in the plane of the four pole surfaces (at each pair of tips) are measured to be 0.072 $\hat{x}$ T, 0.095 $\hat{y}$ T, -0.095 $\hat{y}$ T, and 0.25 $\hat{x}$ T. These ratios match expected values from the basic trap design (a 1:1:1:3 magnitude ratio to conserve magnetic field). The y- and z-components of the magnetic field are less than 0.025T within ±250 μm from the trap center and less than 0.05T within ±500 μm. This level of magnetic field and gradient corresponds to negligible forces along y- or z- directions to within 50 μm of the trap center. At a distance of 250 μm, the force in the y-direction is at most 10% of the force along x-direction and increases to less than 30% at a distance of 500 μm (Figure 13).

With the same trap configuration, the field gradient along the x-axis is fairly uniform and the magnitude of the field varies by less than ±10% over a distance of ±500 μm. This is also in good agreement with the *Maxwell* simulation. If we assume a cell surface area of 100 μm^2, we can exert a force that is constant to within 10% over 2500 cells simultaneously at full confluency.

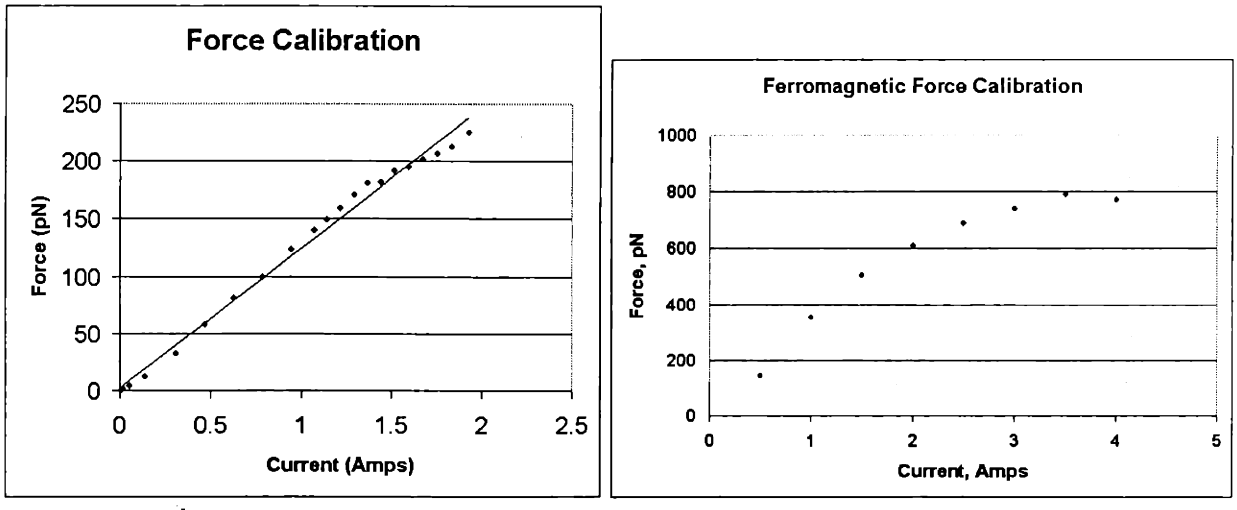

(A) (B)

Figure 14. Calibration plot, of (A) the Dynal paramangetic 4.5 μm diameter beads, and (B) the ferromagnetic beads. The line in (A) is drawn for reference so that the effects of saturation near 1.5 amps is more clear; the saturation of the ferromagnetic beads is much more pronounced by the gradual decrease of the force-current slope.

The calibration reveals the range of forces that can be obtained using this trap. The maximum force that can be obtained using super-paramagnetic beads is over 200 pN (Figure 14A). The force can be increased further using solid iron microspheres (Ben Fabry), where the force reached almost 800 pN with the application of 4 amps (Figure 14B).

The octpolar magnetic trap setup allows control of the amplitude of the forces, the frequency of the oscillations (as well as exerting a static force), and the duration of the applied force. Currently, it is possible to control the direction of the force in the plane of the sample region (the x-y plane), and in the near future, the program will incorporate a z-direction control. This trap, then, can exert precisely controlled forces on the micromagnetic beads, and subsequently, the cells, while using two-photon microscopy to quantitatively gather cell data.

To test the suitability of the workstation to examine cells, a temperature test was done. Under ambient conditions, the trap's temperature did not exceed 50°C at the poles, and did not exceed 35°C in the sample region when the trap was used at half power (100 pN) for one hour. Under forced convection conditions with a fan, the temperature at the sample region stayed at about 36°C for up to four hours at 100 pN. Therefore, the temperature is not inimical to cell viability for this period of time.

3.3 Molecular Assay of the Cell

3.3.1 Reporter Beta-Lactamase and CCF-2/AM

One of the molecular assays of the cell is to measure the gene expression of the cell. In order to assay the gene expression of cells in a non-invasive way that maintains the individual cell information, a reporter assay system, called the beta-lactamase/CCF-2 technique (Zlokarnik and others 1998) was used. The system uses a molecule called CCF-2/AM, which is an acetyloxy-methoxy ester composed of a coumarin and fluorescein molecule linked by a cephalosporin group. The AM ester allows this compound to enter the cell, and upon entering the cell, the natural esterases cleave the esters off, leaving the CCF-2 with a negative charge and preventing it from leaving the cell.

Once inside the cell, the CCF-2 becomes fluorescent as the AM-ester quenching groups are cleaved by cellular esterases. An intact CCF-2 molecule can undergo FRET (fluorescent resonance energy transfer), so that when the coumarin is excited, its blue fluorescence is attenuated by resonance energy transfer to the fluorescein, which then fluoresces green. A cell

with intact CCF-2 will appear green when stimulated at the excitation wavelength of coumarin. If beta-lactamase (an anti-penicillin enzyme) is present, it will cleave the cephalosporin linkage between the coumarin and fluorescein molecules, preventing FRET from occurring. Thus, the coumarin will no longer transfer its excitation energy to the fluorescein and the cell will fluoresce blue when coumarin's excitation wavelength is applied (Figure 15).

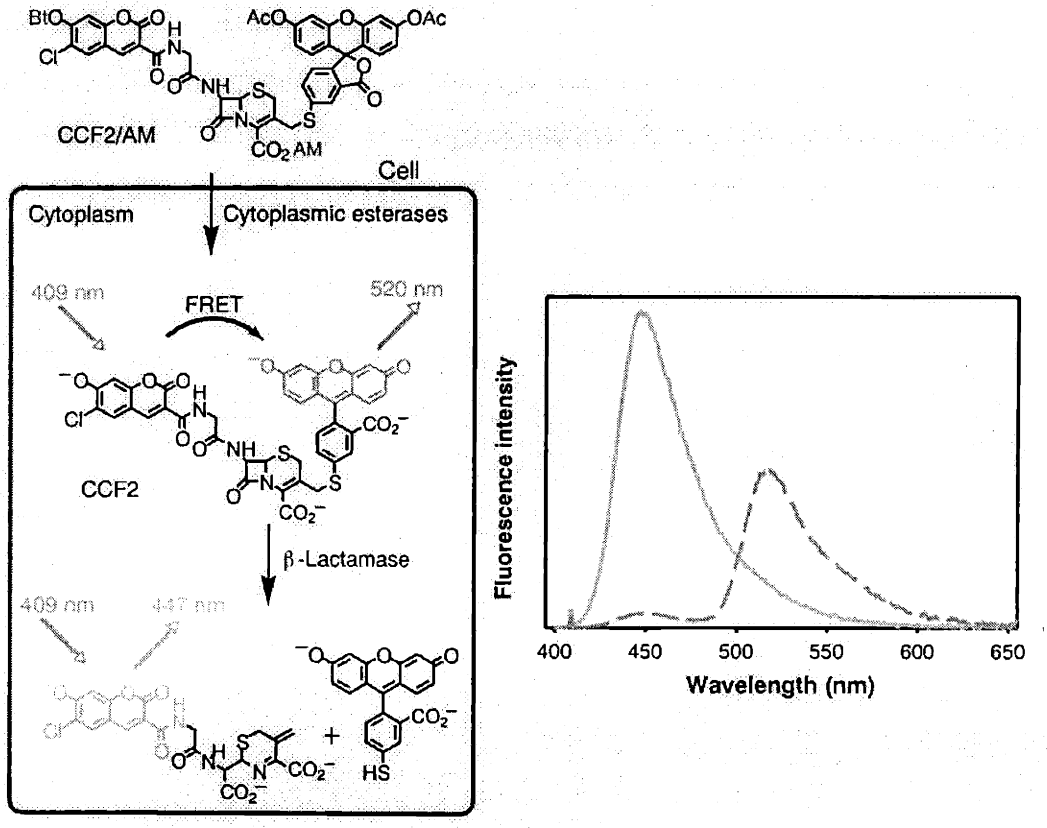

Figure 15. The CCF-2/AM mechanism for giving a fluorescent readout of the internal cellular concentration of beta-lactamase. Adapted from (Zlokarnik and others 1998).

3.3.2 Beta-Lactamase Plasmid Construction

By inserting a gene with a mechanosensitive promoter coupled to the beta-lactamase gene, a non-invasive readout of the promoter's activity can be acquired by examining the cell with fluorescence microscopy. In order to insert the promoter-beta-lactamase construct into cells, plasmid constructs were created by using bacterial recombination techniques. The promoters used were PCR-generated complete promoters (from GenBank) for the mouse EGR-1 gene (NCBI Accession number X12617) and the human PAI-1 gene (NCBI Accession number X06692). The promoters from these PCR products have been tested for responsiveness with

serum stimulation and luciferase reporting, and the promoters were also sequenced to exclude mutation. A SV-40 (simian virus 40) promoter construct was also created in order to establish a positive control, since the SV-40 promoter is normally active in all mammalian cells. The promoters from PCR products were cloned into TA cloning vectors, amplified and purified with Maxiprep DNA isolation (Qiagen), and then restriction digested and ligated into the beta-lactamase vector (Packard Instruments, and Aurora Biotechnology). The beta-lactamase vector was then amplified in bacteria again and purified with Maxiprep. These plasmids were then stored at -20°C until use.

3.3.3 Beta-Lactamase Plasmid Transfection

Cells were transfected with Lipofectin (Gibco) or Superfect (Gibco). These are chemical transfection reagents, and the manufacturer's protocol for transfection was followed. In order to increase the transfection efficiency, different ratios of plasmid DNA to reagent were tried. A typical protocol follows:

First, the transfection reagent was placed into a sterile container, and incubated (15-60 minutes). The plasmid DNA was then added to the transfection solution, and the mixture was incubated for an additional 10-30 minutes. The cells were removed from the incubator, and the media was aspirated. These cells were then rinsed with buffer to remove media, and the transfection mixture was placed on the cells. After incubating at 37°C for 3-5 hours, the cells were placed back in media, either with or without the transfection mixture removed.

Cells transfected this way were used one to three days later. For transformed cells such as CHO or 293 cells, this technique yields above 50% transfection, meaning that more than 50% of the cells show signs of expressing the gene of interest when assayed. For primary cells, however, this method typically yields less than 10% transfection rates. Transfection rates were determined by the use of a CMV-GFP vector (cytomegalovirus driving green fluorescent protein). An example of transfected HASMCs shows the blue and green cells associated with tbe beta-lactamase system, and also shows the relatively low transfection rate provided by these chemical means (Figure 16).

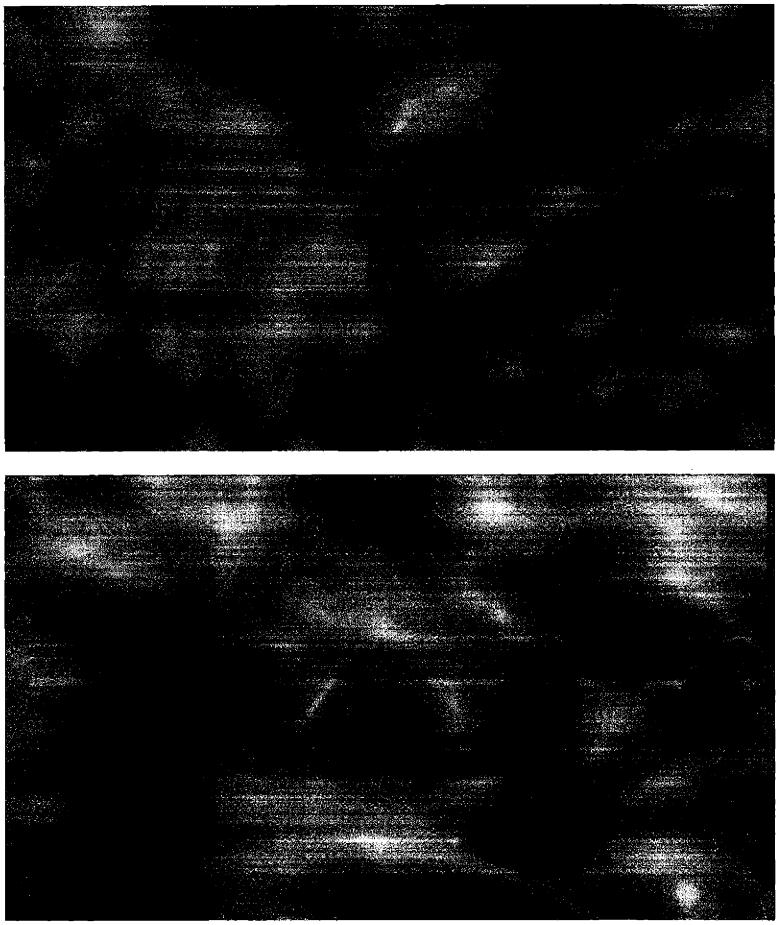

Figure 16. Two images showing HASMCs, with the top field representing controls (no transfection) and the lower field showing SV-40 transfection (using Superfect), loaded with CCF-2. A triple pass-filter was used to take these images on an Olympus BX-60 fluorescent microscope. Note the few blue cells in the lower field, indicating that only a small percentage of the cells were successfully transfected with the plasmid. Magnification 20x.

3.3.4 Adenoviral Construction and Infection

To obtain higher transfection efficiency for the primary cells, adenoviral constructs were used. An adenovirus with constitutive expression of green fluorescent protein was used to transfect cells and the transfection efficiency was near 90%. Replication-deficient adenoviruses (E1 and E3 deficient) were constructed, with different promoters driving the beta-lactamase gene. The promoters included the CMV-promoter for a positive control, and a promoterless vector for the negative control and the EGR-1 and PAI-1 promoters mentioned before. The adenoviral construction was performed using the method developed by He et. al. (He and others 1998) using a shuttle vector with the desired promoter and reporter gene and an adenoviral backbone vector constructed using bacterial recombination (Figure 17). The viral vector was

then transfected into 293A packaging cells and repeatedly amplified by using the viral product from one transfection to infect the next generation. The level of expression desired may be controlled by altering the number of viruses used per cell (typically 10-100 viruses per cell are used).

As an infection control, a CMV-GFP virus was constructed using the same protocol. HASMC cells were infected with different amounts of the virus and assayed to determine the lowest concentration of virus that would yield >90% transfection rates in the HASMCs. Then, 293A cells were infected with different concentrations of each of the viruses. The rate of cell lysis was gauged as a function of time, so that the relative concentrations of the different viruses could be determined. It was estimated, by assuming that a multiplicity of infection (MOI) of 5-15 yields a 50% lysis in 293A cells, that the nominal infection MOI for HASMCs is about 10.

One concern regarding the use of adenoviruses to transfect (infect) the cells with the reporter beta-lactamase is that the adenovirus may have other molecular effects on the cell. These effects may interfere with the reporter by causing the promoter to be constitutively upregulated, or may prevent the promoter from being upregulated in response to mechanical stresses. Thus, a Northern blot was performed on cells infected and the results compared to the cells that were not infected. The results indicate that while the process of infection can slightly increase the basal expression of the mRNA, the effects of mechanical stresses are still present (Figure 18). In fact, the use of chemical transfection may cause a larger increase in basal expression compared to the virus, although this was not clear in a repeat of the Northern blot on different cells.

The basic adenovirus infection protocol was to plate the cells and let them attach overnight. The media was then removed from the cells and replaced with media containing enough adenovirus to infect >90% of the cells as determined previously. The amount of virus would be scaled according to the number of cells in the container. The adenovirus was then left to infect the cells overnight, and aspirated the next day. The cells were washed at least twice in buffer and then replaced in serum-free media. The cells would be used one to three days following the removal of the virus. The adenovirus to be used was stored at –20°C, with the main stock stored at -80°C.

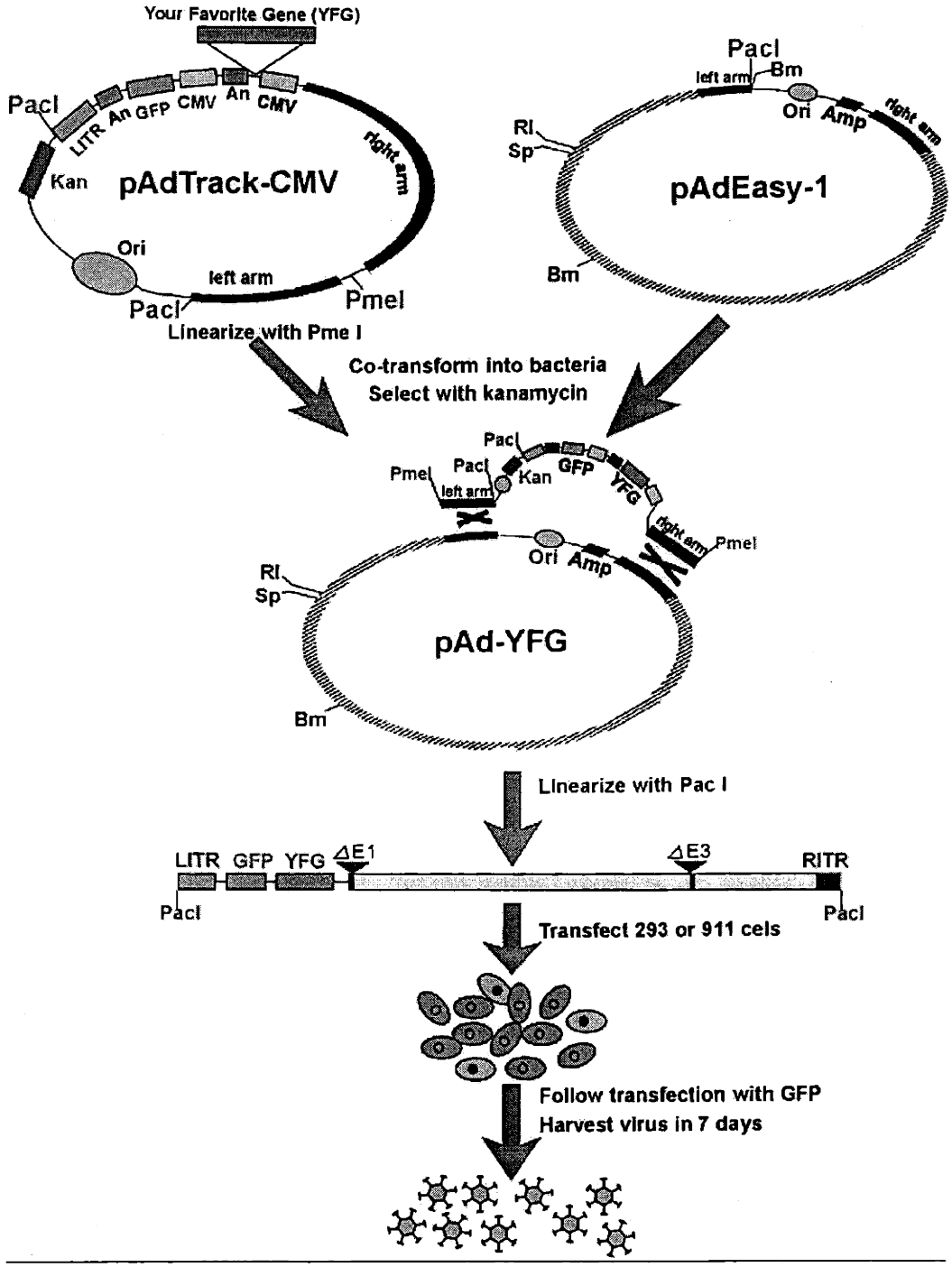

Figure 17. The system used for creating replication-deficient adenoviruses (from He). In the study, a different shuttle vector (shown here as pAdTrack) was used, since expressed GFP interferes with the green fluorescence of the fluorescein in the CCF-2. Instead the pShuttle or pShuttle-CMV was used.

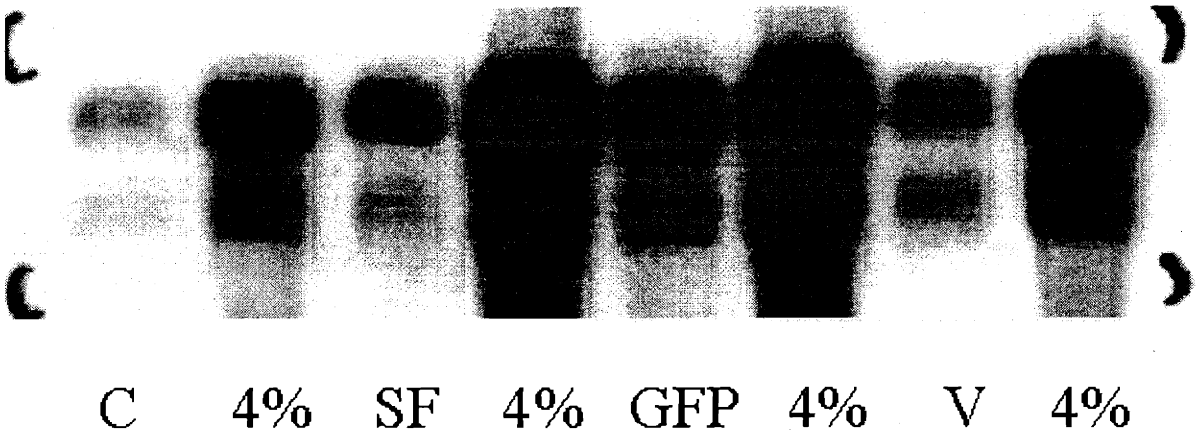

Figure 18. The Northern blot of HASMCs to test if the adenoviral infection causes a change in cell behavior. The 28S band is the upper arc on either side, and the 18S band is the lower arc on either side. The lanes are C=control, SF = Superfect transfection reagent, GFP = CMV driven GFP transfected by Superfect, and V = CMV driven GFP adenovirus infected cells. The 4% to the right of each lane is the identical condition, placed under a 4% strain for xx hours. This Northern is performed on the PAI-1 mRNA. Note the upregulation in all cases, but a slightly higher basal (no-strain) expression for all of the altered cells, with the CMV-GFP transfected by Superfect lane showing the highest basal level.

3.4 Two-photon Microscope

3.4.1 Motivation for Using a Two-photon Microscope

The octopolar magnetic trap can be used to apply a stress on cells, but a system needs to be developed to assay the cellular responses. While imaging in bright-field (standard light illumination) is sufficient for examining cellular deformation, more in-depth techniques are required to establish changes in molecular behavior of the cells. In addition, the method for examining the molecular changes must maintain the single-cell information. The use of the fluorescent reporter CCF-2 with the beta-lactamase system does this, but in order to examine the cells over a period of time, a less injurious detection system needs to be used. This is because the standard ultraviolet (UV) fluorescent microscope will cause photobleaching of the dye as well as cell injury and possibly death if the cells are exposed repeatedly for extended periods of time (greater than a few minutes).

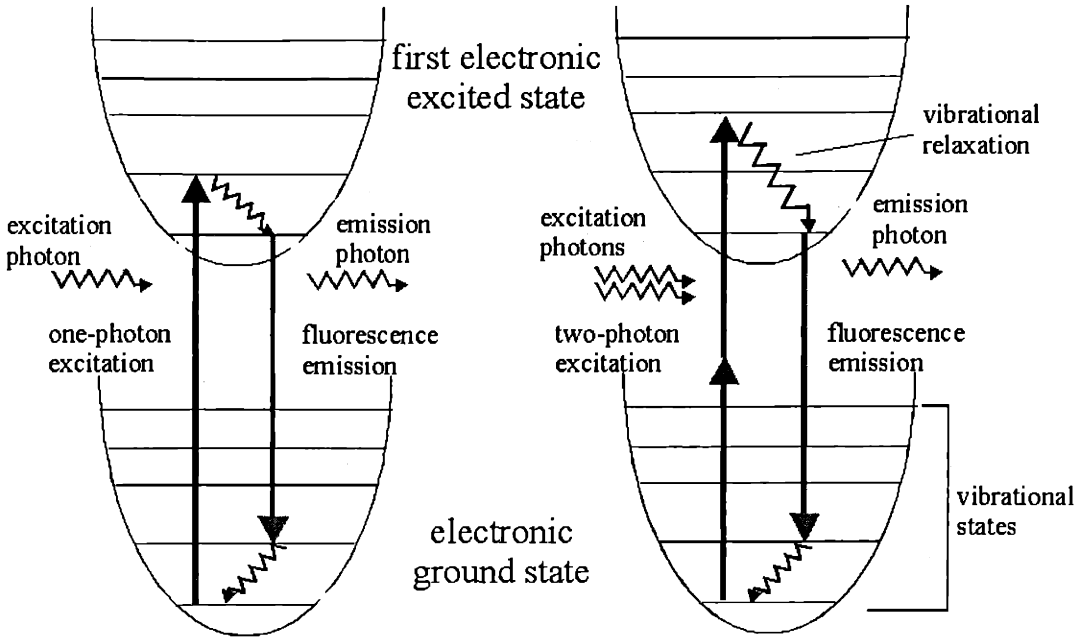

Figure 19. Schematic of the two-photon effect: by using two lower energy photons (right side) a fluorophore can be excited similarly to using one high-energy photon (left side).

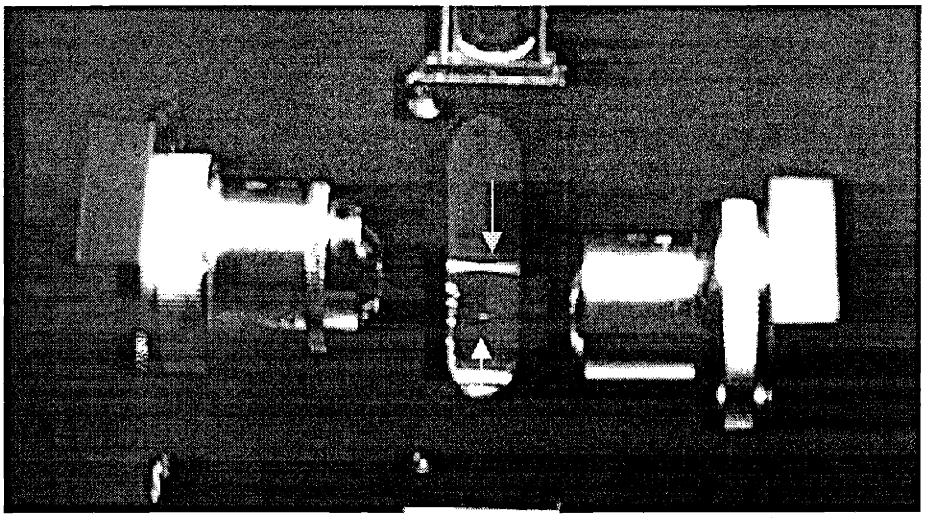

Figure 20. Comparison of two-photon and standard (wide-field) fluorescence. The standard laser excitation, entering from the left excites the entire region (top arrow) while the two-photon system excites only a small volume of the same fluorophore.

A two-photon microscope is a laser-driven fluorescence microscope that relies on two lower energy photons (red to infrared, or IR) to excite a fluorophore instead of a single high energy photon (typically UV) (Figure 19). In order to have a high probability of having two of

the lower energy photons incident on the same fluorophore, the laser needs to be focused on the specimen. By shifting the focal point, a scanned image is obtained because the excitation only occurs in a small region (Figure 20). Two-photon microscopy has the advantage that because it scans a small section at a time, it is possible to take data for a longer period of time without injuring or photobleaching the specimen.

3.4.2 Instrumentation of the Two-photon Microscope

The instrumentation and design of a basic multi-photon microscope has been described in several previous publications (So and others 1998; So and others 1995). The multi-photon excitation microscope design is based on a mode-locked Titanium-Sapphire laser (Mira 900, Coherent Inc., Palo Alto, CA). A Glan-Thomson polarizer is used to control the excitation power. The beam expanded laser light is directed into the microscope via a galvanometer-driven x-y scanner (Cambridge Technology, Watertown, MA). Images are generated by raster scanning the x-y mirrors. The excitation light enters the Zeiss Axiovert microscope (Zeiss Inc., Thornwood, NY) via a modified epi-luminescence light path. The scan lens is positioned such that the x-y scanner is at its eye-point, while the field aperture plane is at its focal point. Since the objectives are infinity-corrected, a tube lens is positioned to re-collimate the excitation light. The scan lens and the tube lens function together as a beam expander that over-fills the back aperture of the objective lens. The dichroic reflects the excitation light to the objective. The dichroic mirrors are custom-made short pass filters (Chroma Technology Inc., Brattleboro, VT) that maximize reflection in the infrared and transmission in the blue-green region of the spectrum. Typical image sizes range from 40 to 200 microns on a side. The objective axial position is driven by a piezo-motor interfaced to a computer. The typical image acquisition time is about two seconds for a single x-y plane.

The fluorescence emission is collected by the same objective and transmitted through the dichroic mirror along the emission path. An additional barrier filter is needed to further attenuate the scattered excitation light because of the high excitation intensity used. Since two-photon excitation has the advantage that the excitation and emission wavelengths are well-separated (by 300-400 nm), short pass filters such as 2 mm of BG39 Schott glass filter (CVI Laser, Livermore, CA) eliminate most of the residual scatter with a minimum attenuation of the fluorescence. A de-scan lens is inserted between the tube lens and the photomultiplier tube (PMT) to re-collimate

the excitation and ensure that the emission light strikes the PMT at the same position, independent of scanner motion. The fluorescence signal at each pixel is detected by an R5600-P PMT (Hamamatsu, Bridgewater, NJ), which is a compact single photon counting module with high quantum efficiency.

The setup of the two-photon microscope and the octopolar trap is schematically shown in Figure 21.

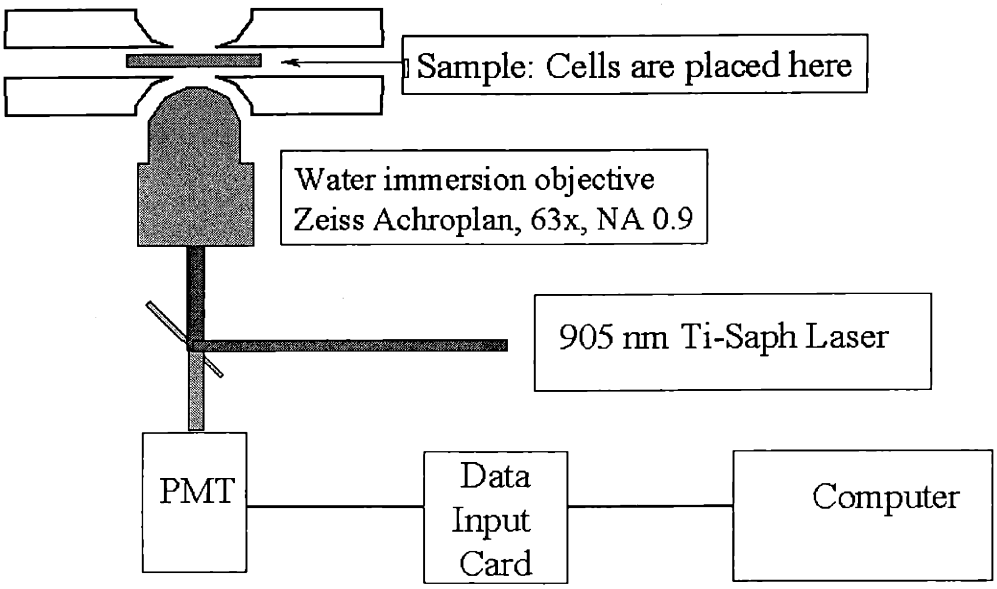

Figure 21. The integration of the two-photon system and the octopolar magnetic trap to be able to scan specimens while exerting a stress on it. It is possible to substitute the unipolar magnetic trap for the octopolar, but it would be difficult to determine the distance from the pole-tip to the magnetic bead without adding another camera to the system.

3.4.3 The "Fast-Scan" Two-photon Microscope

A second two-photon system based on a high speed polygonal scanner was developed to take very fast three-dimensional sections of large specimens (up to mm by mm in size) (Kim and others 1999b). This "fast-scan" system is used for taking fluorescent images of a large area. A single three-dimensional image stack consisting of fifty slices can be imaged in about four seconds (at 256 by 256 pixel resolution). When taking fluorescence images for quantitative analysis, it is important to have the focus in the same plane, usually the location where the fluorescence is maximal. However, due to irregularities in the specimen and the microscope stage, scanning a large section can be problematical because the focus can change planes. By scanning a three-dimensional section across the specimen, one can then extract the maximum

fluorescence slice from each scanned region, and reconstruct the specimen as a single large image at the focal plane, circumventing this problem.

3.5 Octopolar Magnetic Trap Results: Molecular Assays

3.5.1 Control Response

HASMCs were first infected with the CMV driven beta-lactamase and the no promoter (NP) driven beta-lactamase as a test to see if the viruses were functional. The data were taken on two channels, one with a bandpass filter at 525 nm for the green resulting from the fluorescein fluorescence, and one with a bandpass filter at 450 nm, for the blue coumarin fluorescence. Five to ten images of each specimen were acquired with the standard two-photon microscope, and then the images were analyzed. A program was written to calculate the blue to green ratio as:

$$R = \frac{1}{n}\sum_{1}^{n}\left(100 * \frac{F_g - F_b}{F_g + F_b}\right),$$

where F_g is the green fluorescence, F_b is the blue fluorescence and the sum is taken over all the pixels above a threshold in the entire image (of number n). This ratio was used instead of F_b/F_g because the latter term has a large range, from zero to infinity, and is sensitive to changes in F_g for low fluorescence intensities. The ratio R varies from –100 to 100, with –100 indicating a sample had only blue fluorescence and 100 indicating that the sample had only green fluorescence. In order to count only cells, a threshold for the green fluorescence was determined where the background would be attenuated but the majority of the cell information would be left intact. The R ratio would only be calculated for the pixels that crossed the threshold. This level varied from experiment to experiment, but was the same for all specimens in the same experiment. For the beta-lactamse studies, the ratio ranges from just under 0 to 100, since the fluorescein in the cells is excited independently by two-photon, so that even when there is no FRET, green fluorescence is present.

The experiments on the constitutive promoters indicate that the CMV adenovirus worked very well, with almost 100% infection rates, and that the NP version did not have any significant signal, although surprisingly, there were a few cells that were blue. The quantitative analysis also reveals that there is little time sensitivity of the reporters, indicating that the dye does not spontaneously and significantly degrade over the course of a few hours (Figures 22,23). The NP beta-lactamase showed little changes in time-course, even when exposed to a chemical stimulus

(PMA) and the placement of magnetic beads (Figure 24). This last test served as a control against false positive readings that may have little or nothing to do with the mechanical response of the promoters.

3.5.2 PAI-1 Response

HASMCs were infected with the PAI-1 mediated beta-lactamase adenovirus, and quantitative assays were done using the two photon microscope to test the response of the promoters to known a agonist, fetal calf serum. The cells were placed in serum-free media post infection. On the day of the experiment, the cells were loaded with CCF-2, assayed, and then one of the specimens was placed in media containing 10% serum. An assay was then taken at 6 hours after a CCF-2 reload (Figure 25). The results indicate that serum does not cause the production of more beta-lactamase molecules in this time period as compared to control. The variance of the data is quite large, indicating that there is fairly large variability in expression among the cells.

3.5.3 EGR-1 Response

Since the PAI-1 viral reporter did not respond well to chemical induction and because PAI-1 is a relatively slow responding promoter (requiring some six to twenty-four hours to establish induction in Northern blots), the EGR-1 promoter was used. HASMCs infected with EGR-1 driven beta-lactamase, however, expressed a large baseline, so that cells that were left in serum-free media after infection showed a blue-green ratio near zero immediately upon assay. This indicates that the baseline EGR-1 expression is high enough to create thousands of beta-lactamase molecules.

To circumvent this problem, an inhibitor of beta-lactamase, clavulanic acid, was used to surpress the initial expression of EGR-1. After infection, cells were placed in a 300 μM concentration of clavulanic acid (United States Pharmacopeia, Rockville, MD) as suggested by Dr. Zlokarnic of Aurora Biotechnology. The cells were left in the clavulanic solution until the day of the experiment. In this case, it is not the amount of blue-green that is indicative of the promoter activity, but rather the rate that the blue-green ratio decreases. In other words, if the rate that the promoter makes new beta-lactamase is increased, a larger number of CCF-2 molecules will be cleaved and the cell's blue-green ratio will decrease more quickly. An

experiment was done at room temperature, where four EGR-1 specimens were tested. A control EGR-1 specimen was used as the baseline since it has no stimuli and would thus reflect the constitutive activity of the cell. The three other specimens were either loaded with beads only, loaded with PMA (an EGR-1 agonist), or loaded with beads and placed in the magnetic trap under 120 pN of force for one hour. After one hour, the cells were reloaded with CCF-2 again and assayed hourly. The reload is necessary since the magnetic trap's effect on cells with beads seems to cause leaks (a "magnetoporation effect") that cause the CCF-2 to exit the cell, or be degraded to the extent that assays cannot be done immediately. The results indicate that there is no detectable difference between any of the stimuli, as compared to control (Figures 26, 27).

Different variants of this experiment were performed where cells were placed in the 37°C incubator to help control temperature, the concentration of clavulanic acid was changed, the cells were left in the CCF-2 solution to avoid reloading of the dye, and different lengths of stimuli were used. The results were mostly ambiguous – while there appeared to be a consistent mild induction of EGR-1 by the magnetic trap, it was not clear that the induction was caused to a large extent by the mechanical stresses applied to the cell. One major concern was the lack of temperature control in the specimen. The controls were either placed at room temperature (23°C) or in the cell incubator (37°C), while the cells in the active magnetic trap were often exposed to temperatures throughout this range, since the trap is initially at room temperature, and then gradually warms to 37°C over the course of an hour. Controls where the specimens were sequentially loaded in the magnetic trap without beads were also inconclusive, partially because the temperature of the magnetic trap would be different at the start of the second specimen. One attempt was made to control temperature by placing the magnetic trap into a 37°C incubator and pre-warming it to 37°C before the start of each experiment, but the trap then exceeded 37°C during the experiment, and the results were not robust.

To exemplify the effects of temperature on meolcular expression in cells, a Northern blot was performed on cells that were stretched at room temperature and compared to cells stretched at 37°C. The results indicate that there is significantly less upregulation of the mRNA expression at room temperature, compared to the changes seen at 37°C (Figure 28).

The chemical induction of the promoters consistently showed substantial upregulation; however, the amount of expression was not consistent among different smooth muscle cell lines.

Thus, this system can be used for studying the molecular responses of cells, but only if many factors, such as temperature, have been controlled. There still remains the possibility that despite all controls, the magnetic trap cannot exert enough force to induce a molecular response. One way to test this hypothesis is to test if the trap can exert enough force to deform the cells. It is a reasonable expectation that in order for a cell to detect mechanical stresses, the stresses must be of sufficient magnitude to actually cause cell deformation. This is supported by the fact that cell strain studies using Northern analysis show that for low strains, the molecular signal is much weaker as compared to higher strains (Figure 29).

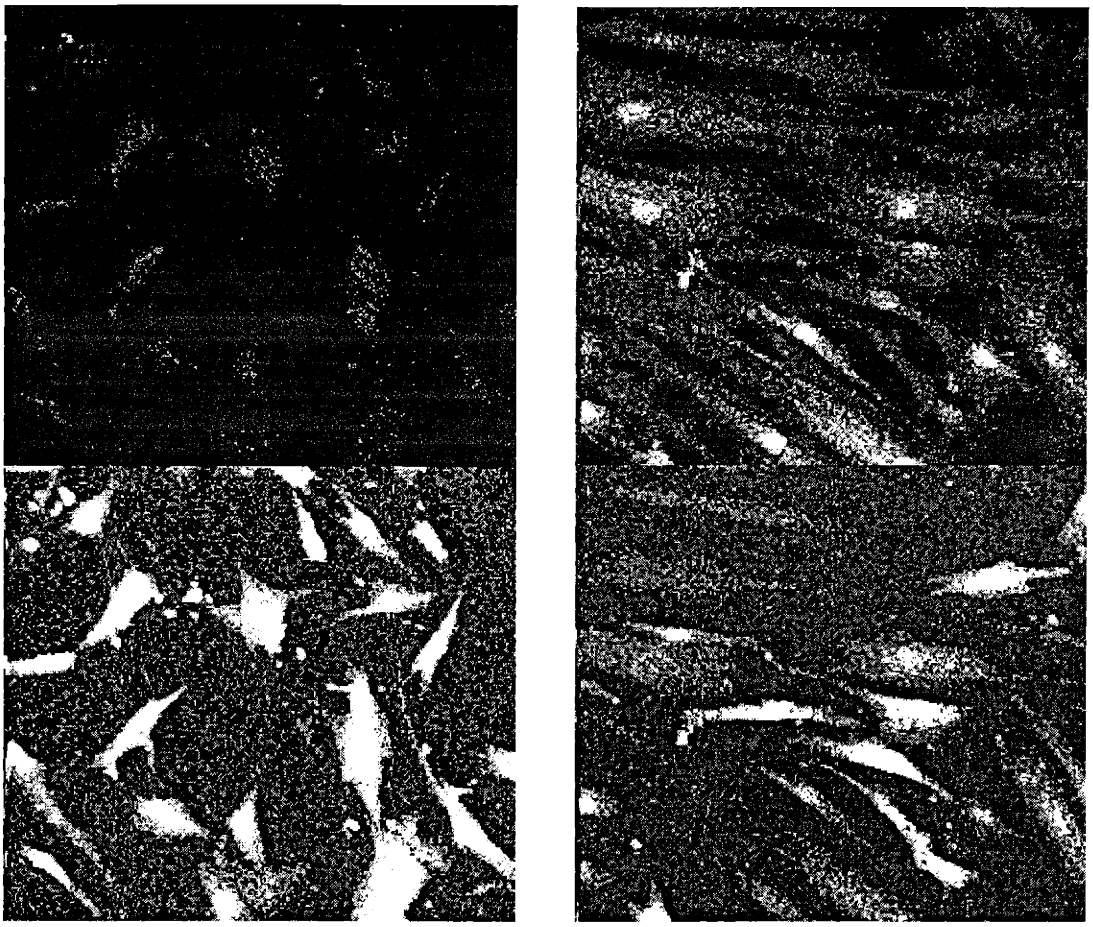

Figure 22. Two-photon images of control (left) and CMV (right) beta-lactamase infected HASMCs. The upper field in each image is the blue channel, and the lower is the green channel. Note the increased fluorescence in the blue channel for the CMV-beta-lactamase infected cells. The blue fluorescence in the control image is likely due to autofluorescence or the partial degradation of the dye, CCF-2.

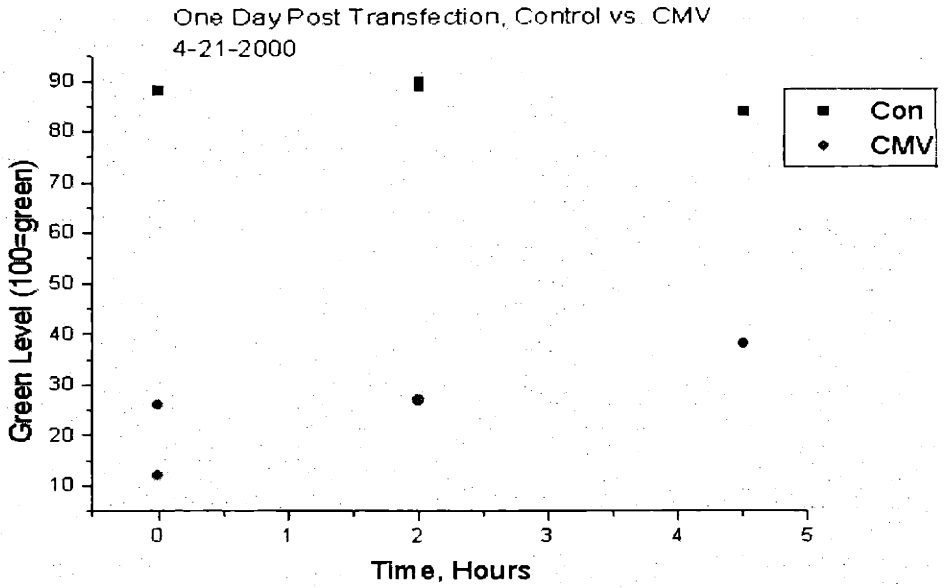

Figure 23. The time course of the blue-green ratio of control and CMV-beta-lactamase infected HASMCs. There is only slight degradation after 3-4 hours, but by keeping the cells immersed in the CCF-2 solution even this degradation disappears.

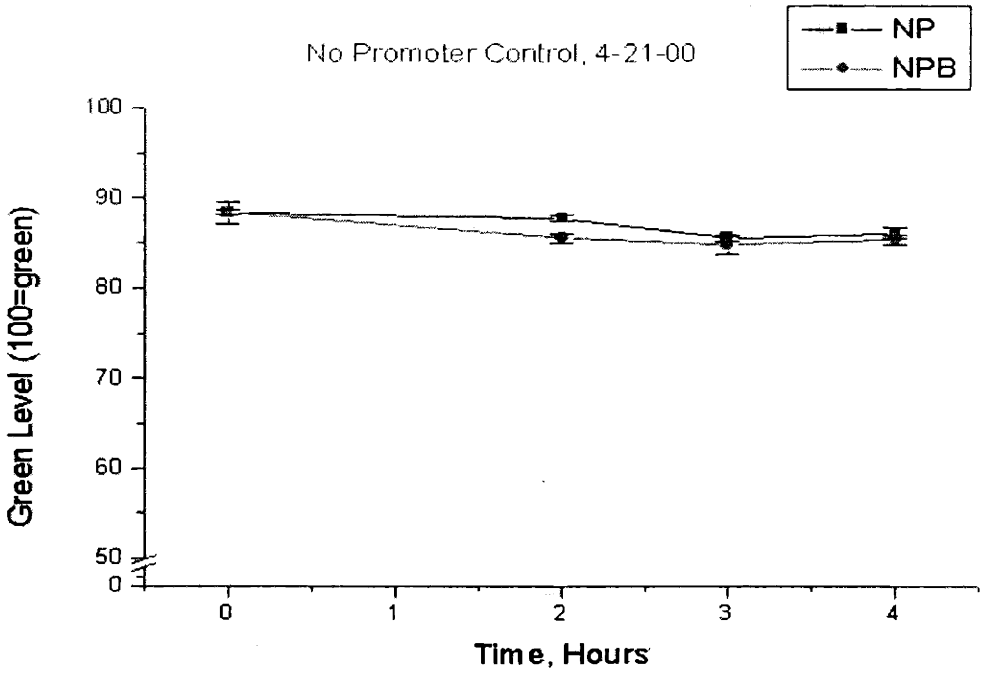

Figure 24. The no promoter adenovirus was used to infect HASMCs. After the infection, the cells were loaded with CCF-2 and assayed for four hours. There was little change in the blue-green ratio for the cells alone (NP) as well as for the cells exposed to PMA and magnetic beads (NPB).

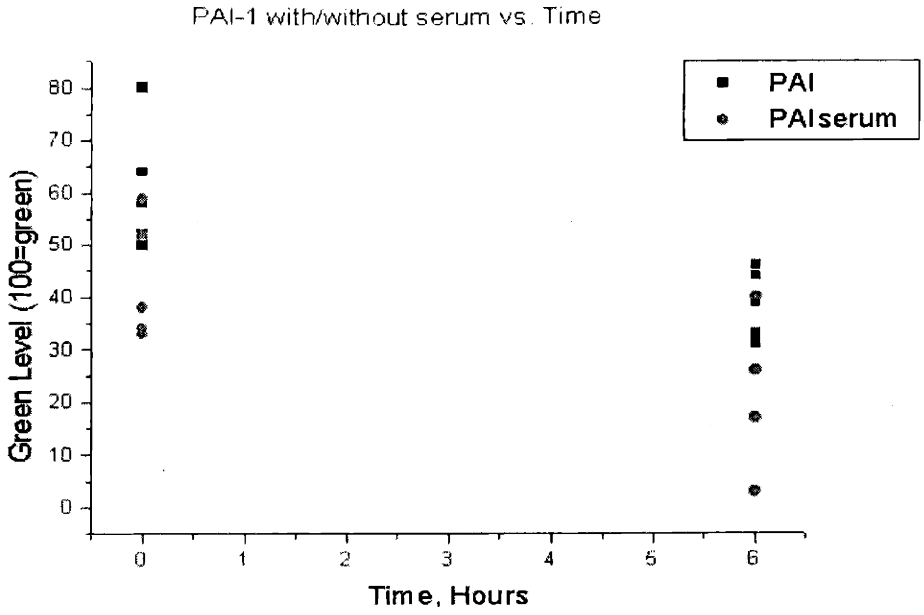

Figure 25. Induction of the PAI-1 promoter using serum. No clear change is observed.

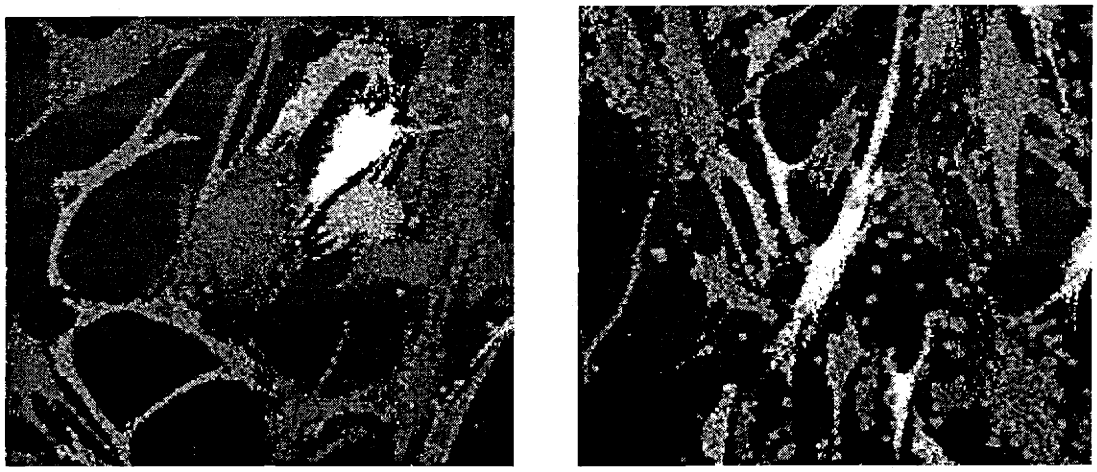

Figure 26. EGR-1 beta-lactamase infected HASMC, as control (left) and magnetic trapped for 1 hour in the octopolar magnetic trap (right). The magnetic beads are visible in the right image.

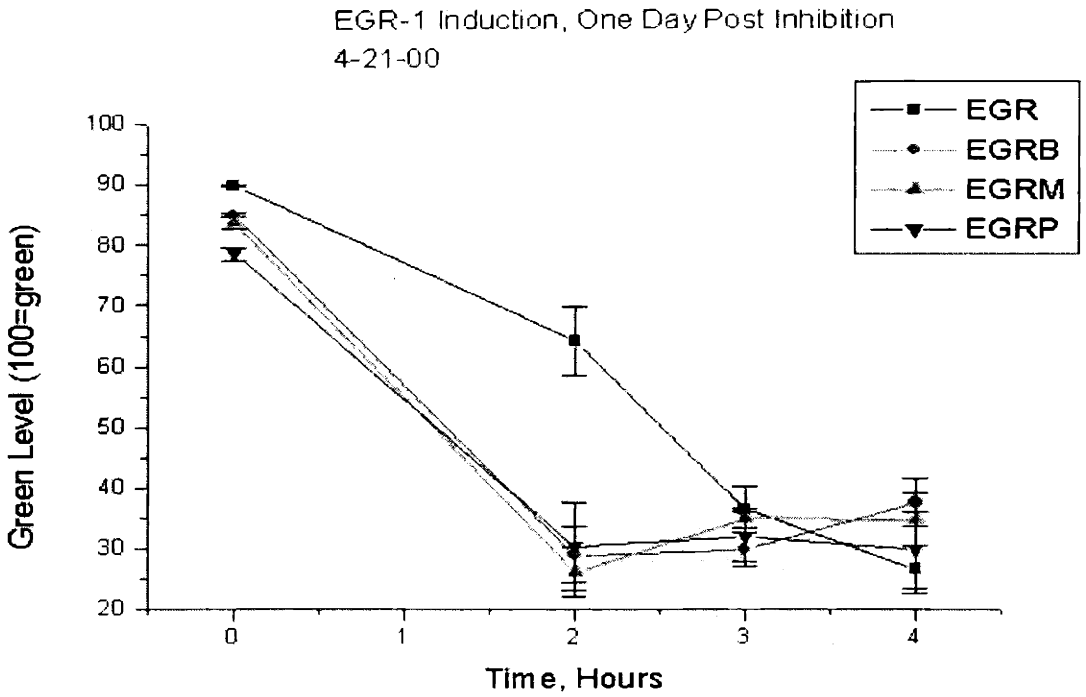

Figure 27. EGR-1 induction with clavulanic acid, m=stimulus in mag trap for 1 hour at 1.25 V, b= beads only and p=pma only, all at room temp

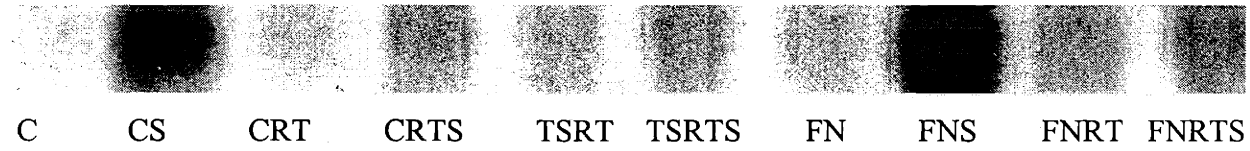

Figure 28. Northern blot showing the effects of temperature on the expression of EGR-1 in HASMCs. The specimens were placed at 37°C unless otherwise noted. The lanes are C: control, CS: control with 4% strain for 1 hour, CRT: control at room temperature, CRTS: control at room temperature with 4% strain for 1 hour, TSRT: TS2/16 coated magnetic beads loaded onto the cells at room temperature, TSRTS: TSRT with 4% strain for 1 hour, FN: fibronectin coated magnetic beads loaded onto the cells, FNS = FN with 4% strain for 1 hour, FNRT: FN at room temperature, and FNRTS: FNRT with 4% strain for 1 hour. Note the attenuated upregulation in the room temperature specimens with stretch, as well as the very mild upregulation due to the addition of the magnetic beads.

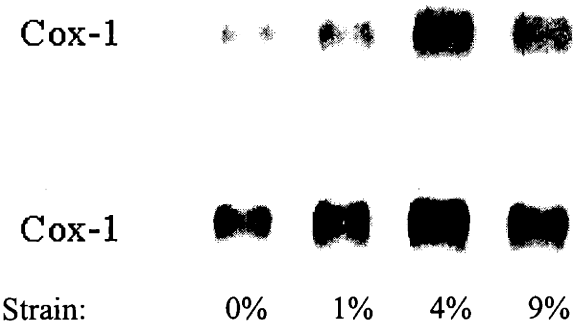

Figure 29. Effects of different strains on cyclooxygenase-1 response. The response at 1% is very weak, compared to the response at 4%. This result supports the notion that cells are sensitive to large deformations, although it does not exclude the effects of force.

3.6 Octopolar Magnetic Trap Results: Cell Deformation Assays

3.6.1 Methods for Cell Deformation

There are many ways that the octopolar magnetic trap could be used to probe the physical response of the cells. The method employed in this study took full advantage of the design of the trap to work in conjuction with the two-photon microscope.

HASMCs were plated on glass coverslips, and allowed to ingest 0.5 μm diameter fibronectin coated polystyrene beads (Duke Scientific) overnight. On the day of the experiment, magnetic beads (4.5 μm, fibronectin coated) were placed on the cells and allowed to attach. The specimen was then placed on the two-photon microscope stage inside the magnetic trap. A section of the specimen was identified which contained a cell with an attached magnetic bead, and at least two polystyrene beads attached to the coverslip but not on the actual cell itself. The polystyrene beads serve as markers, and are used to eliminate the residual specimen stage movement (approximately 100 nm) during activation of the magnetic transducer. A three-dimensional image stack was then acquired using the two-photon microscope, with a z-spacing of 0.14 μm and a x-y resolution of 512 by 512 pixels, with each pixel representing about 0.15 microns. This set of data is called the "before" images. The magnetic trap was then turned on and a one-minute delay was instituted to allow the section to stabilize. The forces used in this study ranged from 50 to 120 pN. The three-dimensional stack was then recorded again, called the "after" images. Each data block took approximately 20 minutes to complete. All images were sampled at a finer scale than diffraction limited resolutions. The image blocks were post-

processed with a blind deconvolution program (AutoDeblur, Autoquant, Watervliet, New York) to further improve image resolution.

3.6.2 Post-Processing Deformation Data

Using endocytosed polystyrene beads as markers, any solid body displacement and rotation of the coverslip can be eliminated by matching the polystyrene beads' positions in the "before" and "after" image stacks. Then, a cross-correlation program (Insight, TSI, St. Paul, MN) was used to determine local displacements. The program takes an interrogation region, a subsection of the "before" images, 128 pixels by 128 pixels, and calculates a cross-correlation factor with respect to the "after" images. By shifting the interrogation region in the x and y directions, the cross-correlation function is obtained for all possible displacements. The x and y shifts which maximize the cross-correlation function corresponds to the displacement. By choosing many interrogation regions over the entire "before" picture, a map of the displacements is obtained. The images were also qualitatively analyzed for cell deformation by examining the acquired cell images.

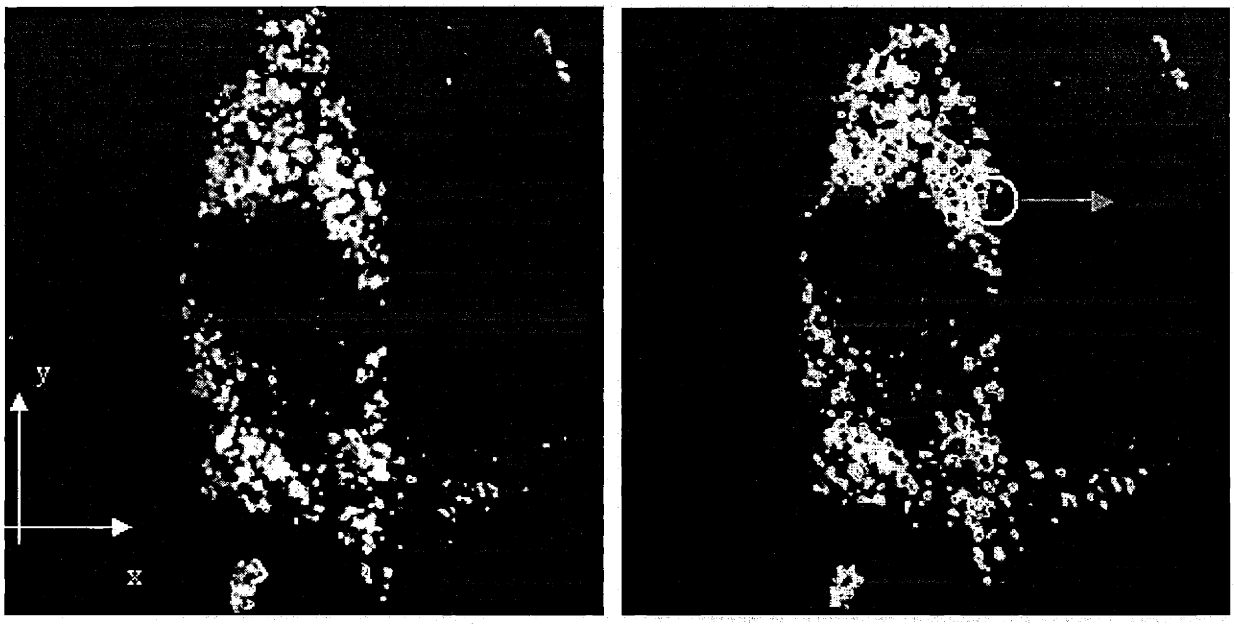

Figure 30. Low force (50 pN) results on a HASMC. The bead location is shown by the white circle on the right image, and the arrow indicates the direction of force.

Application of 50 pN is sufficient to show deformation in the cellular structure as determined by ingested beads (Figure 30). The cell structure shows an apparent stretching and rotation. Curiously, the stretching is almost perpendicular to the direction of the applied force. At larger forces (120 pN), the global stretching and rotation is even more evident, and the development of a large local deformation near the location of the magnetic bead becomes evident (Figure 31). The global deformation can be quantified using a cross-correlation algorithm, which yields displacement vectors based on analysis of an interrogation region 128 by 128 pixels (Figure 32). While the resolution of the vectors is not optimal, using this method allows the generation of a displacement map with subcellular resolution. The magnitudes of local cell deformation are quantified and can be used to calculate cell stretching and rotation. The vectors increase in size from the bottom of the image to the top (increasing y), indicating that the displacements are increasing in magnitude. In addition, the displacement vectors exhibit a non-uniform horizontal component, indicating that the cell has rotated.

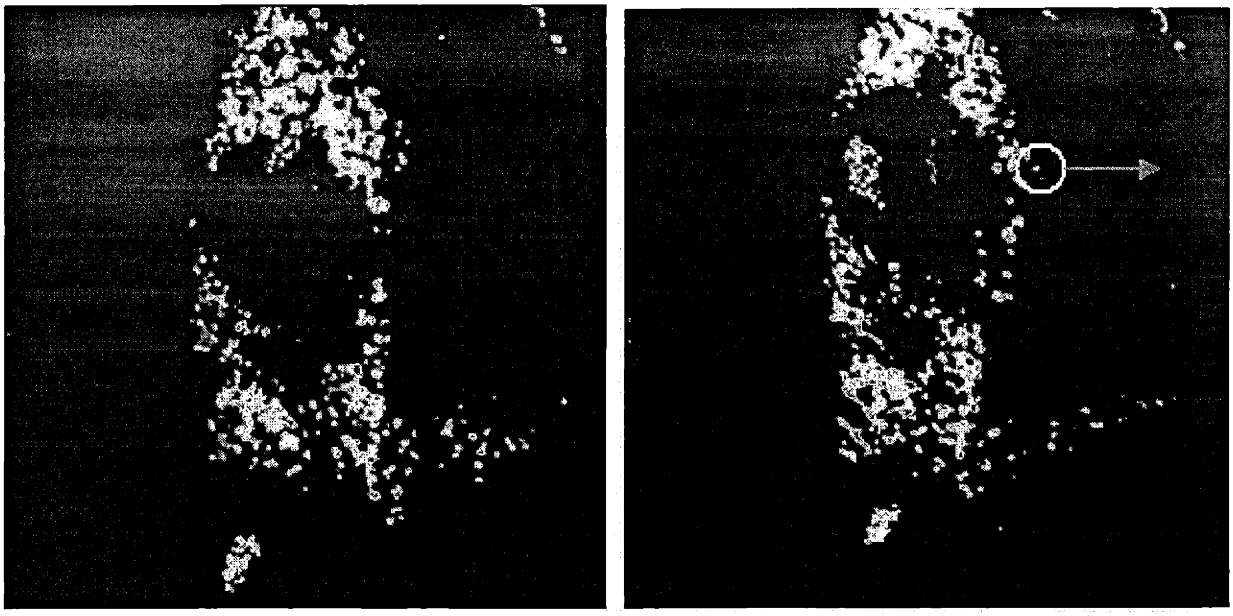

Figure 31. The application of high force (120 pN) on the same cell as shown in figure 29. Note the higher deformation and the apparent rotation of the cell clockwise as compared to the control on the left.

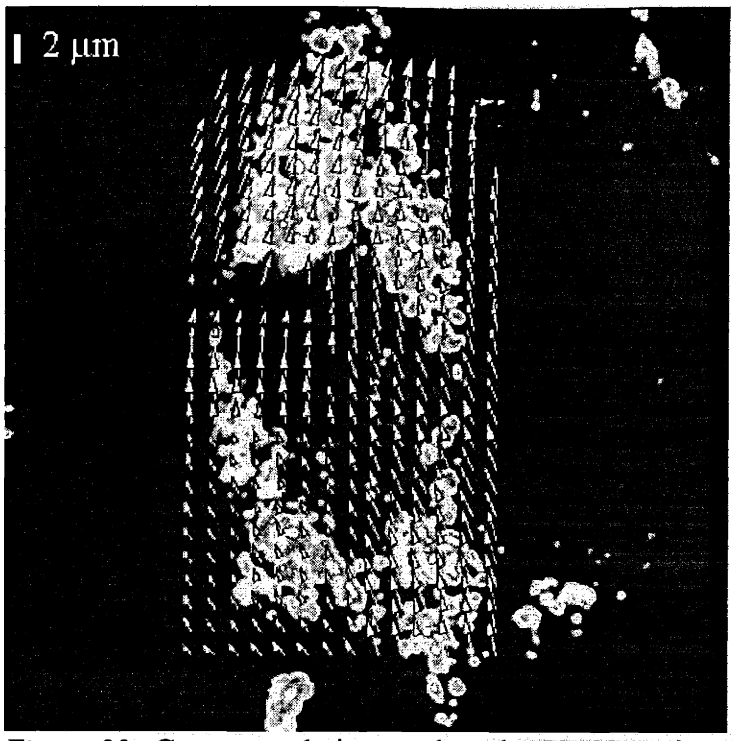

Figure 32. Cross-correlation used on the 50 pN section. Note the increase in the y-magnitude of the vectors, and the change in x-component from negative to positive as y increases. This indicates that the cell is stretching in the y-direction and rotating clockwise. The vectors are scaled by a factor of 2 in the TSI Insight program to generate this figure.

3.6.3 Controls For Remodeling and Vibrations

Over a period of 20-30 minutes required to acquire the data, it is possible that the cell has migrated or significantly remodeled itself even without any forces on the cell. In order to test this hypothesis, a "before" three-dimensional image block was acquired of another cell, and the sample holder was then gently tapped to create a global translation and rotation without actually stressing the cell, and the "after" image block was then acquired. The image-blocks were processed and show minimal or no displacements at all (Figure 33). While this data was taken at half the resolution of the previous data set, cross-correlation analysis shows that the displacement vectors in the non-stressed cell image are at about a factor of three smaller than those of the stressed cell, and these vectors are located predominantly off the cell itself.

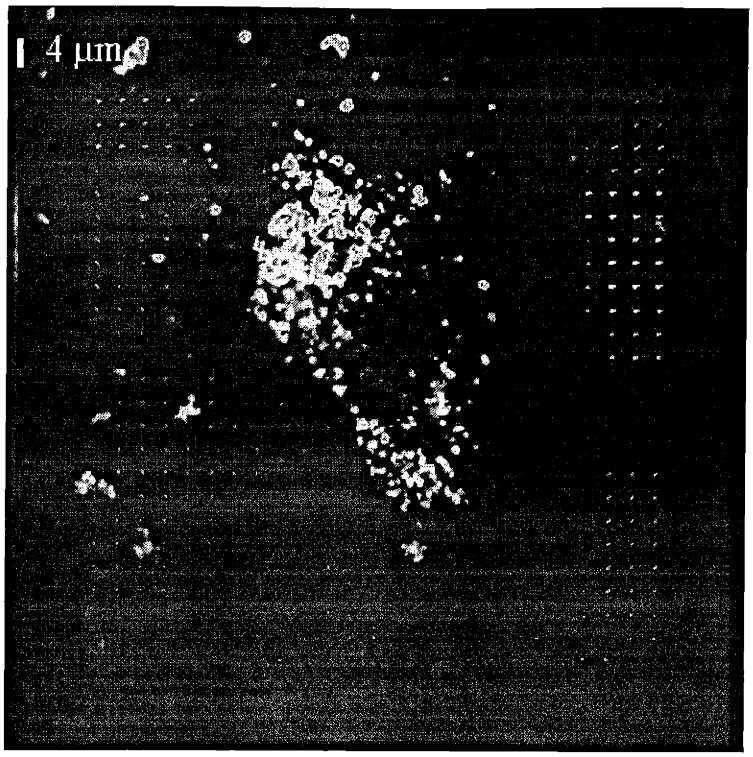

Figure 33. A cell with no bead, and no magnetic trapping, processed for displacement. Due to resolution differences, the vectors are half the size of Figure 31, but numerical analysis indicates that the vector sizes are small compared to that of the specimen with a magnetic bead and force. The vectors are scaled by a factor of 2 in the TSI Insight program to generate this figure as well, but this data was taken at a lower resolution than Figure 32.

A second test was performed where a cell with no magnetic beads attached was placed in the magnetic trap (called a "temperature control", a "before" data clock acquired, and the trap activated to produce 120 pN of force. The "after" data block was then acquired and compared to the before. Changes in cell shape and location was present, but less significant compared to that of a cell with a bead on it (Figure 34). These results suggest that without an applied force, the cell does not migrate or remodel to the same extent as under a mechanical stress. The magnetic field, vibrations from operating the trap, and the temperature effects from the trap do not result in a significant change in cell morphology.

Despite these controls, there are still other possibilities that could explain the deformation data. If the cell was in the process of remodeling, the fact that scanning was from a bottom-to-top direction may have resulted in an artifical shift that appears as a deformation. Even if this was the case, however, the amount of shifting is lower for control specimens when compared to cells with applied stresses.

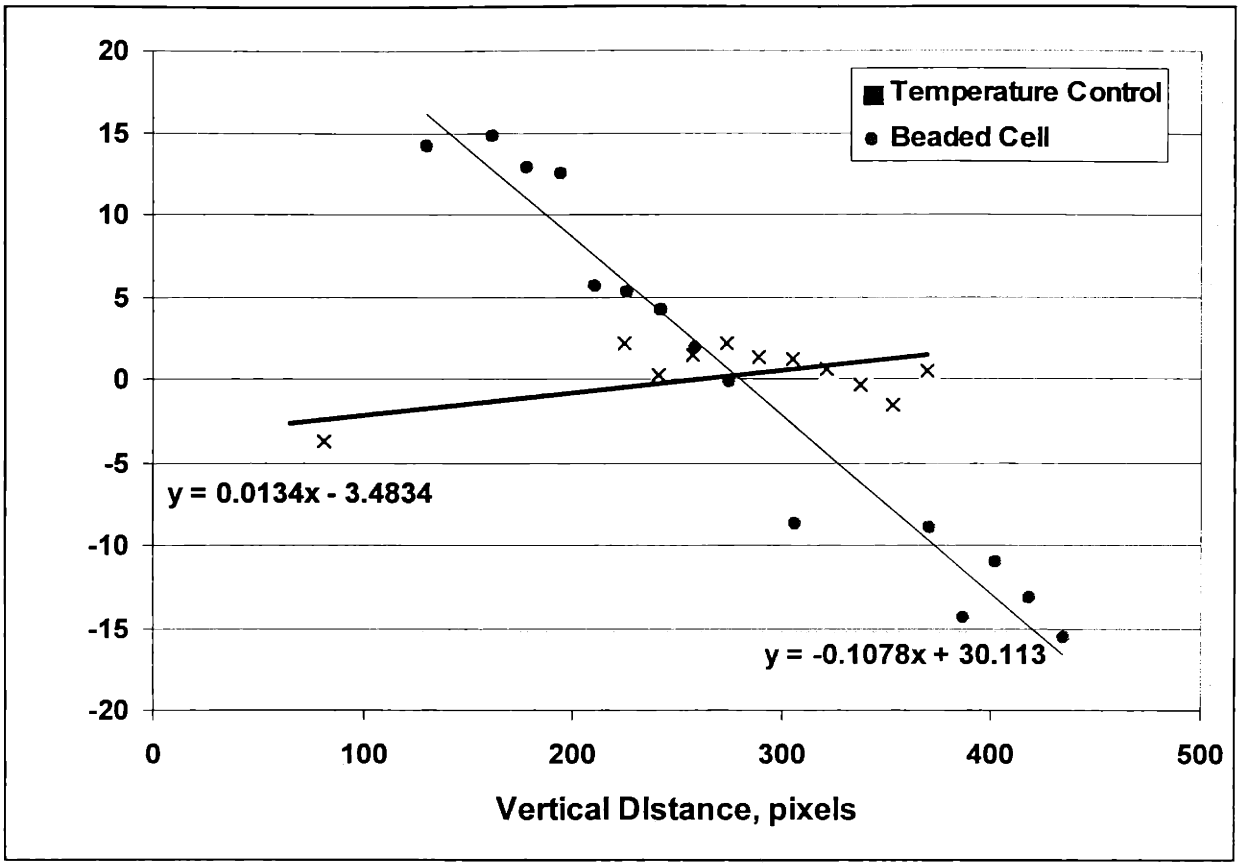

Figure 34. Plot of the normalized y-displacements of a cell without a bead (temperature control) and a cell with a single bead. Both cell data were taken at 120 pN, or about 1.25 V of driving current. Outliers were removed, especially invalid displacements and displacements near the nucleus. The displacements were averaged and then shifted so that the average is zero for the purposes of comparison. The cell with a bead on in has about a factor of 7 more stretch than the control cell, as calculated by using the slopes of the best fit lines. While the deformations are not likely to be linear in reality, the slopes are likely indicative of the extent of deformation.

3.6.4 Reconstruction of Data in a Different Plane

Since the images form a complete three-dimensional block of data, the deformation can be visualized from a different perspective. Images reconstructed in the vertical planes (cut-plane) show that the deformation is not limited to the surface (Figure 35). The largest deformations are somewhat limited to the upper half of the cell, but they pervade the cell to the nucleus. One possible artifact that can be noticed is the beads' tendency to line in vertical columns. This is not likely to be caused by a single bead due to the intermittent nature of some of the columns. It is not currently known why beads appear to line up in these columns.

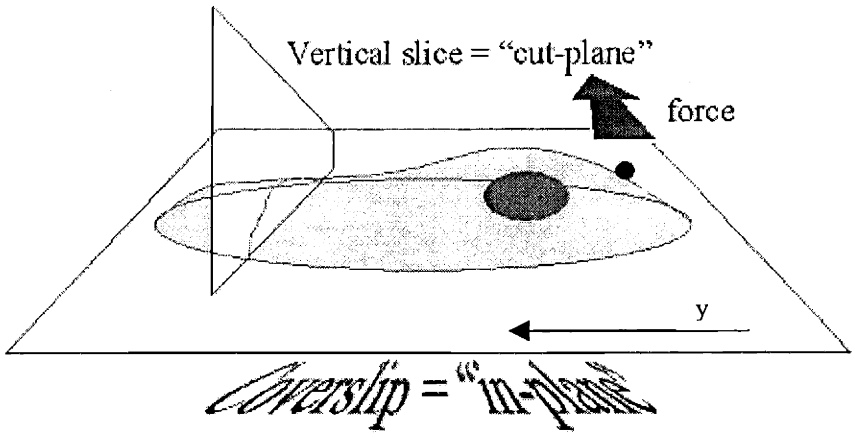

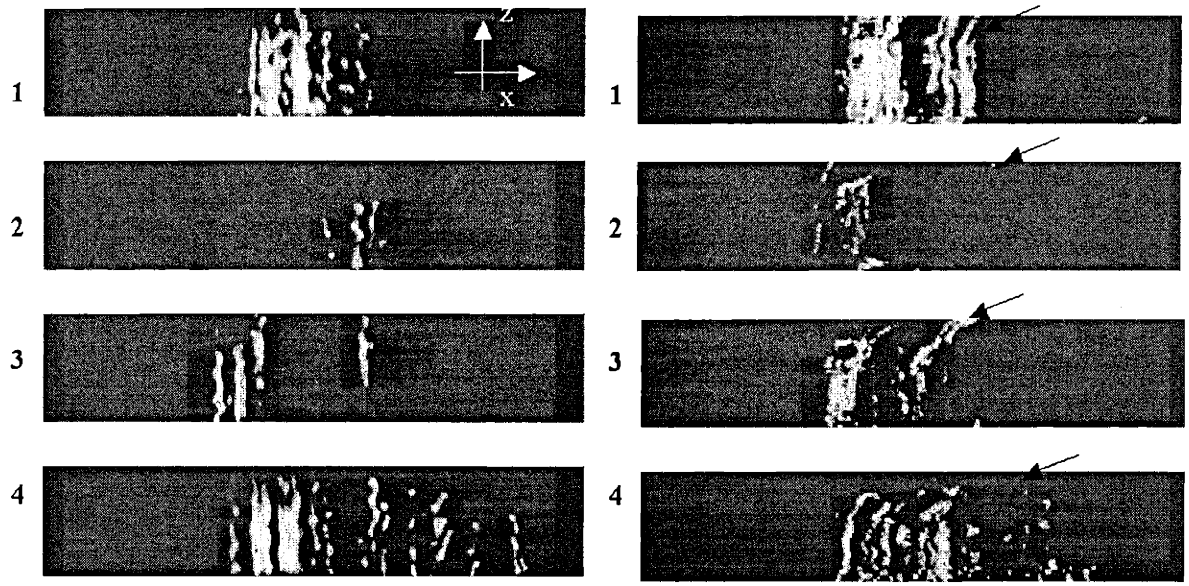

Figure 35. Vertical slices of a cell before and after stress is applied. These reconstructed two-photon images are taken from the same data set as used for Figure 30 (120 pN). The vertical direction is the z-axis, representing the axis parallel to gravitation. The top of the cells appears flat because the images were truncated. These images show slices at (1) 50, (2) 150, (3) 250, and (4) 350 pixels from the top of the image in figure xx. The cell deformation (indicated by arrows) is clearly in the direction of the applied stress, and while this deformation is mostly limited at the top half of the cell, it also clearly penetrates the cell to the nucleus.

3.6.5 Discussion of Octopolar Cell Deformation

Cells respond physically to mechanical forces, albeit in this experiment, several minutes elapsed between the application of the force and the assay. It is possible that the cell's response

was more of a long-term remodeling, and that the initial deformations caused by a purely material response of the cells were too small to be detected. In fact, experiments on HASMCs in real-time using a video camera and white light showed only marginal movement of the magnetic beads, and when polystyrene beads on the cell surface were tracked they rarely showed any displacement.

Despite the application of reasonably high forces (200 pN), then, very little strain can be seen, except at the medium- to long-term, which could be accounted for by cell remodeling and migration. This appears to contradict the results from other cell types, such as the results from Ingber (using a single pole trap at 180 pN on F9 embryonic carcinoma cells, and detecting 200 nm mean displacements (Alenghat and others 2000)). One possible explanation for this is that the HASMCs used in this experiment are physically stiffer than other cell types; that is, the elastic modulus or shear modulus is significantly higher than the modulus of the F9 cell, and thus, will result in greatly diminished strain upon the application of identical forces. In order to test this hypothesis, a new system capable of exerting much larger forces than 200 pN would be required. Due to spatial limitations and the optimization performed on the octopolar trap, it was unlikely that another uniform field magnetic trap could be constructed that would give significantly higher force. This is supported by the simulations, which showed that the magnetic trap pole tips and core were already at saturation.

To exert higher forces, but in a similar fashion to the octopolar magnetic trap, a single pole trap was adapted from the same poles used for the octopolar trap. This single pole trap was tested and was able to exert upwards of 10 nN of force, a fifty-fold increase in force levels. It was hypothesized that there is a large differences in cell moduli between cell types, which would explain the lack of observable deformation in the HASMCs despite the fact that other cells have been deformed with comparable or less stress. In order to test this hypothesis, the single pole trap was used to probe the physical response of three different cell types, using the same range of forces and the same cell model.

4.0 Single Pole Experiment :Cell Moduli Determination

4.1 Introduction: Techniques to Probe Single Cells

4.1.1 Magnetic Twisting Cytometry

While there is a wide variance in elastic moduli as reported from the literature (from one to 10^6 Pa), it is instructive to consider groups that have used one technique to examine different cell types. For example, Ingber et al has done multiple studies with the magnetic twisting cytometer (MTC) on various cell types (Ingber and others 1995; Lee and others 1998; Tagawa and others 1997; Yoshida and others 1996). The range of moduli ("stiffnesses") reported under similar loads varies from 0.8 Pa to 250 Pa, in response to varying stresses. These results were consistent with the predictions of the tensegrity model that the stiffnesses are linearly proportional to the stresses applied. The model was intended to help explain why a range of stiffnesses was reported even in the same experiment on the same cell. Interestingly, there was little variation in moduli at similar stresses among the different cell types used when probed with magnetic twisting cytometry, including bovine capillary endothelial cells, bovine pulmonary smooth muscle cells, feline cardiac myocytes and COS cells. These moduli span from less than 1 Pa to 100 Pa, with the highest value (human airway smooth muscle cells) being 250 Pa (Wang and others 2001). In one study, both bovine capillary endothelial cells and bovine pulmonary smooth muscle cells were plotted on the same graph, showing that the smooth muscle cells are about 10-20% stiffer than the endothelial cells (Wang and Ingber 1995).

There are problems with drawing conclusions from reviewing twisting cytometry, however. First, only a few of the studies actually looked at the stiffness with different mechanical loads. In these cases, the emphasis was on determining whether the stiffness is a (linear) function of applied stress, and not on whether the calculated stiffness is a good representative of how difficult it is to deform the cells. That is, the emphasis is on relative changes in modulus rather than the absolute value of the modulus itself. In addition, there are some inherent limitations of magnetic twisting cytometry. For instance, there is the possibility that the magnetic beads' attachments will vary, leading to changes in bead movement based solely on rolling. There is also a study that indicates that the technique used for calculating stiffnesses in MTC used by Ingber's group is incomplete, due to the fact that the stress the bead applies to a cell is a function of the angle that the bead rotates, and this was not apparently taken

into account (Butler and Kelly 1998). Interestingly, when the rotation was taken into account, the fact that stiffness is a linear function of stress is no longer as clear; in fact it is reported that the increase in stiffness actually decreases with stress (Potard and others 1997).

4.1.2 Other Techniques to Probe Single Cells

Other techniques have been used to determine stiffnesses, or moduli of various cell types. These techniques often use different methods for calculating stiffness compared to MTC and to each other. The techniques are briefly reviewed here together, since no technique has had as extensive study on different cell types by the same group as MTC. Atomic force microscopy (AFM) uses a small conical probe tip to press on cells (Braet F 1998; Hofmann and others 1997; Shroff and others 1995). By calibrating the cantilever and measuring it's deflection, either a map of the cell surface or the force-displacement relationships can be obtained. One advantage to using AFM is that the location of the cell being probed can be controlled precisely. Cell poking uses an indenter similar to AFM, but the probe is not as fine or precisely controlled (Petersen and others 1982). Microplate manipulation moves two parallel plates closer together or farther apart, with the cell adhered on both sides (Thoumine and Ott 1997). By looking at the cell's aspect ratio and measuring the force required to compress or stretch the cell, it is possible to determine mechanical properties of the cells. Finally, micropipette aspiration uses a hollow pipette to partially vacuum a cell or a portion of a cell into the interior of the pipette (Sato and others 1996). The pressure difference across the cell and the amount of the cell that is aspirated are related to the mechanical properties of the cells.

All of these techniques (and MTC) have been used to examine cells, but they have different limitations. Micropipette aspiration and microplate manipulation requires the cells to be suspended, so normally adherent cells cannot be studied in their natural environment. Microplate manipulation permits a cell to attach to a substrate, but only for a short period of time, so that the cell likely does not have a chance to spread. AFM, because of the small size of the probe tip, is very susceptible to heterogeneities in cells and is sometimes injurious to cells. Cell poking has not been used recently with the advent of AFM. None of these techniques, including MTC, allow for easy acquisition of a strain field away from the site of the probe.

4.1.3 Single-Pole Magnetic Trapping

Magnetic and optical trapping are techniques that apply a force on a cell via a bead attached to a cell. These techniques have many advantages. First, the use of different bead diameters allows the force to be applied to regions of different areas, resulting in a wide range of stresses that can be applied, although this is somewhat limited by the fact that force decreases with decreasing bead diameter. Second, the bead can be coated with a large variety of adhesion molecules, such as fibronectin, laminin, and antibodies to cell surface receptors. This allows the stresses to be applied to specific targets on the cell surface, which is useful for studying the involvement of certain receptors to signaling. Finally, the magnetic trap applies a precise force of any desired waveform while the optical trap applies a precise displacement, insofar as the maximum force exerted by the laser is not exceeded. Thus magnetic and optical trapping are the methods of choice for attempting to determine the elastic modulus of various types of cells. Optical trapping, however, is generally limited in forces to under 100 pN, and furthermore, is a strain-controlled stimulus if feedback is not applied. Magnetic trapping can generate forces in the range from 10 pN to over 10 nN (10^{-9} N = 1 nanoNewton), permits force control and temperature control (for the single pole trap). In contrast to magnetic twisting cytometry, the force applied on a bead with single pole trapping is well-characterized and does not change significantly if the bead does not move more than a few diameters. In addition, the application of a linear force results in a deformation across the cell that can be mapped and analyzed more readily than that resulting from a twist. Thus, single pole magnetic trapping is one of the best ways to probe the physical behavior of cells in response to mechanical forces.

4.2 The Single Pole Magnetic Trap

The single pole magnetic trap was used for the high force experiments. The advantages of the single pole trap are that it can generate much higher forces than the octopolar trap, the geometry of the single pole trap is simple, so that there is more room to maneuver and to add in the Bioptechs temperature-controlled stage, and the operation is more straightforward, since any current running through the coils of the pole will generate a magnetic field. The main disadvantage of a single pole trap is that the force is a function of the distance from the pole (or unipole), which means that calibrations need to be done more carefully and the bead-tip distance needs to be recorded along with any other data. However, since the force generated by a single

pole decreases rapidly away from the tip, this variance in force has the additional benefit that multiple experiments can be done on the same sample, since the stress applied to one region is limited in range.

The single pole trap consisted of a pole wrapped 550 times with copper wire (Figure 36).

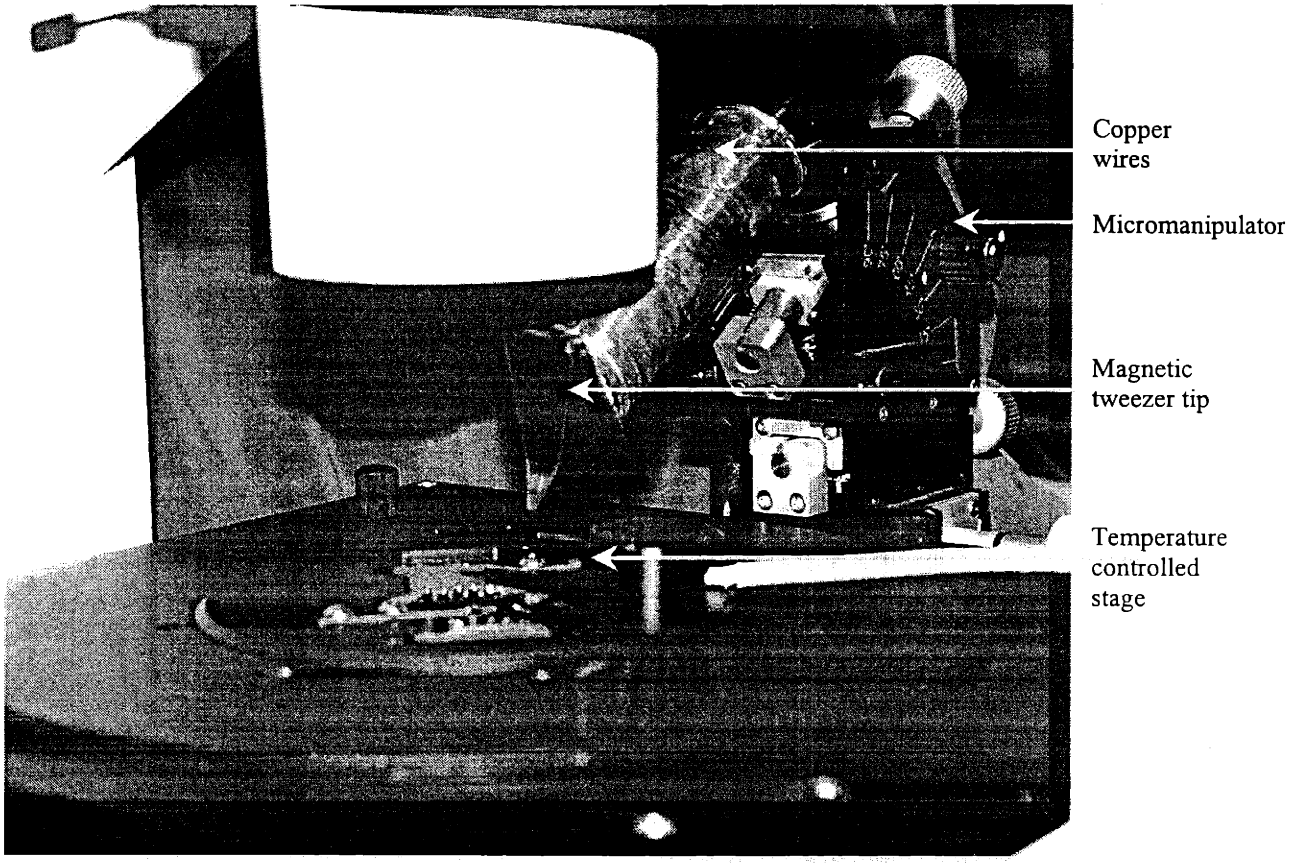

Figure 36. Photograph of the unipolar setup, showing the magnetic pole, Bioptechs temperature controlled stage, and the micromanipulator for positioning the pole.

The wire and geometry of the tip was identical to the poles used for the octopolar trap. The pole was placed in a 5 degree-of-freedom micromanipulator (MX110R, SD Instruments, OR) so that spatial adjustments can be made if necessary. Calibration was performed using a high viscosity fluid, polysiloxane, with a viscosity of 12,500 centistokes. Bead tracking was performed the same way as for the octopolar trap, but the bead was tracked through its entire range of motion, since the force, and thus the bead velocity, was constantly changing. A Matlab (Mathworks, Natcik, MA) program was written to convert the particle positions into a force.

Control of the magnetic trap is via the same program as for the octopolar trap. A RAID (redundant array of independent drives) controller on Stripe (0) with two 7200 RPM 60 GB hard

drives (IBM, Armonk, NY) was used to take 30 frames per second movies (as avi files = audio video interleave) of the cell bead motions in order to track many beads simultaneously. Matlab programs were written in order to track the beads' motions through the movie and to yield bead displacements as a function of time (Appendix B).

4.3 Single Pole Trap Characterization

The single pole trap was calibrated in a similar manner to the octopolar trap. A sample calibration curve is shown in figure 37. After the bead data is acquired, the Matlab program takes the instantaneous displacement curve, averages the data over 5 points (two before the data point, the data point, and two after the data point), then uses Stokes' formula to calculate the force.

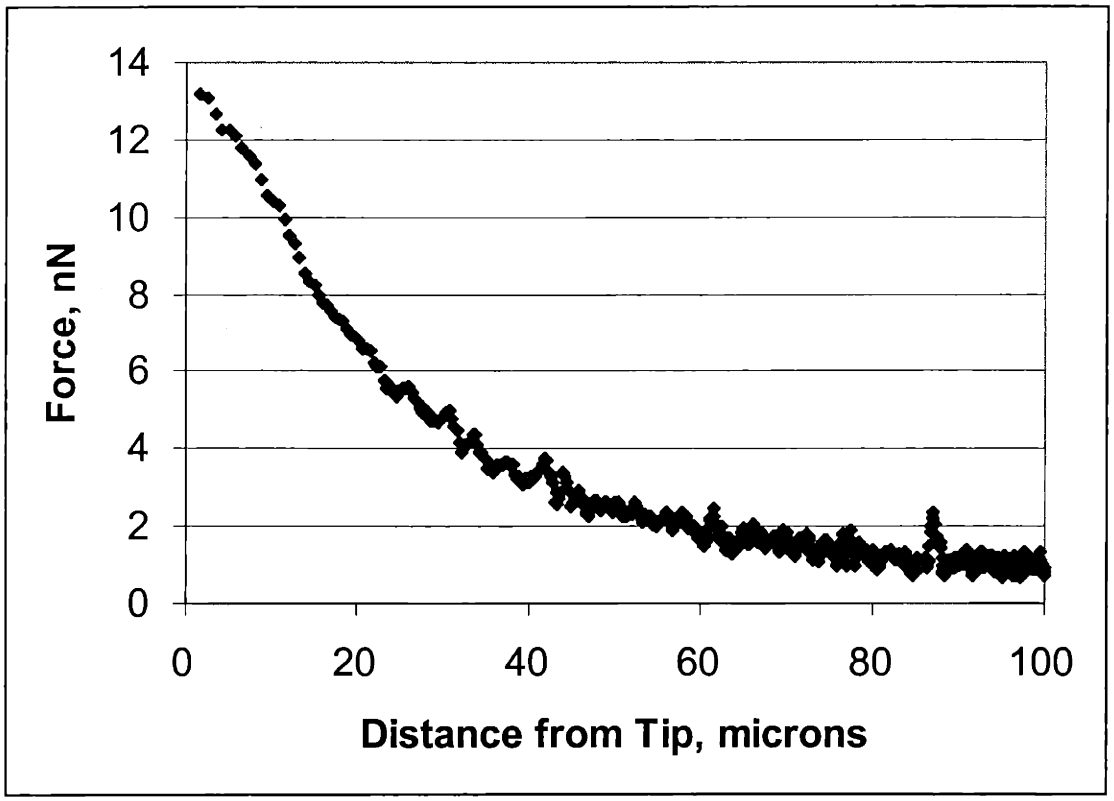

Figure 37. Sample calibration curve. This plot represents the instantaneous, partially smoothed force plot for a Dynal bead at 1 V of force driving the single pole (1 volt drives about 1/5 amps through this design).

This procedure is repeated for 5 beads at four different voltage levels (0.5, 1, 1.5, and 2 V driving the pole). The calibration curves for each voltage level are then averaged in intervals of

5 microns away from the magnetic pole tip. Figure 38 shows the mean force in the intervals for each voltage level.

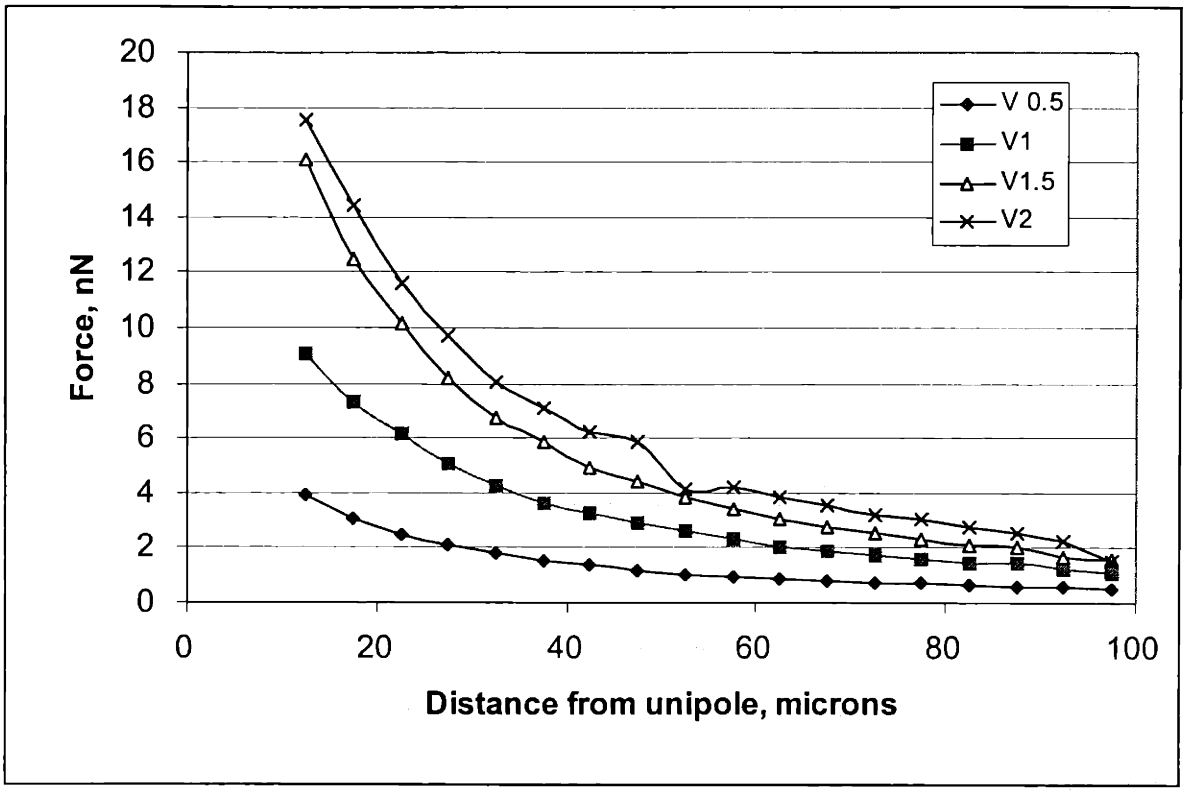

Figure 38. Calibration curves for the pole, at 0.5, 1, 1.5 and 2 V. The 2 V curve is very close to the 1.5 V curve, indicating that 2V is in saturation. The distance represented by the x-axis is from the tip of the pole.

4.4 Cell Studies

4.4.1 Experimental Methods

Cells were plated on Bioptechs gaskets with FN coating and allowed at least one day to attach and spread. On the day of the experiment, 1-5 μL of the 2.6 μm polystyrene beads (at 1%) with passively adsorbed FN were placed in the gaskets and allowed to attach to the cells for 2.5-3 hours at 37°C in a cell culture incubator. One hour before the start of the experiment, 0.5-1 μl of the 4.5 μm magnetic beads ($4*10^8$ beads/ml), coated with FN, were placed in the gaskets and allowed to attach. The beads (both types) were sonicated for about 2-3 minutes in a sonicator bath, to break up bead clusters. The actual concentration of the FN beads was lower than the given concentration since the clusters that remained were allowed to precipitate and not used for the experiment.

After the beads attached, the media was removed, and the gasket was washed once with PBS with calcium and magnesium to remove unbound beads, and then placed in PBS with calcium and magnesium for the experiment. The gasket was placed on the temperature controlled microscope stage. A video camera (DAGE-MTI 100, Michigan City, IN) was used to acquire movies. The specimen was observed with a 63x water-immersion Achroplan objective (Zeiss, Thornwood, NY) with a conversion factor of 0.228 microns per every pixel. The movies were acquired at a rate of 30 frames per second by the RAID controllers.

The single pole magnetic trap was positioned to appear in the field of acquisition. The tip was moved until it just touched the gasket, which was determined by noting when the specimen's focus started changing. Then, a movie was taken with the pole off for 3 seconds and on for 3 seconds, repeated once (for a total of about 12 seconds). Movies were taken for a single area at 0.5, 1, 1.5 and 2 V, and five areas were acquired, for a total of 20 movies. The movies were decomposed into component images (sample image in figure 39), and a Matlab program was used to track the magnetic beads and the surrounding polystyrene beads as a function of time. Other Matlab routines were written to calculate the force exerted on the magnetic bead (since the distance from the magnetic trap tip to the bead can be determined) as well as the relative angle and distance from the magnetic bead to a tracked polystyrene bead.

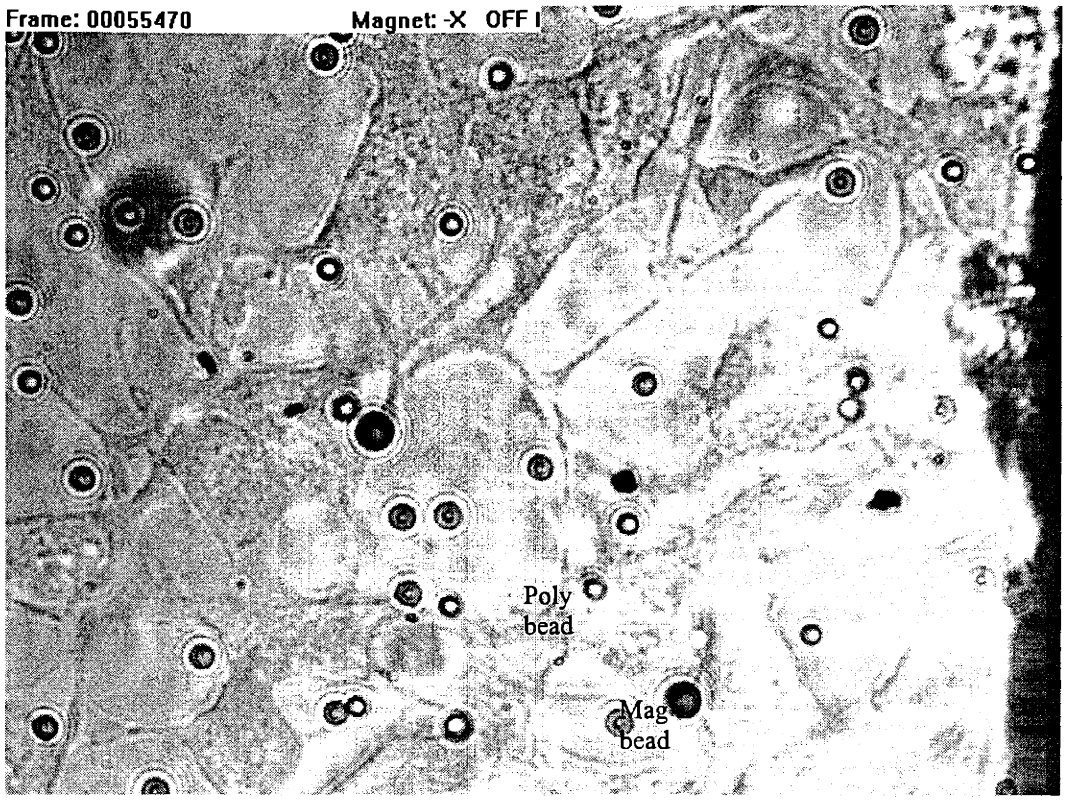

Figure 39. Sample image from the movie data acquired for 293A cells. The dark shadow at the right is the tip of the magnetic trap. The larger beads are the magnetic beads, and the smaller ones are the polystyrene beads.

4.4.2 Cell Model and Analysis

The data from the experiments yields the displacement field around the magnetic bead. In order to turn this information into a cell modulus, a model is required. A useful model for magnetic trapping comes from Boulbitch (Boulbitch 1999). Briefly, the cell's membrane and underlying cytoskeleton ("cortex" components) are treated as a thin elastic continuum plate with homogeneous properties. This cortex is then linked to the rest of the cell and the cell substrate by a series of prestressed and unstressed fibers, which collectively serve to add an additional restoring term to the plate equations. Once the restoring term is added (similar to a spring), the applied force is treated as a spatial impulse force (representing a small area of applied force relative to the size of the cell), and a Fourier transform is used to obtain the solution - the displacements over the cell membrane. This solution to the equation of mechanical equilibrium is:

$$u_x(r) = \frac{F_0}{2\pi\mu^*}\left\{\begin{array}{l}\frac{1}{2}K_0(\kappa r) + \frac{1-\sigma}{4}K_0(\kappa_1 r).....\\ .....-\cos 2\theta\left[\frac{K_1(\kappa r)}{\kappa r} - \sqrt{\frac{1-\sigma}{2}}\frac{K_1(\kappa_1 r)}{\kappa r} + \frac{1}{2}K_0(\kappa r) - \frac{1-\sigma}{4}K_0(\kappa_1 r)\right]\end{array}\right\}$$

where u_x is the x-displacement of the membrane (and subsequently, the polystyrene bead) at a distance r from the point of applied force (the magnetic bead), F_0 is the magnitude of the applied force, θ is the angle of the polystyrene bead with respect to the magnetic bead, K_0 and K_1 are the modified Bessel functions of the second kind of order 0 and 1, respectively, and κ and μ^* are parameters to be fit (Bausch and others 1998; Boulbitch 1999). The y-displacement was not used because those displacements are small, and thus will mostly be within instrumentation noise.

The x-displacements of the polystyrene beads, the angle and radius of the polystyrene bead with respect to the magnetic beads and the applied force were grouped for each cell type, then a Matlab program was used to minimize the least-squares error of x-displacements from the data to the displacement equation presented above using the Nelder-Mead method. The starting conditions for κ and μ^* were the final values determined by Sackmann for the reported fibroblast experiment (Bausch and others 1998). The minimization procedure was repeated ten times, with slight modifications of the starting conditions, and the negative or imaginary results were discarded. Generally, the final parameters were the same for each type of cell, regardless of the initial guess. Convergence was set to the default Matlab tolerances.

Once κ and μ^* are determined, the shear modulus of the cell composite membrane (or cell "envelope") can be approximated as:

$$\mu = \mu^*/h,$$

where h is the thickness of the composite membrane. The composite membrane consists of the lipid membrane and an underlying cortex. The cortex is composed of actin filaments and has been hypothesized to contribute to the rounding of cells in suspension (Zhelev and others 1994; Karl and others, 1999; Henson JH 1999). Using Sackmann's values of h=0.1 μm for the composite membrane, one can estimate the shear modulus of the cell composite membrane. Table 1 lists the values of κ and μ^* obtained through data analysis, as well as the estimated shear

moduli. The stiffness, or modulus, of the rest of the cell can be estimated from these two parameters (κ and μ^*) as well, and is done in section 4.7.

Cell	κ (1/m)	μ^* (Pa*m)	μ (Pa)
293A	$2.89*10^5$	$1.07*10^{-4}$	1,070
HASMC	$1.8*10^5$	$3.2*10^{-3}$	32,000
HSVEC	$4.7*10^5$	$2.2*10^{-4}$	2,200

Table 1. Least squares fit for the parameters for each cell type, with the displacement data of each cell type taken in aggregate.

4.4.3 Comparisons of Theory and Experiment

One complication from this analysis is that for the HASMCs and HSVECs, a significant portion of the data consisted of zero-displacement points, meaning that the displacement of the polystyrene beads is less than noise (noise being about 20-30 nm). The least-squares minimization routine was run a second time with all of the zero-point data removed, and Table 2 shows the results.

Cell	κ (1/m)	μ^* (Pa*m)	μ (Pa)
293A	$2.8*10^5$	$1.1*10^{-4}$	1,100
HASMC	$1.4*10^5$	$1.2*10^{-3}$	12,000
HSVEC	$2.1*10^5$	$5.4*10^{-4}$	5,400

Table 2. Least squares fit for the parameters for each cell type, with the zero-displacement data removed.

As the results indicate, the shear modulus does not change by more than a factor of 3 when the zero-displacement data removed. The true shear modulus of the cell, using this model, is likely between the values computed for both cases. It is possible that some of the zero-displacement data is not valid, due to bead detachment or endocytosis, but it is likely some of the zero-displacement data is valid and will change the modulus from the values displayed in Table 1. Valid zero-displacement points might result from beads that do move, but are below the resolution of the camera, beads that have been engulfed by the cells and thus do not represent the cell surface properties, or beads located on a folded portion of the lipid membrane. In the last case, the magnetic bead displacement would simply stretch out the membrane without significantly moving the polystyrene bead. However, the actual explanation for these data is not yet known.

An unexpected result in eliminating the zero-displacement data is that the HSVECs (and to a lesser extent, 293 cells) appeared to become stiffer with the removal of the data that one would expect to contribute to a stiffer result. This result is explained by the fact that the shape of the curve (as determined by κ) changes in addition to the stiffness. Thus, while the average displacement for a given force level may increase when the zero-displacement points are removed, the change of the shape of the displacement curve away from the magnetic bead results in an increased stiffness. This partially highlights the limitation of the model to take into account the zero-displacement data as true zero-displacement data (as opposed to data that, because of inherent errors, appears zero). It is reasonable to say that the results obtained are only good for order of magnitude approximations, and that in order to increase the precision of the measurements, a more robust model and more experiments would be required.

A comparison of the experimental and theoretical displacement fields is presented in figure 40 on the next few pages. The theoretical results (called "model" in the figures) are the x-displacements from the Sackman/Boulbitch model, using the κ and μ^* from the Matlab analysis, calculated at the same coordinates as the polystyrene beads in the experiments, with the magnetic bead located at the origin.

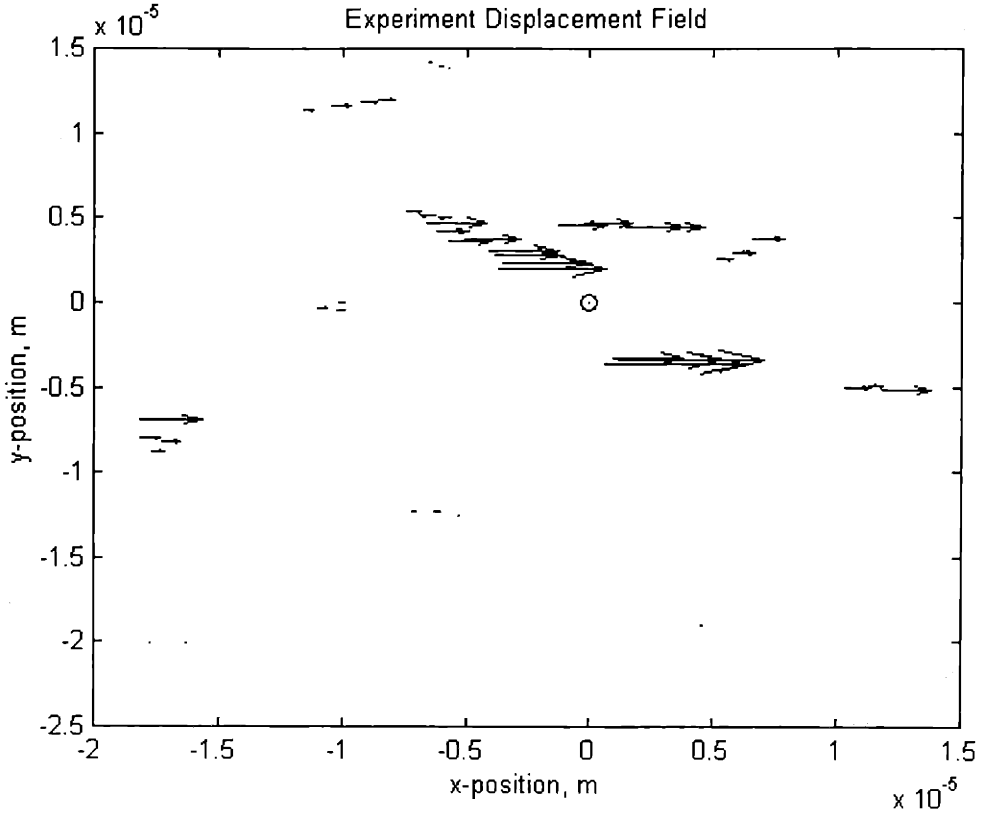
Experiment Displacement Field
x 10^-5
1.5
1
0.5
0
-0.5
-1
-1.5
-2
-2.5
y-position, m
-2
-1.5
-1
-0.5
0
0.5
1
1.5
x-position, m
x 10^-5

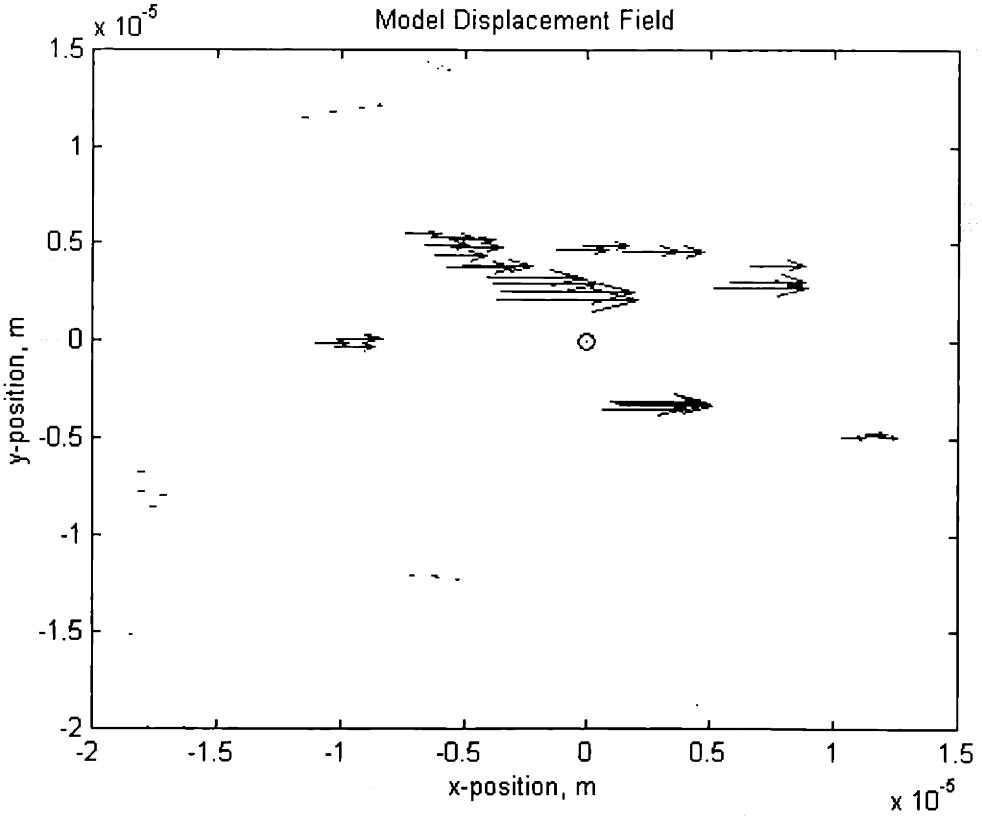
Model Displacement Field
x 10^-5
1.5
1
0.5
0
-0.5
-1
-1.5
-2
y-position, m
-2
-1.5
-1
-0.5
0
0.5
1
1.5
x-position, m
x 10^-5

293A cells

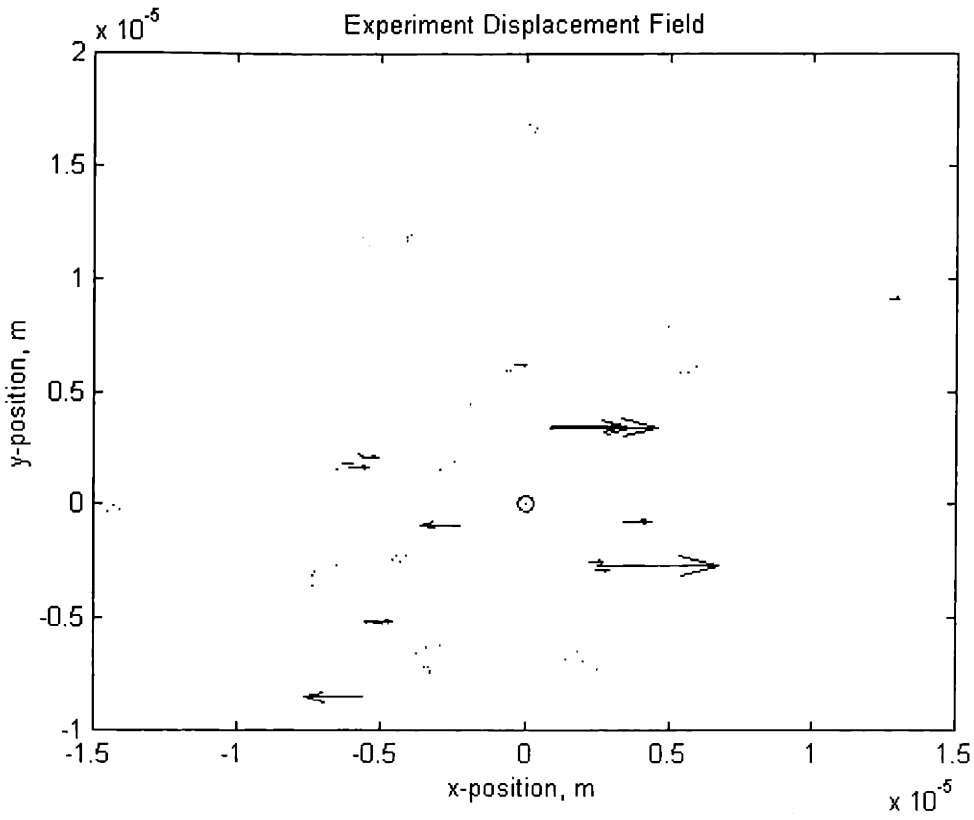
Experiment Displacement Field
x 10^-5
2
1.5
1
0.5
0
-0.5
-1
-1.5
-1
-0.5
0
0.5
1
1.5
y-position, m
x-position, m
x 10^-5

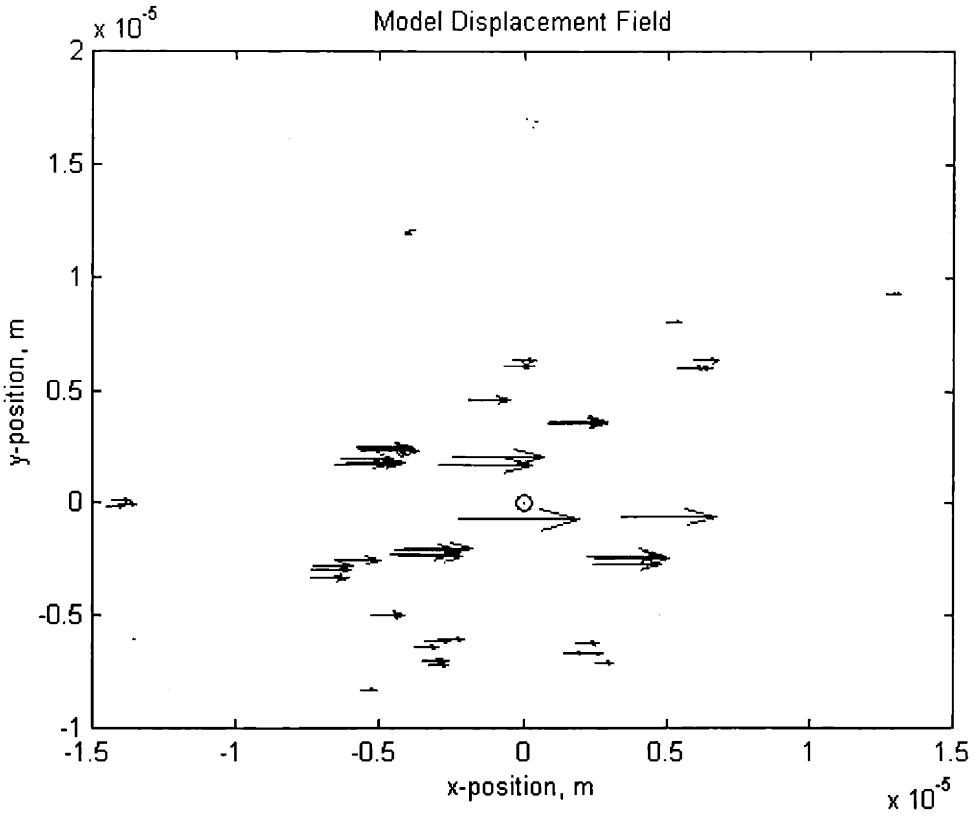
Model Displacement Field
x 10^-5
2
1.5
1
0.5
0
-0.5
-1
-1.5
-1
-0.5
0
0.5
1
1.5
y-position, m
x-position, m
x 10^-5

HASMC

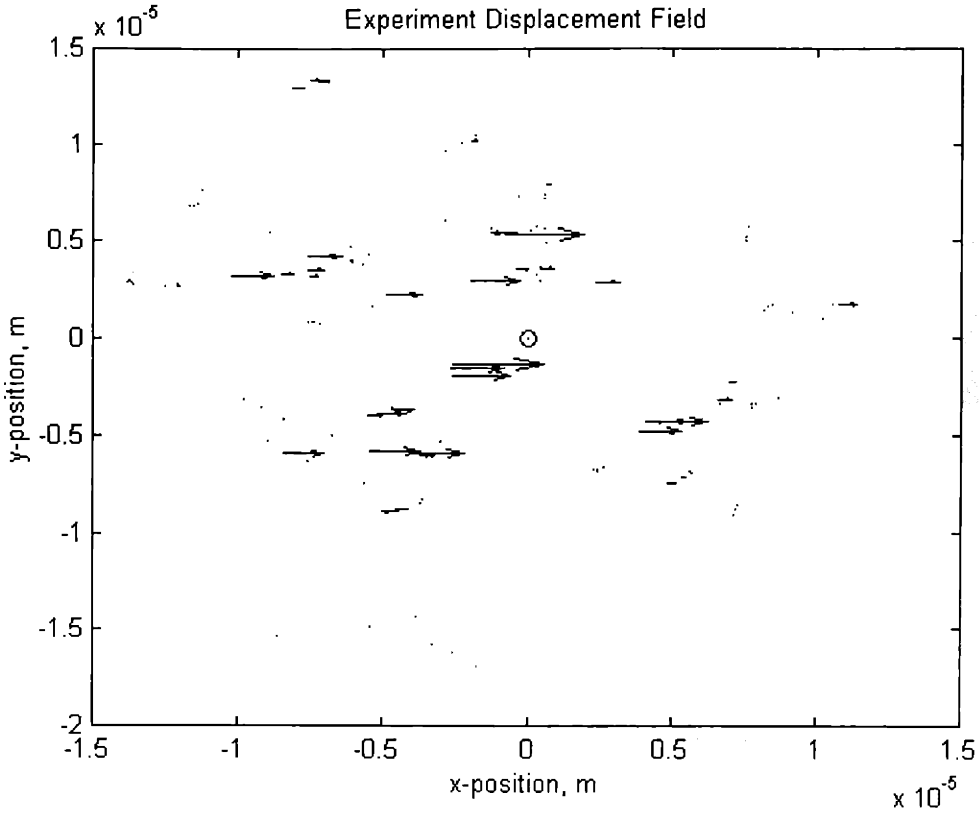
Experiment Displacement Field
x 10^-5
1.5
1
0.5
0
-0.5
-1
-1.5
-2
y-position, m
-1.5
-1
-0.5
0
0.5
1
1.5
x-position, m
x 10^-5

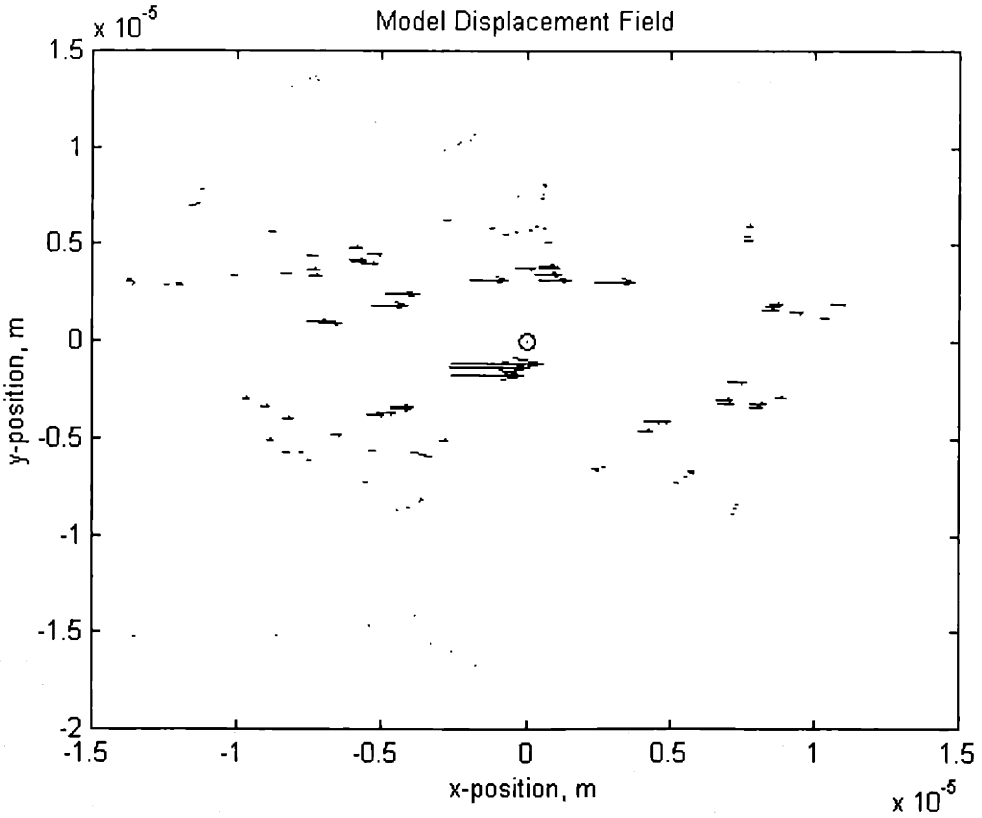
Model Displacement Field
x 10^-5
1.5
1
0.5
0
-0.5
-1
-1.5
-2
y-position, m
-1.5
-1
-0.5
0
0.5
1
1.5
x-position, m
x 10^-5

HSVEC

Figure 40. Experimental and theoretical displacement fields of the mechanical response of the polystyrene beads. The magnetic bead is located at the origin, denoted with an "o." The vectors are scaled to fit inside the plot. The top images of each set represent the experimental data, and the lower plot represents the displacements predicted by the theoretical model at the same locations relative to the magnetic bead.

The relative magnitudes of the vectors are similar, and the displacements tend to decrease with increasing radius. This tendency is shown more clearly in Figure 41, where the theta term (angle) is ignored. The spread of data is present partially because the same radius can lead to different displacements, depending on θ (theta, the angle the polystyrene bead is at relative to the magnetic bead).

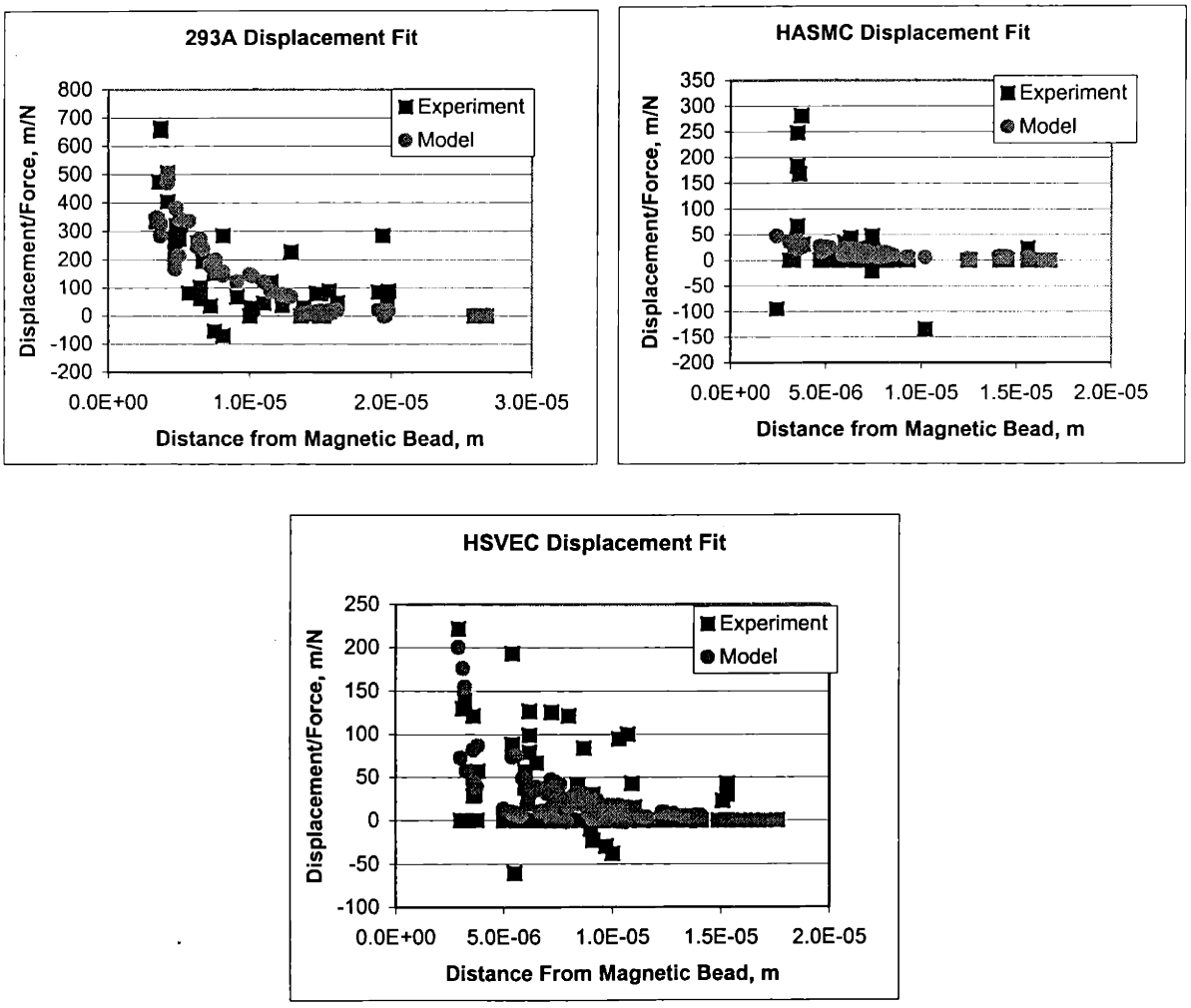

Figure 41. Plot of polystyrene bead displacement (normalized by the applied force) as a function of distance away from the magnetic bead. There is still a spread of data since the angle of the polystyrene bead to the magnetic bead is not accounted for.

4.5 Discussion of Cell Strain Experiments

The strain experiments performed with the single pole trap show that the shear moduli of the cells are within a factor of 30 of each other, when fitted to Boulbitch's model. This result is in contrast to the literature in aggregate, where cells may have as much as six orders of magnitude of variance in modulus. A tighter range in moduli can be obtained by considering only those studies using the same method on different cells. For example, both Ingber's studies and AFM studies span about span two orders of magnitude, although the actual range shares no overlap (Ingber: 1 to 250 Pa, AFM: 1 to 100 kPa). Thus, the real question is: which range of moduli is most representative of cells?

4.5.1 Results From Other Techniques

From the experiments that were performed and a critical review of the literature, it is very likely that the range of stiffnesses for almost all cells fall in the order of 1-10 kPa. Surprisingly, this number spans many cell types and even species (Bausch and others 1998; Braet F 1998; Hofmann and others 1997; Rotsch and others 1999; Thoumine and Ott 1997). Differences in protocol can explain some results. For example, in Figure 4 of the Introduction, it is shown that stiffnesses determined by AFM spans from 1 to 100 kPa. However, in the literature used in making this plot, there are only three calculated stiffnesses: 2 kPa (Braet F 1998), 10 kPa, and 100 kPa (Hofmann and others 1997) from three separate studies (the third study did not explicitly calculate stiffness). Furthermore, the 100 kPa result is derived from an experiment where an actin filament (stress fiber) was deliberately targeted and probed, yielding an inflated stiffness. That study, which also probed the cell without such targeting, also revealed that the modulus of the cell body is actually only about 10 kPa.

The other high stiffness from Figure 4 is that from Sackmann and Bausch's single pole study. Bausch et al actually found that the stiffness of the fibroblast that they used was in the range of 2-4 kPa (Bausch and others 1998). It is not clear why the Stamenovic represented the stiffness as being almost 100 kPa.

Thus, the main departure from the conclusion that cells are in the range of 1-10 kPa in stiffness is the result of many studies using magnetic twisting cytometry, which would seem to be softer than found with other techniques. It is possible to explain this discrepancy based on the specific technique used. For example, Ingber's use of MTC has been challenged in its use of

initial stress, as opposed to a strain-corrected stress. This is important because as the bead rotates, the twisting force decreases as the angular displacement of the bead increases. However, groups that have corrected for this factor failed to find significantly higher moduli (Maksym and others 2000; Potard and others 1997). The biggest factor contributing to lower modulus from using MTC is probably that the magnetic beads are prone to rolling when a torque or force is applied, because the bead is attached only on the bottom to the cell.

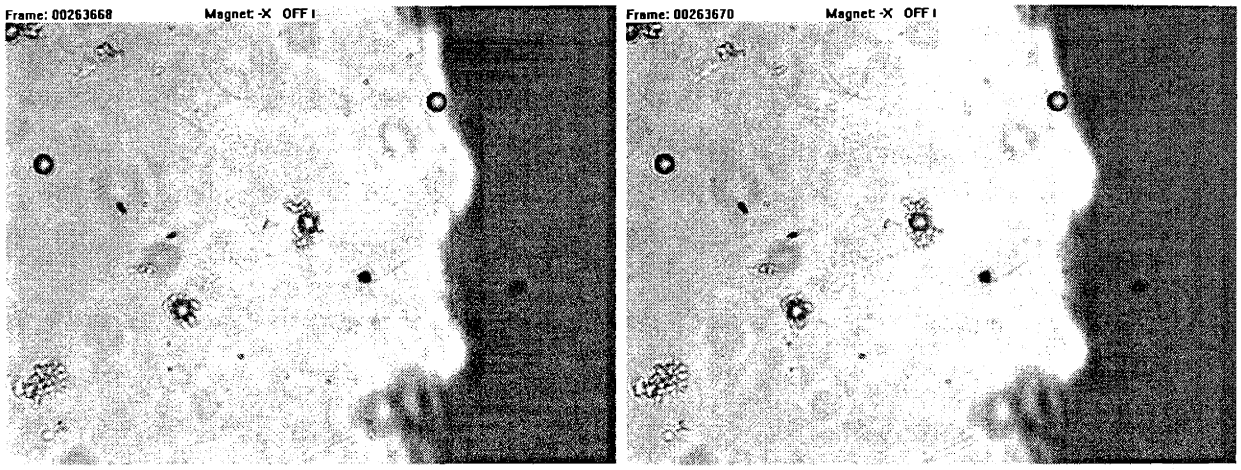

Figure 42. Images of bead rolling. Magnetic beads with attached polystyrene beads are bound to 293a cells. On the left, the magnetic trap is on, and on the right, the magnetic trap is off. Note the different distribution of the polystyrene beads around the magnetic beads, especially the one indicated by the arrow.

The phenomenon of bead rolling was captured using the single pole magnetic trap in movies (Figure 42). From the experiments done to calculate the moduli, substantial variations in rolling were observed. In some cases, the bead rolled about a non-central location, causing the bead to pivot. In other cases the bead was firmly stuck and did not roll significantly. Still other cases were observed where the bead rolled 90° (Figure 42). This conclusion is supported by examining the extremely large distribution in raw displacements of the magnetic beads on the same plot as the polystyrene beads (Figure 43). Large variations in bead behavior have also been seen by other groups using a single pole trap (Alenghat and others 2000).

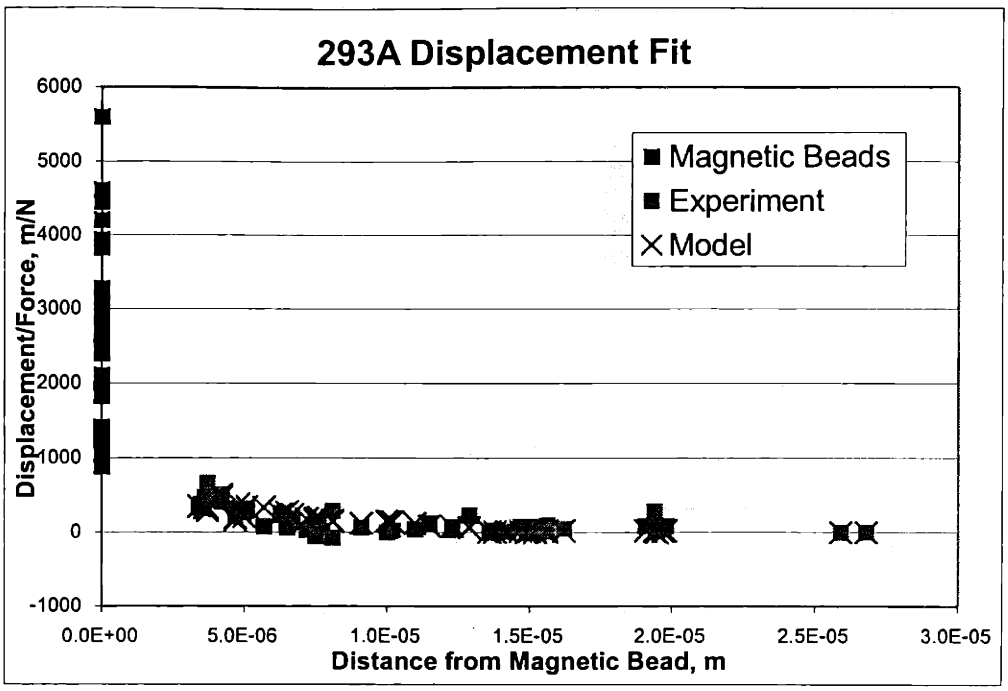

Figure 43. The same plot as Figure 40 (A), but with the magnetic bead displacement data shown as well. Both displacements have been normalized for force, so the remaining variation of the magnetic beads comes from physical differences (cell stiffness variation or bead rolling).

Bead rolling, then, represents a major reason why magnetic twisting cytometry and magnetic manipulation cannot be done reliably on magnetic beads alone. If the beads roll, then the apparent strain will seem larger than it really is, because the bead will not have had the full resistance of the material to oppose its motion. For example, if a perfectly attached bead moves 250 nm without rolling, while another bead rolls by 60°, the difference in total displacement will be different by a factor of 10, and subsequently, so will the stiffness.

It is reasonable to conclude that twisting cytometry tends to underestimate the magnitude of cell stiffnesses. To determine whether, when corrected for rolling, MTC will give estimates of stiffnesses in the range of 1-10 kPa, would require more experiments with the twisting cytometer and the development of either a cell twisting model or a way of measuring the extent of bead rolling, neither of which is trivial. The use of polystyrene beads is advantageous since there is little force acting on the polystyrene beads to cause it to roll, and subsequently, the motion is almost exclusively due to the translation of the local membrane.

Recently, a study using magnetic twisting cytometry concluded that there is a wide heterogeneity in bead behavior when twisting cytometry is performed. This study also found that in the range of 20-30 dyne/cm^2 (close to the stress for many of Ingber's studies) the

observed stiffness can be as much as a factor of four less than the true stiffness if 10% of the beads are unbound. It was determined that a possible reason for the apparent increase in stiffness with increasing stress is not necessarily due to the predictions of tensegrity, but rather a result of elimination of loosely bound beads, indicating that the higher values of stiffnesses are more likely representative of the cell modulus (Fabry 1999).

4.5.2 Actin Gel Study

Surprisingly, studies attempting to characterize the mechanical properties of actin gels also resulted in a range of moduli, despite the fact that these gels are much simpler when compared to cells. Various studies on actin preparations with different equipment yielded moduli that ranged from one to several thousand pascals. However, one group that duplicated the experiments found that the variation was likely due to the disruption of the actin network in the preparation and not the equipment (Janmey and others 1994). This result serves as a warning that in order to characterize the mechanical behavior of anything, even nonliving substances, requires careful consideration of the technique used as a whole, and not just the instrumentation alone.

4.6 Limitations and Uncertainties of the Analysis

4.6.1 Range of Moduli

There is an uncertainty associated with the use of magnetic trapping and the Sackmann/Boulbitch model. Since the cell is not a simple plate, and likely has viscous behavior, the estimates of stiffnesses should not be viewed as highly precise. There is the uncertainty associated with the measurements of about 20-30 nm from noise and about 200 nm from post-processing, mainly due to interference from shadows or passing beads. The latter is the main cause of the negative displacement data, which appears in less than 3% of the total data. If the data acquired in this study is combined with the data in the reviewed literature, it is reasonable to conclude both that most cells are on the order of 1-10 kPa in stiffness, and that there is yet insufficient data to increase the precision of this conclusion. In order to test the goodness-of-fit of the data, the Boulbitch model was recalculated for the 293A cells, using stiffnesses a factor of three higher and lower than that resulting from the optimization, and plotted on the same plot as

the experimental data. The data are bracketed very well by this range, and thus it is reasonable to say that the modulus is accurate to within a factor of 3 each way, or a factor of 10 (Figure 44.).

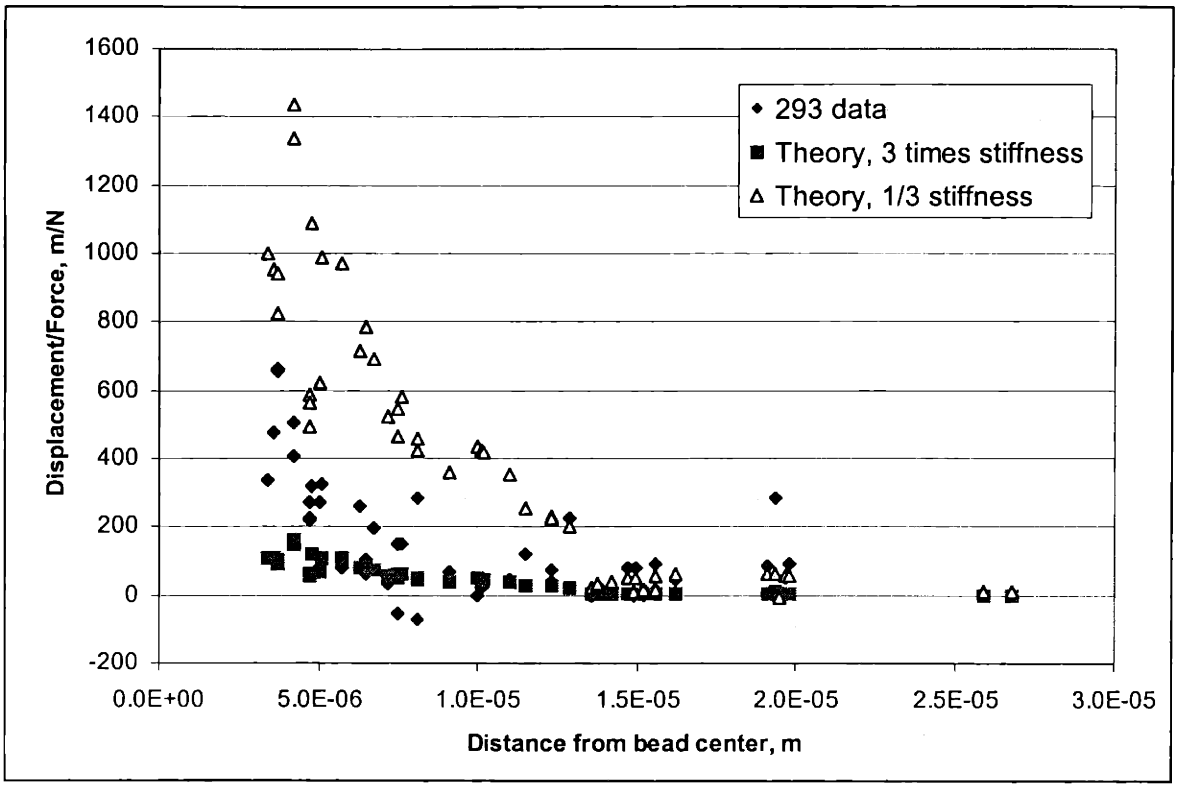

Figure 44. Experimental data for 293 cells plotted with stiffness at three times and a third of the stiffness calculated for the best fit. The great majority of the data lies between these two values, thus it is reasonable to conclude that there is no more than an order of magnitude variation in shear modulus.

It is also reasonable, although somewhat more tentative, to conclude from this study that HASMCs are stiffer than either the HSVECs or the 293A cells. The extent to which the HASMCs are stiffer is not well characterized and would require more repetitions of experiments to establish a more precise figure, but from this study one would expect that HASMCs are about 5 to 15 times stiffer than 293a cells, for example.

4.6.2 Other Factors and the Influence of Cell Height

Other limitations of the magnetic trapping technique and analysis can affect the results presented in this study. First, while there was some temperature control (by the Bioptechs system), there was no control over the evaporation of the buffer used to cover the cells when the experiment was in progress. Cells were exposed to room air for as much as thirty minutes.

Evaporation would mean that the concentration of salts would change with time. This is not likely to be a major factor, since at the end of the experiment when the cells were being discarded, usually 80% of the buffer was recovered. This problem can be alleviated in the future by using a constant perfusion of warmed buffer, which would also serve to keep the temperature more stable.

Second, it is possible that the differences in cell stiffnesses between the 293A cells and the HASMCs are even smaller. The cell with the lowest stiffness could also happen to have the largest cell height. A thicker cell will likely displace more, and the model used to determine the moduli did not explicitly take into account the cell height. While the model does in fact relate cell height to the parameters being fit, height was not explicitly used in the least-squares routine. Thus, some examination needs to be made regarding the sensitivity of the model to thickness.

According to the model (from Sackman),

$$\chi = k_{un} n_{un} + \frac{T n_{st}}{d_c},$$

where $\chi = \kappa^2 \mu^*$ is the coupling constant, n_{un} is the number density of unstressed cytoskeletal attachments to the actin cortex of the cell, with k_{un} representing their average spring constant, n_{st} is the number density of stress fibers under tension T, and d_c is the average height of the cell. Since we now have a relation between the two parameters we fit, we can perform a sensitivity analysis on them. If Tn_{st}/d_c is very small compared to $k_{un}n_{un}$, then there is no dependence on cell height at all, and the differences in stiffnesses that were found remain independent of height.

However, if Tn_{st}/d_c is very large compared to $k_{un}n_{un}$, then cell height is a major determinant in the relation between κ and μ^*. One way to compare the different cell types is to hold κ fixed, and vary d_c to see how sensitive μ^* is to cell height.

Two-photon fast-scanning is used for taking three-dimensional sections of cells, so that the height of cells can be determined. In this case, the cells were scanned from well above to well below the cell (in the z-direction). Then, the number of pixels above background was counted. This count was plotted as a function of z, and the cell height was taken as the Δz from when the count first reached 25% of the maximum pixel count to when it reached 25% a second time (Figure 45).

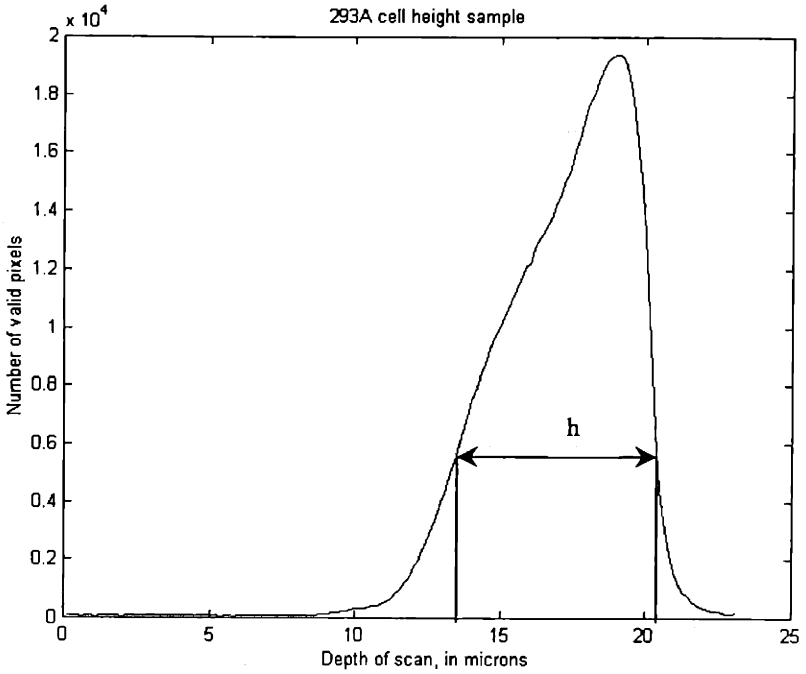

Figure 45. Sample cell height plot of a 293A cell section. The two vertical lines represent the 25% cut-off, and the cell height was calculated as h.

An experiment was done where all three cell types were scanned. The average heights of cells were determined using at least 20-30 cells for each type (table 3).

Cell	Average Height, μm	Standard deviation, μm
293A	8.5	2.8
HASMC	4.2	0.9
HSVEC	2.5	0.3

Table 3. The average heights of cells and the standard deviations of heights.

Using the height data gathered from the fast-scan, one finds that the cell moduli can approach a common value, but not to the point where they are identical (Table 4).

Cell Type	μ with 293a height, Pa	μ with HASMC height, Pa	μ with HSVEC height, Pa
293a	(1,070)	2,170	3,640
HASMC	16,000	(32,000)	54,000
HSVEC	650	1,300	(2,200)

Table 4. The moduli of the cells if the heights were taken into account at the highest sensitivity. The table shows how stiff a given cell type would be if it had the height of a different cell type. Thus, a 293a cell at the height of a HASMC would be 2,170 Pa stiffness instead of the 1,070 Pa that was determined from the deformation data.

The results indicate that the cell height can modify the results by a factor of two, but not much more than that. If we take both cell height and the zero-displacement data points into account, then, the difference in stiffness is reduced from a factor of ten to a factor of five. Thus, the conclusion that cell stiffnesses do not span six orders of magnitude is supported by this analysis.

A more sensitive geometrical parameter is the thickness of the cell cortex, or composite membrane. In this study, it was assumed that the cortex has a thickness of 100 nm. Clearly, it cannot be less than 10 nm, since that is the approximate thickness of the cell membrane alone. It is unlikely to be greater than 1 μm, given that scanning electron microscopy studies on neutrophils placed the estimates at between 0.05 and 0.1 μm. Thus, using 0.1 μm as an estimate of the cell cortex thickness is a reasonable first estimate.

4.6.3 Zero-Displacement Beads

Beads with zero-displacements are incompletely explained. As stated before, it is not clear whether they failed to move because the membrane under them did not move, whether they were somehow endocytosed by the cells (but even if some were, most should not have been, given the relatively short incubation time of the beads on the cells), or whether they were indirectly linked to the cell (say, via a tether or leash that wasn't already under some tension). The end analysis is not greatly affected by this, since the only major result is that the HASMC stiffness increases to 30 kPa when the zero-displacements are included, which is still within the hypothesized range. It may be possible to explain the zero-displacement data by postulating that the polystyrene beads are to some extent non-specifically bound to non-cytoskeletally linked proteins. Thus, when the cell starts deforming, the beads do not move noticeably because they are not linked to the major support structure. Evidence for the dissociation of the cytoskeletal

linked receptors and the non-cytoskeletal linked receptors exists, but has not yet been well established (Pommerenke and others 1996; Yoshida and others 1996).

4.6.4 Lack of Viscous Contributions

A more general concern is that the model used (originally based on thin plate analysis) is elastic and has no viscous terms in it at all. When the data were acquired, there was a three-second period for the bead motion to stabilize the beads, which may not be sufficient. Simpler models of cell membrane mechanics often have dashpots in parallel with other elements, indicating that if left long enough, the displacement would continuously increase, until the cell boundary is reached. This is not quite true, as shown in an experiment where the displacements

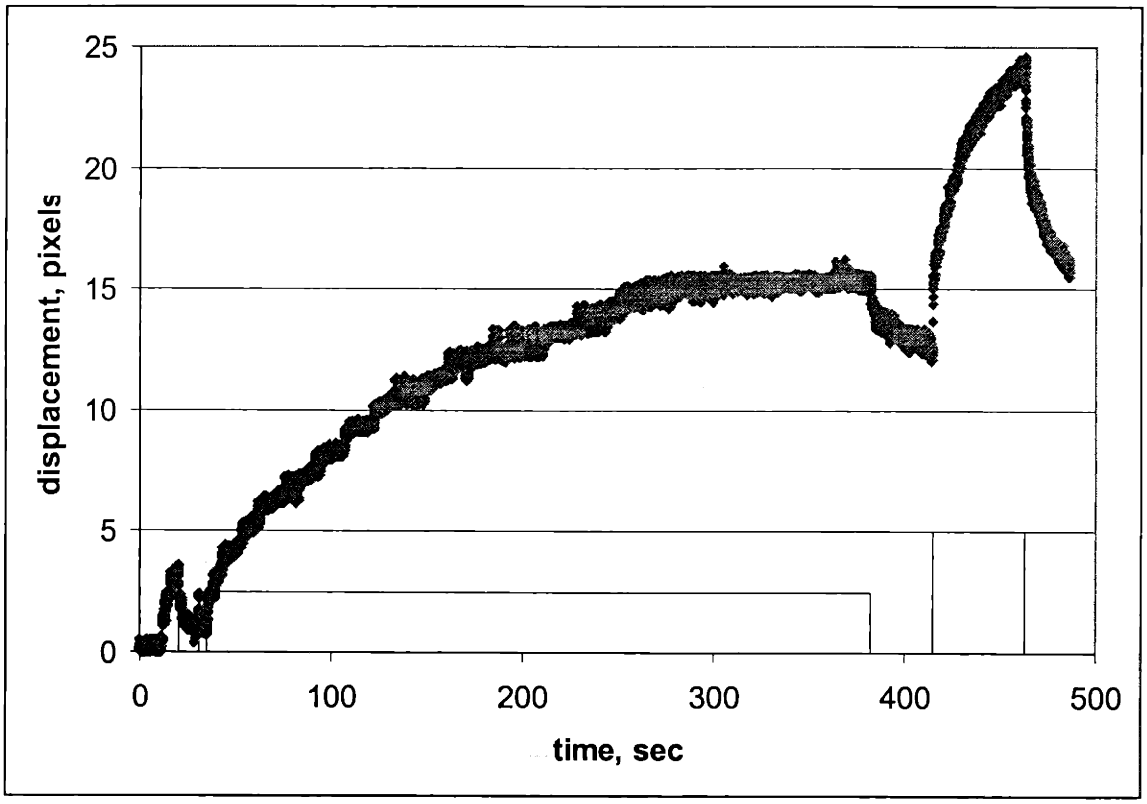

Figure 46. Plot of magnetic bead displacement as a function of time. The thin line represents the power to the magnetic trap, and the thick curve represents the displacement of the magnetic bead in pixels. Note the flattening of the bead displacement under sustained force, from 300 to almost 400 seconds. The bead is not at the limit of its displacement, as shown by the higher force at 410 seconds yielding an even higher displacement.

would gradually decrease until a near-equilibrium was attained (Figure 46). Upon the application of higher forces, the displacements would increase rapidly again, indicating that the bead had not reached the limits of its motion (and in fact, while observing this bead, it was noted that the bead did not approach the visible edge of the 293A cell). There is also concern that if a long wait period was implemented for the bead to reach equilibrium, remodeling could become prominent, which was a concern for the octopolar trap data.

4.7 Finite Element Modeling Comparison

The Sackman/Boulbitch model is linearly elastic, which is one inherent limitation in many, if not all, current cell models. This can be resolved by introducing more accurate models and will almost certainly entail the use of finite-element modeling to obtain the displacement fields. In contrast to the simplified plate-spring model used by Sackmann/Boulbitch, finite element models can model the cell in its geometric entirety, with three-dimensional elements for the cell components.

One preliminary finite element model (FEM) was created to analyze the displacement and stress fields of a cell, 5 μm thick and 10 μm thick, with a shear modulus of 100 Pa. A confluent cell monolayer was treated as a uniform cylinder with diameter 60 μm and a magnetic bead 4.5 μm in diameter at the center of the top of the cell. The cell membrane was treated as a shell element 6 nm thick with elastic properties chosed to match those of the lipid bilayer. The magnetic bead had a fixed 0.5 μm displacement exerted on its center, and had an attachment angle of 30° to the cell's surface. The computer solved for the displacement field (and stresses, etc.) throughout the cell, and the displacements on the cell's surface were then extracted. Interpolation was then performed (triangle based linear interpolation) to obtain the displacements at the locations where the experimental data were gathered. The displacements, normalized by the applied force, were plotted together. The displacement/force ratio from the FEM was adjusted to match those of the experiments as closely as possible. It was found that if one multiplied the displacement/force ratio of the 5 μm thick cell by 2, then the FEM data fit the experimental data, in terms of general trends and magnitudes. For the 10 μm thick cell, no adjustments were needed (Figure 47) (Karcher 2001). One unexpected result of the FEM is that as the cell's thickness increases, it required more force to displace the magnetic bead by the same 0.5 μm. However, the displacements of the membrane increase with increasing cell thickness.

From this analysis, one can conclude that the 293 cells (having an average thickness of 8 μm) from the experiment have a total cell modulus between 50 and 100 Pa. While this is different from the modulus of 1.1 kPa determined from the Boulbitch model, the moduli determined from the Boulbitch model represent the only the stiffness of the membrane and underlying cortex and not of the entire cell. The effective modulus of the finite element cell is very close to 100 Pa, since the cell body represents the significant portion of the cell. That is, the stiffness of the membrane and cortex, being extremely thin compared to the thickness of the cell (10 to 100 nm versus 10 μm), does not contribute substantially to the total modulus. To make a valid comparison between the stiffnesses of the models, the modulus of the cell body would have to be determined from the experimental data and compared to 100 Pa.

This can be done by taking the coupling constant, χ, where $\chi=\kappa^2\mu^*$ and multiplying by a length scale. The coupling constant represents the elastic "spring" contribution from the cell body, and is a good representation of the stiffness of the cell body, mainly the cytoskeleton. Assuming that the length scale (taken to be the characteristic diameter of the cell) of a 293A cell is 10 μm, we obtain a spring constant (which can be interpreted as a shear modulus of the cell body by the setup of the model) of 89 Pa, which is in very good agreement with the finite element model. Thus the difference in experimental membrane modulus (1 kPa) and in the finite element membrane modulus (10 Mpa) does not affect the membrane displacements.

The magnetic bead rolling is more prominent in the FEM, partly due to the small contact angle with the cell. As an illustration, for the 5 μm thick cell, the magnetic bead moved 0.5 μm under 14.3 pN of force (14.7 pN for the 10 μm thick cell). This gives a displacement/force ratio of 35,000 m/N. When compared to the magnetic beads of 293a cells with a ratio of 100-6000 m/N, one can say that if the bead attachments are similar, then, neglecting the effects of cell thickness, the stiffness of the 293 cells as scaled from the FEM lie between 500 and 35,000 Pa. It is likely that the beads in the experiments are attached better than 30° on average, although it is not presently known what the average attachment actually is.

FEM is useful for cell studies because it offers a way to change one facet of cell models at a time, which helps to show the sensitivity of parameters to the same applied stresses. This is something that cannot yet be done experimentally. FEM could also model the three-dimensional aspect of cell geometries, such as heights that vary across a cell. The estimates of shear moduli of the main cell body are close (within 15%) when comparing preliminary results

between the FEM and the parameters derived from the experiments using the Sackmann/Boulbitch model. However, this comparison should not be taken as a validation of the moduli determined through either method. There is currently insufficient information on the uncertainties associated with either model. For example, some of the calculations based on the Sackmann/Boulbitch model are based upon order of magnitude estimations, such as the membrane cortical thickness and the characteristic length of the 293A cells. The two models represent different methods of approaching the problem of cell deformation, and while it is encouraging that the models yield similar results, more work needs to be done before the computed moduli can be considered truly representative of a given cell.

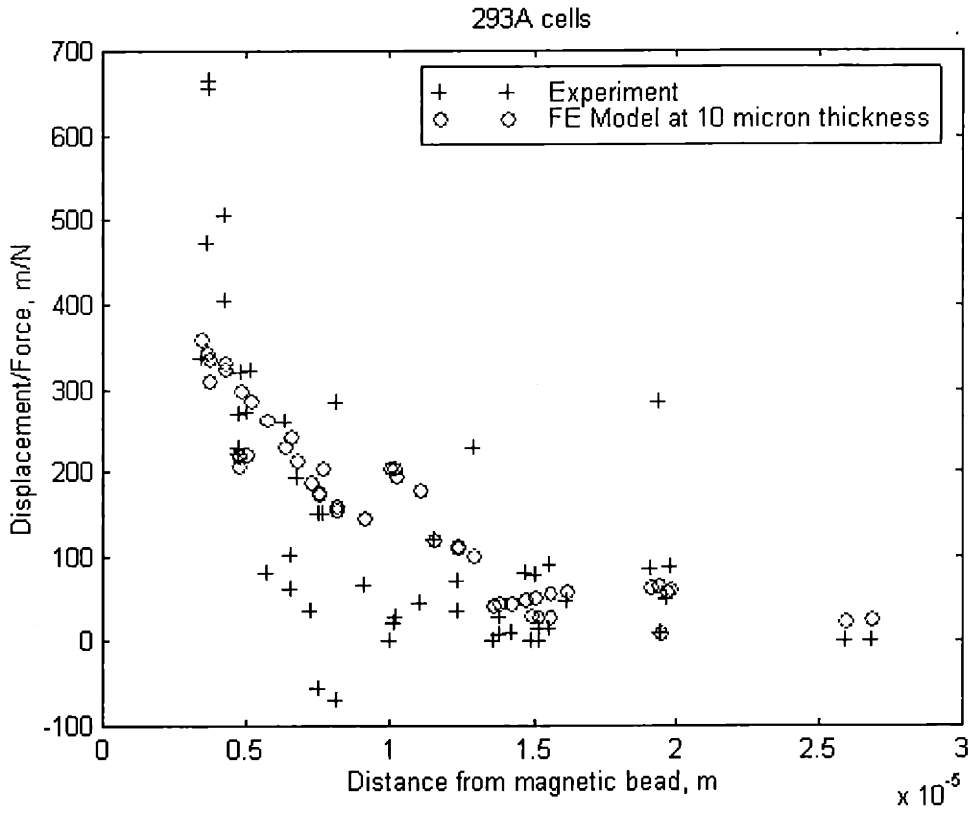

Figure 47. Comparison of the 10 μm cell FEM predictions and experimental displacements on 293A cells (average cell height 8 μm). The finite element model results were interpolated using Matlab to match the coordinates from the experiment.

5.0 General Discussion

The basic theme of this study was to examine at the single cell level the molecular regulation of cells to mechanical forces, in an attempt to link together the known external and internal responses.

An octopolar magnetic trap capable of producing uniform forces on the order of a few hundred pNs over an area of 500 × 500 μm^2 was designed. This micromanipulator was integrated with a high-resolution two-photon microscope so that 3-D images of deformation fields in biological specimens could be taken and analyzed. The development of this octopolar magnetic trap represents a significant step in the experimentation of cell mechanics. It is the first device that provides a robust way to study structural, biochemical, and genetic changes in biological systems with 3-D resolution. It can exert a uniform force across many hundreds of cells, while allowing the single cell information to remain intact. The user can perform both molecular assays as well as gather information of the purely physical response. This feature is vital for studying a variety of mechanical-cellular problems, where the responses of many cells must be averaged to obtain statistically relevant results. Some examples include the study of calcium flux of mechano-activated channels and mechanically activated gene induction. The statistical nature of these processes requires the study of a large number of cells.

This magnetic manipulator was used to probe the molecular response of human aortic smooth muscle cells. The results from mechanical stimulus were not clear, even though the controls behaved as predicted. It was postulated that due to high cell stiffness, the deformation was not sufficient to cause a response, and to test this hypothesis the octopolar trap was used to deform the cells. By using endocytosed polystyrene beads, the octopolar trap was able to generate a physical response that could be examined in 3D. Even when the applied stress is planar and is generated at a single focal location, it was found that cellular deformation occurs in all three dimensions. Different projections of the three-dimensional reconstruction of the data indicate that the deformations are not restricted to the surface – they extend through the cytoplasm to the nucleus. Similar results were observed in flow induced cytoskeletal deformation in endothelial cells (Helmke and others 2001). The data support the notion that the nucleus itself changes shape when a stress is applied on the cell, which is consistent with a step-strain analysis done by Ingber et al (Bojanowski and others 1998; Maniotis and others 1997).

However, this data suggests that the nuclear deformation could be induced by global continuum cellular changes as well as fibrous interconnections between the cell membrane and nucleus. Unfortunately, this information was not quantitative enough to permit an accurate calculation of the relative stiffness of the cell. In our static loading study, it is clear that global displacements becomes the dominant response mechanism on a time scale of minutes. These global motions are likely to be caused by physical processes that are different from those that generate the smaller, more instantaneous local displacements. One may postulate that these global displacements may involve active processes such as cellular cytoskeleton remodeling or focal adhesion shifting (Mathur and others 2000).

Thus, the single pole trap was built in order to gauge the nearly instantaneous physical response of the cells. Displacement mapping experiments were performed on three different cell types over a range of forces (1-10 nN). The data were fit into a model by Boulbitch and Sackmann, who used similar instrumentation to probe fibroblasts. The results suggest that the range of cell stiffnesses is actually much smaller than expected, only on the order of 1-10 kPa, which is consistent with the majority of the studies. The difficulty in obtaining molecular responses in the octopolar study is not likely due to a lack of deformation in the cells, but rather a combination of cell conditions, such as temperature and possibly cell confluence. Cell confluence can be an important factor, because when the single pole magnetic trap was used to probe HASMC's molecular responses using PAI-1, the molecular response was also not clear. However, the effects of confluence were highlighted by the fact that in the PAI-1 driven beta-lactamase cells, the blue signals were clearly present in the lower confluence region. No such dependency is seen in the control or the CMV driven beta-lactamase, which means that the PAI-1 promoter itself can be influenced by cell-cell contact (Figure 48).

While there are some limitations to the devices, such as a lack of temperature control for the specimens and the upper limit of applied forces being 200 pN for the octopolar trap, these are not insurmountable concerns. The introduction of a perfusion line will help resolve both the temperature considerations and the changing salt concentration due to evaporation. The limitation of the force of the octopolar trap can be more serious, but given that cells are more similar in stiffness than previously thought it is likely that, once the other factors have been

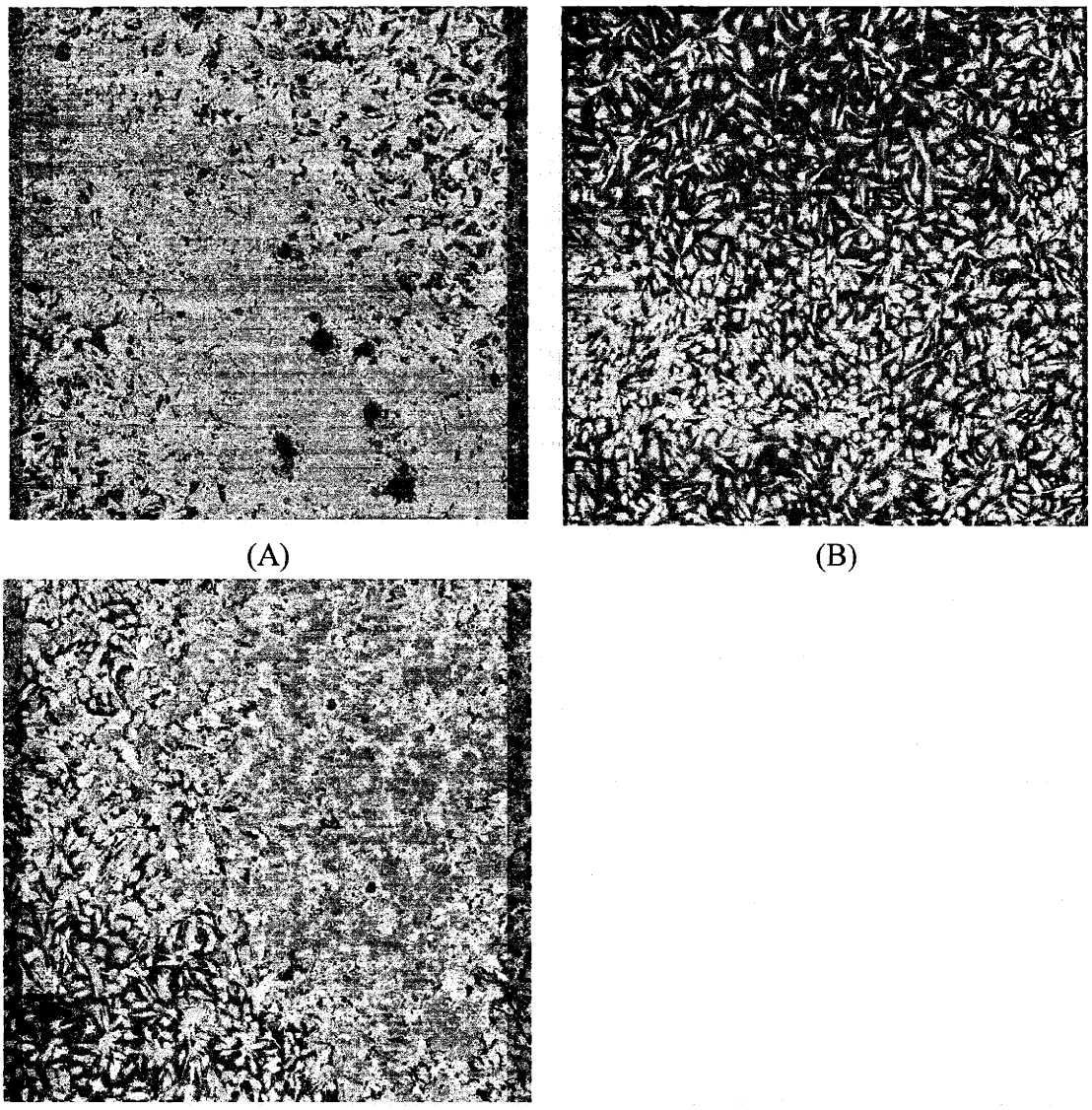

Figure 48. HASMC gene induction by confluence. The images are fast-scan composites of (A) control cells, (B) cells infected with CMV beta-lactamase adenovirus, and (C) cells infected with PAI-1 beta-lactamase adenovirus. There was no additional stimulus applied to any of these specimens. Note the relative uniformity in expression in (A) and(B) but the higher blue expression in lower confluence regions in (C). The false color images show green as orange, but blue as blue for increased contrast.

accounted for, a molecular response is possible. Other groups, using lower forces, have reported molecular responses in aggregate, thus there is every chance that the 200 pN force generation is sufficient for this purpose (Pommerenke and others 1996) (Goldschmidt and others 2001).

Finally, it is possible that the generated magnetic field itself can cause biological effects when cells are being studied. Magnetic field responses of biological systems have not been well-characterized, so detailed studies with a magnetic micromanipulator such as the ones used in this study need to include controls to eliminate the effects of the field. However, it is clear these magnetic traps provide the capabilities to systematically study the cellular mechanical response to establish a more comprehensive model of cell mechanics and behavior.

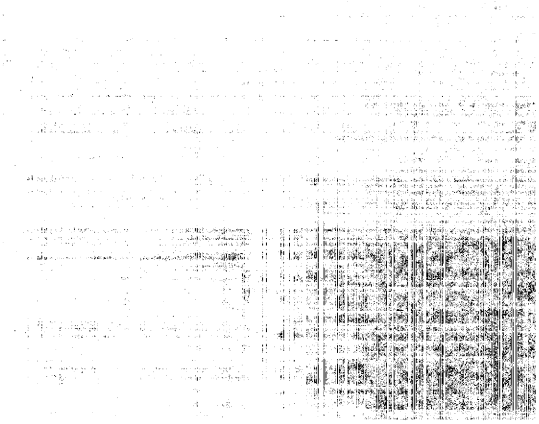

6.0 Future Work

More work needs to be done on cell mechanics before a complete cell model can be established. Probably the most important direction that needs to be explored is that of linking the external cellular deformation properties with the internal molecular regulation pathways. In order to achieve this, it is important to develop tools such as the octopolar magnetic trap that makes it possible to measure both the cell's physical properties and assay the cell's molecular response.

An important future improvement of the octopolar magnetic trap involves improving its mechanical stability. When the trap is toggled on/off, there is a noticeable movement in the sample section as viewed through the microscope (on the order of a hundred nanometers). This stability problem may be addressed in the future by the introduction of support struts, or by local encasements of the trap joints in plastic or epoxy. If the trap is intended for repeated uses, fatigue may result and can cause the trap force to change with time. For this study, the solid body displacement has been corrected by attaching latex particles to the coverslip as reference points. By stabilizing the trap, one can map the displacement fields of the cell with quantitative accuracy, so that the deformation data and the molecular data can be acquired using the same device.

One test that could be done with magnetic twisting cytometry is to use a much higher level of torques to see if the increasing stress-stiffness pattern is present. If the conclusions of this study are correct, then at high torques there should not be significant change in stiffness with increasing stresses, and the stiffness should be on the order of 1-10 kPa.

Future experiments that can measure the height of beads attached to cells could help narrow the range of moduli further. However, a model would need to be developed that can account for the cellular topology, because current models typically assume constant cell height or omit height entirely.

A more complete cell model needs to be developed. It is likely, given the progressive complexity of the models being developed, that such models will require computational models to make predictions. An analysis of Ingber's tensegrity model is already mathematically complex, even when limited to a few struts (Stamenovic and others 1996). Such a model would need to take into account the viscous behavior, heterogeneity, and hysteresis of the cell, but these

effects are poorly understood at this point in time, at least from a quantitative perspective. The use of finite-element modeling can be very useful to help identify important variables that should be included in cell models and targeted for experimental study.

In the short term, the single pole magnetic trap can be used to perform molecular studies. Because the forces generated by the single pole trap are sufficient to measurably deform cells, even to the point of cell detachment, it is a good place to start testing whether molecular responses can be stimulated. A good preliminary study would entail plating cells at a fixed confluence (such as full confluence), and then using the unipolar trap to stress beads attached to the cells under temperature controlled, slow perfusion conditions. The molecular response of the cells would range from the beta-lactamase assay to using RT-PCR (reverse transcriptase polymerase chain reaction) to determine the change in genetic expression. Some Northern analyses can be performed, such as gauging the effect of temperature on chemical induction of promoters. Such information is useful for determining whether the induction by mechanical means shares a pathway with that of chemical means. Finally, polystyrene beads (in the red fluorescence region) can be used to gauge the displacements of the beads with respect to time, in order to see if there is cell stiffening, so that all of the components of mechnaotransduction can be unified.

7.0 References

Alenghat FJ, Fabry B, Tsai KY, Goldmann WH, Ingber DE. 2000. Analysis of cell mechanics in single vinculin-deficient cells using a magnetic tweezer. Biochem Biophys Res Commun 277(1):93-9.

Amblard F, Yurke B, Pargellis A, Leibler S. 1996. A magnetic manipulator for studying local rheology and micromechanical properties of biological systems. Biophys. J. 67(3):818-27.

Bao X, Lu C, Frangos JA. 2001. Mechanism of temporal gradients in shear-induced ERK1/2 activation and proliferation in endothelial cells. Am J Physiol Heart Circ Physiol 281(1):H22-9.

Bausch AR, Ziemann F, Boulbitch AA, Jacobson K, Sackmann E. 1998. Local measurements of viscoelastic parameters of adherent cell surfaces by magnetic bead microrheometry. Biophys J 75(4):2038-49.

Bojanowski K, Maniotis AJ, Plisov S, Larsen AK, Ingber DE. 1998. DNA topoisomerase II can drive changes in higher order chromosome architecture without enzymatically modifying DNA. J Cell Biochem 69(2):127-42.

Boulbitch AA. 1999. Strain of a biomembrane cause by a local tangential force: Application to magnetic tweezer measurements. Physical Review B 59(3):3402-7.

Braet F RC, Wisse E., Radmacher M. 1998. Comparison of fixed and living liver endothelial cells by atomic force microscopy. Appl. Phys. A 66:S575-S578.

Brown TD, Bottlang M, Pedersen DR, Banes AJ. 1998. Loading paradigms--intentional and unintentional--for cell culture mechanostimulus. Am J Med Sci 316(3):162-8.

Butler JP, Kelly SM. 1998. A model for cytoplasmic rheology consistent with magnetic twisting cytometry. Biorheology 35(3):193-209.

Butler PJ, Norwich G, Weinbaum S, Chien S. 2001. Shear stress induces a time- and position-dependent increase in endothelial cell membrane fluidity. Am J Physiol Cell Physiol 280(4):C962-9.

Chang G, Spencer RH, Lee AT, Barclay MT, Rees DC. 1998. Structure of the MscL homolog from Mycobacterium tuberculosis: a gated mechanosensitive ion channel. Science 282(5397):2220-6.

Chen CS, Mrksich M, Huang S, Whitesides GM, Ingber DE. 1997. Geometric control of cell life and death. Science 276(5317):1425-8.

Cheng GC, Briggs WH, Gerson DS, Libby P, Grodzinsky AJ, Gray ML, Lee RT. 1997. Mechanical strain tightly controls fibroblast growth factor-2 release from cultured human vascular smooth muscle cells. Circ Res 80(1):28-36.

Chicurel ME, Chen CS, Ingber DE. 1998. Cellular control lies in the balance of forces. Curr Opin Cell Biol 10(2):232-9.

Davies PF. 1995. Flow-mediated endothelial mechanotransduction. Physiol Rev 75(3):519-60.

Davies PF, Barbee KA, Volin MV, Robotewskyj A, Chen J, Joseph L, Griem ML, Wernick MN, Jacobs E, Polacek DC and others. 1997. Spatial relationships in early signaling events of flow-mediated endothelial mechanotransduction. Annu Rev Physiol 59:527-49.

Davies PF, Polacek DC, Handen JS, Helmke BP, DePaola N. 1999. A spatial approach to transcriptional profiling: mechanotransduction and the focal origin of atherosclerosis. Trends Biotechnol 17(9):347-51.

Fabry BM, G. N.; Hubmayr, R. D.; Butler, J. P.; Fredberg, J. J. 1999. Implications of heterogeneous bead behavior on cell mechanical properties measured with magnetic twisting cytometry. Journal of Magnetism and Magnetic Materials 194:120-125.

Feng Y, Yang JH, Huang H, Kennedy SP, Turi TG, Thompson JF, Libby P, Lee RT. 1999. Transcriptional profile of mechanically induced genes in human vascular smooth muscle cells. Circ Res 85(12):1118-23.

Fung YC. 1990. Biomechanics: motion, flow, stress, and growth. New York: Springer-Verlag. 569 p.

Goldschmidt ME, McLeod KJ, Taylor WR. 2001. Integrin-mediated mechanotransduction in vascular smooth muscle cells: frequency and force response characteristics. Circ Res 88(7):674-80.

Gu CX, Juranka PF, Morris CE. 2001. Stretch-activation and stretch-inactivation of Shaker-IR, a voltage- gated K+ channel. Biophys J 80(6):2678-93.

Haidekker MA, L'Heureux N, Frangos JA. 2000. Fluid shear stress increases membrane fluidity in endothelial cells: a study with DCVJ fluorescence. Am J Physiol Heart Circ Physiol 278(4):H1401-6.

He TC, Zhou S, da Costa LT, Yu J, Kinzler KW, Vogelstein B. 1998. A simplified system for generating recombinant adenoviruses. Proc Natl Acad Sci U S A 95(5):2509-14.

Helmke BP, Thakker DB, Goldman RD, Davies PF. 2001. Spatiotemporal analysis of flow-induced intermediate filament displacement in living endothelial cells. Biophys J 80(1):184-94.

Henson JH. 1999. Relationships between the actin cytoskeleton and cell volume regulation. Microsc Res Tech 47(2):155-162

Hofmann UG, Rotsch C, Parak WJ, Radmacher M. 1997. Investigating the cytoskeleton of chicken cardiocytes with the atomic force microscope. J Struct Biol 119(2):84-91.

Ingber DE. 1997. Tensegrity: the architectural basis of cellular mechanotransduction. Annu Rev Physiol 59:575-99.

Ingber DE, Prusty D, Sun Z, Betensky H, Wang N. 1995. Cell shape, cytoskeletal mechanics, and cell cycle control in angiogenesis. J Biomech 28(12):1471-84.

Jacobson K, Sheets ED, Simson R. 1995. Revisiting the fluid mosaic model of membranes. Science 268(5216):1441-2.

Janmey PA, Hvidt S, Kas J, Lerche D, Maggs A, Sackmann E, Schliwa M, Stossel TP. 1994. The mechanical properties of actin gels. Elastic modulus and filament motions. J Biol Chem 269(51):32503-13.

Karcher H. 2001. Finite Element Modeling and Analysis of Magnetocytometry: Single Cell Micromanipulation using Magnetic Beads [Rapport de stage d'option scientifique]. Cambridge: MIT/Ecole Polytechnique. 32 p.

Karl I, Bereiter-Hahn J. 1999. Tension modulates cell surface motility: A scanning acoustic microscopy study. Cell Motil Cytoskeleton 43(4):349-359

Khachigian LM, Anderson KR, Halnon NJ, Gimbrone MA, Jr., Resnick N, Collins T. 1997. Egr-1 is activated in endothelial cells exposed to fluid shear stress and interacts with a novel shear-stress-response element in the PDGF A- chain promoter. Arterioscler Thromb Vasc Biol 17(10):2280-6.

Khachigian LM, Collins T. 1997. Inducible expression of Egr-1-dependent genes. A paradigm of transcriptional activation in vascular endothelium. Circ Res 81(4):457-61.

Khachigian LM, Lindner V, Williams AJ, Collins T. 1996. Egr-1-induced endothelial gene expression: a common theme in vascular injury. Science 271(5254):1427-31.
Kim BS, Nikolovski J, Bonadio J, Mooney DJ. 1999a. Cyclic mechanical strain regulates the development of engineered smooth muscle tissue. Nat Biotechnol 17(10):979-83.
Kim KH, Buehler C, So PTC. 1999b. High-speed, two-photon scanning microscope. Appl. Opt. 38(28):6004-9.
Koh SD, Sanders KM. 2001. Stretch-dependent potassium channels in murine colonic smooth muscle cells. J Physiol 533(Pt 1):155-63.
Lee KM, Tsai KY, Wang N, Ingber DE. 1998. Extracellular matrix and pulmonary hypertension: control of vascular smooth muscle cell contractility. Am J Physiol 274(1 Pt 2):H76-82.
Leung DY, Glagov S, Mathews MB. 1976. Cyclic stretching stimulates synthesis of matrix components by arterial smooth muscle cells in vitro. Science 191(4226):475-7.
Maksym GN, Fabry B, Butler JP, Navajas D, Tschumperlin DJ, Laporte JD, Fredberg JJ. 2000. Mechanical properties of cultured human airway smooth muscle cells from 0.05 to 0.4 Hz. J Appl Physiol 89(4):1619-32.
Malek AM, Izumo S. 1995. Control of endothelial cell gene expression by flow. J Biomech 28(12):1515-28.
Maniotis AJ, Chen CS, Ingber DE. 1997. Demonstration of mechanical connections between integrins, cytoskeletal filaments, and nucleoplasm that stabilize nuclear structure. Proc Natl Acad Sci U S A 94(3):849-54.
Mathur AB, Truskey GA, Reichert WM. 2000. Atomic force and total internal reflection fluorescence microscopy for the study of force transmission in endothelial cells. Biophys J 78(4):1725-35.
McAllister TN, Frangos JA. 1999. Steady and transient fluid shear stress stimulate NO release in osteoblasts through distinct biochemical pathways. J Bone Miner Res 14(6):930-6.
Morawietz H, Ma YH, Vives F, Wilson E, Sukhatme VP, Holtz J, Ives HE. 1999. Rapid induction and translocation of Egr-1 in response to mechanical strain in vascular smooth muscle cells. Circ Res 84(6):678-87.
Mow VC GF, Tran-Son-Tay R, Hochmuth RM. 1994. Cell Mechanics and Cellular Engineering. New York: Springer Verlag.
Ookawa K, Sato M, Ohshima N. 1993. Morphological changes of endothelial cells after exposure to fluid- imposed shear stress: differential responses induced by extracellular matrices. Biorheology 30(2):131-40.
Park JBL, R. S. 1992. Biomaterials: An Introduction. New York: Plenum Press. 394 p.
Petersen NO, McConnaughey WB, Elson EL. 1982. Dependence of locally measured cellular deformability on position on the cell, temperature, and cytochalasin B. Proc Natl Acad Sci U S A 79(17):5327-31.
Pommerenke H, Schreiber E, Durr F, Nebe B, Hahnel C, Moller W, Rychly J. 1996. Stimulation of integrin receptors using a magnetic drag force device induces an intracellular free calcium response. Eur J Cell Biol 70(2):157-64.
Potard US, Butler JP, Wang N. 1997. Cytoskeletal mechanics in confluent epithelial cells probed through integrins and E-cadherins. Am J Physiol 272(5 Pt 1):C1654-63.
Pourati J, Maniotis A, Spiegel D, Schaffer JL, Butler JP, Fredberg JJ, Ingber DE, Stamenovic D, Wang N. 1998. Is cytoskeletal tension a major determinant of cell deformability in adherent endothelial cells? Am J Physiol 274(5 Pt 1):C1283-9.

Reusch HP, Chan G, Ives HE, Nemenoff RA. 1997. Activation of JNK/SAPK and ERK by mechanical strain in vascular smooth muscle cells depends on extracellular matrix composition. Biochem Biophys Res Commun 237(2):239-44.

Rosales OR, Isales CM, Barrett PQ, Brophy C, Sumpio BE. 1997. Exposure of endothelial cells to cyclic strain induces elevations of cytosolic Ca2+ concentration through mobilization of intracellular and extracellular pools. Biochem J 326(Pt 2):385-92.

Rotsch C, Jacobson K, Radmacher M. 1999. Dimensional and mechanical dynamics of active and stable edges in motile fibroblasts investigated by using atomic force microscopy. Proc Natl Acad Sci U S A 96(3):921-6.

Satcher RL, Jr., Dewey CF, Jr. 1996. Theoretical estimates of mechanical properties of the endothelial cell cytoskeleton. Biophys J 71(1):109-18.

Sato M, Ohshima N, Nerem RM. 1996. Viscoelastic properties of cultured porcine aortic endothelial cells exposed to shear stress. J Biomech 29(4):461-7.

Shen J, Luscinskas FW, Gimbrone MA, Jr., Dewey CF, Jr. 1994. Fluid flow modulates vascular endothelial cytosolic calcium responses to adenine nucleotides. Microcirculation 1(1):67-78.

Shroff SG, Saner DR, Lal R. 1995. Dynamic micromechanical properties of cultured rat atrial myocytes measured by atomic force microscopy. Am J Physiol 269(1 Pt 1):C286-92.

Singer SJ. 1972. A fluid lipid-globular protein mosaic model of membrane structure. Ann N Y Acad Sci 195:16-23.

Singer SJ. 1982. Structure of the cell surface. Natl Cancer Inst Monogr 60:25-30.

Singer SJ, Nicolson GL. 1972. The fluid mosaic model of the structure of cell membranes. Science 175(23):720-31.

Sleep J, Wilson D, Simmons R, Gratzer W. 1999. Elasticity of the red cell membrane and its relation to hemolytic disorders: an optical tweezers study. Biophys J 77(6):3085-95.

So PT, Konig K, Berland K, Dong CY, French T, Buhler C, Ragan T, Gratton E. 1998. New time-resolved techniques in two-photon microscopy. Cell Mol. Biol. (Noisy-le-grand) 44(5):771-93.

So PTC, French T, Yu WM, Berland KM, Dong CY, Gratton E. 1995. Time-resolved fluroescence microscopy using two-photon excitation. Bioimaging 3:49-63.

Stamenovic D, Coughlin MF. 1999. The role of prestress and architecture of the cytoskeleton and deformability of cytoskeletal filaments in mechanics of adherent cells: a quantitative analysis. J Theor Biol 201(1):63-74.

Stamenovic D, Coughlin MF. 2000. A quantitative model of cellular elasticity based on tensegrity. J Biomech Eng 122(1):39-43.

Stamenovic D, Fredberg JJ, Wang N, Butler JP, Ingber DE. 1996. A microstructural approach to cytoskeletal mechanics based on tensegrity. J Theor Biol 181(2):125-36.

Tagawa H, Wang N, Narishige T, Ingber DE, Zile MR, Cooper Gt. 1997. Cytoskeletal mechanics in pressure-overload cardiac hypertrophy. Circ Res 80(2):281-9.

Thoumine O, Ott A. 1997. Time scale dependent viscoelastic and contractile regimes in fibroblasts probed by microplate manipulation. J Cell Sci 110(Pt 17):2109-16.

Wang N, Butler JP, Ingber DE. 1993. Mechanotransduction across the cell surface and through the cytoskeleton [see comments]. Science 260(5111):1124-7.

Wang N, Ingber DE. 1994. Control of cytoskeletal mechanics by extracellular matrix, cell shape, and mechanical tension. Biophys J 66(6):2181-9.

Wang N, Ingber DE. 1995. Probing transmembrane mechanical coupling and cytomechanics using magnetic twisting cytometry. Biochem Cell Biol 73(7-8):327-35.

Wang N, Naruse K, Stamenovic D, Fredberg JJ, Mijailovich SM, Tolic-Norrelykke IM, Polte T, Mannix R, Ingber DE. 2001. Mechanical behavior in living cells consistent with the tensegrity model. Proc Natl Acad Sci U S A 98(14):7765-70.

Yang JH, Briggs WH, Libby P, Lee RT. 1998. Small mechanical strains selectively suppress matrix metalloproteinase- 1 expression by human vascular smooth muscle cells. J Biol Chem 273(11):6550-5.

Yao X, Kwan H, Huang Y. 2001. Stretch-sensitive switching among different channel sublevels of an endothelial cation channel. Biochim Biophys Acta 1511(2):381-90.

Yoshida M, Westlin WF, Wang N, Ingber DE, Rosenzweig A, Resnick N, Gimbrone MA, Jr. 1996. Leukocyte adhesion to vascular endothelium induces E-selectin linkage to the actin cytoskeleton. J Cell Biol 133(2):445-55.

Zhao S, Suciu A, Ziegler T, Moore JE, Jr., Burki E, Meister JJ, Brunner HR. 1995. Synergistic effects of fluid shear stress and cyclic circumferential stretch on vascular endothelial cell morphology and cytoskeleton. Arterioscler Thromb Vasc Biol 15(10):1781-6.

Zhelev DV, Needham D, Hochmuth RM. 1994. Role of the membrane cortex in neutrophil deformation in small pipets. Biophys J 67(2):696-705.

Zlokarnik G, Negulescu PA, Knapp TE, Mere L, Burres N, Feng L, Whitney M, Roemer K, Tsien RY. 1998. Quantitation of transcription and clonal selection of single living cells with beta-lactamase as reporter. Science 279(5347):84-8.

Appendix A: Cell Culture Techniques

Smooth Muscle Cells

These cells were isolated from leftover aorta from heart transplants. They are cultured in DMEM (Bio-Whittaker) supplemented with glutamine, penicillin/streptomycin to help prevent bacterial contamination, and 10% fetal calf serum (company). The cells are used from passage two through six, although often by passage five the cells have slowed their growth rate. Passage one is considered the first flask that is seeded with cells, with the explant-in-petri-dish counted as passage zero.

These cells are fed twice a week, by aspirating the existing media off the cells and replaceing with the same amount of media, corrected for evaporation. In a T150 flask (150 cm^2 of culture area) this takes 20 ml. For a T25 flask (25 cm^2 of culture area) this takes 5 ml. For a 6-well plate (10 cm^2 area per well) this takes 2 ml per well.

The cells are split whenever they reach full confluency. That is, when the cells completely cover the available culture area in the flask. The cells are split by first aspirating the media off the cells, and rinsing the cells with Hanks buffered saline solution, without calcium and magnesium (5 ml in T150 flask). The Hanks is aspirated and the trypsin is placed on the cells (5 ml for a T150 flask, although as little as 3 ml can be used). The cells are incubated at 37°C for 2-3 minutes, sometimes longer if the cell confluency is higher, but no longer than 5-6 minutes. The cells are then washed with DMEM+FCS (5 ml) to inactivate the trypsin. The cells are then centrifuged at 1500-1700 RPM (about 100-200 g). The supernatant is aspirated and the pellet of cells is resuspended in 10 ml DMEM+FCS (or 5 ml, if the cell confluency was low). For propogation purposes, the cells are placed at 1/3 concentration. Thus, if the pellet was resuspended in 10 ml DMEM+FCS, then a 3 ml sample of the cell suspension would be placed in a new T150 flask with 17 ml DMEM+FCS for further passaging.

Otherwise, a 35 µl sample would be taken of the cell suspension and inserted into both sides of a hemocytometer (roughly 17 µl for each side). Four square sections would be counted and averaged, and the average would be multiplied by 10,000 to get the concentration of cells/ml of suspension. The appropriate number of cells would be calculated from this number and the cells would be plated with known cells/cm^2 concentration. Typically, for low seeding one uses 8,000-10,000 cells/cm^2, but nominally the cells are plated at near confluency due to their slow growth rate, so they are plated at 16,000-18,000 cells/cm^2. If complete confluence is required, the cells are plated at 25,000 cells/cm^2. Care must be taken with overplating these cells since these cells can grow in layers, on top of each other. These cells normally look thin and fibrous, much like one would expect muscle fibers to look like.

These cells are hardy, so they can take room temperature incubations for extended periods. They can survive in low media conditions, and will not detach easily even in Hanks w/o Ca and Mg. They typically grow slowly, requiring passage usually only after 2-3 weeks, although in some cases the cells grow much faster than that.

293A Cells

These are transformed cells, and thus do not have the same passage limitations as the HASMCs. These cells are also kept in the same DMEM+glutamine+penicillin/streptomycin and 10% FCS as the HASMCs.

These cells are split weekly, and not fed during the week. The split is done similarly to HASMCs, with the difference that the cells are placed at 1/10 concentration. That is, the cells are resuspended in 10 ml DMEM+FCS and then 1 ml of cell suspension is taken and placed in a new T150 flask with 19 ml DMEM+FCS. The growth rate of these cells is very fast – if the split was 1/3 concentration, they would reach full confluence in 2-3 days.

Cell counting is done the similarly to HASMCs. The 293A cells are smaller, so the plating density is usually higher. For low confluency, the cells are plated at 25,000-30,000 cells/cm^2, but for full confluency, the cells are plated at 45,000-50,000 cells/cm^2. This takes into account the faster growth rate of the cells.

These cells will not grow on top of each other, and look like cobblestones. They are easily visualized, even without phase contrast because they are so thick. They are quite fragile, though, and will start to detach if left at room temperature for too long. They will also detach if left in buffer, such as PBS, even with calcium and magnesium present. Thus, loading these cells with CCF-2 is very difficult. It should be noted that these cells will detach in trypsin very quickly, sometimes under 1 minute.

293A cells are also meant for viral infection, having been transformed to express the E1 section of common adenovirus (thus, making up for the E1 deficiency in the adenovirus). Unlike HASMCs, these cells have a very high transfection efficiency from chemical transfection means, usually greater than 50% of the cells will be transfected (opposed to HASMCs being <10%).

Endothelial Cells

These cells were cultured in another lab, so propagation was not performed in lab.

Endothelial cells are kept in a media called M-199, supplemented with 10% FCS, penicillin/streptomycin and a fungus retardant, fungizide. They are plated at 20,000 cells/cm^2 for near-full confluency (although they tend to cluster in the center of the dishes, so that the true confluence varies).

Normally, these cells form cobblestone patterns, similar to 293A cells, and like 293A cells, will not grow on top of each other.

Generalities

Cells are plated directly on cell-culture treated plastic, such as for 6-well plates, culture flasks (T25, T75, and T150), and petri dishes. For glass (Bioptechs gaskets, coverslips, silicone membranes) the surface needs to be treated with fibronectin. The typical way of coating these is

to place enough fibronectin in Hanks with calcium and magnesium to cover the surface. The concentration of fibronectin used is typically 2 μg/ml Hanks. The plates are then left overnight at 4°C, although for certain cell types and surfaces, as little as 1 hour is sufficient. The Bioptechs gaskets, if new, can be used very quickly since they have pre-treated the surfaces. Fibroblasts and endothelial cells can be plated with a few hours incubation. Dishes with fibronectin coating can be left for over a week and still be viable, as long as the fluid level is kept up (there will be evaporation).

Practically all cells can be frozen for later use. This is useful because sometimes cells will grow faster than one can use them, and in the case of HASMCs, the supply is not always guaranteed, so it is a good idea to have some frozen stocks on hand so they can be used in a pinch. However, it is generally best to do at least one experiment to confirm findings from cells that are fresh, since cells that have been thawed sometimes look a bit sick. Interestingly, transformed cells (CHO, 293A) are often very good at being frozen and thawed repeatedly. Freezing the cells is a straightforward procedure: just detach and spin down the cells as if you were going to passage, and then resuspend the cell pellet in a small volume. Typically, one freezes half or third of a T150 flask in a single vial. If this is the case, resuspend the pellet in 2.85 ml DMEM+FCS, and then place 0.95 ml in each of 3 vials. Then add dropwise to each vial 50 μl of DMSO (sterile, cell-culture grade), invert the vial to mix and quickly place the vials in dry ice. Different volumes can be used, just make sure that the DMSO is about 5% of the final volume. Let the vials freeze. The vials can then be transferred to liquid nitrogen tanks (-170°C), or sometimes they can be placed at -80°C for a day before being transferred. The DMSO helps prevent ice crystal-formation that will destroy the cells. To thaw the cells, simply run the vials under warm water, until about 50% thawed, and then transfer to a 50 ml tube with 10ml of DMEM+FCS, pellet with centrifuge, and place in a flask. It is recommended that cells not be used immediately after thaw – wait a week first. Remember that DMSO is toxic to cells.

Appendix B: Beta-lactamase system

The beta-lactamase system uses the dye CCF-2/AM to produce a response. Originally, Aurora Biotechnology developed the beta-lactamase system, but they licensed it to Packard Instruments. The beta-lactamase system used in this study is from Packard Instruments. However, due to policy changes Packard no longer carries the beta-lactamase system. Unfortunately, the beta-lactamase sequence from Packard is not identical to that of Aurora, so the sequence is given here for reference, in addition to the CMV, EGR-1, and PAI-1 promoter sequences. Note that the promoters listed here may be slightly larger than what was finally used since some restriction digestions may cut slightly into either side.

CMV sequence

tagtaatcaattacggggtcattagttcatagcccatatatggagttccgcgttacataacttacggtaaatggcccgcctggctgaccgccca
acgacccccgcccattgacgtcaataatgacgtatgttcccatagtaacgccaatagggactttccattgacgtcaatgggtggagtatttacg
gtaaactgcccacttggcagtacatcaagtgtatcatatgccaagtacgccccctattgacgtcaatgacggtaaatggcccgcctggcatta
tgcccagtacatgaccttatgggactttcctacttggcagtacatctacgtattagtcatcgctattaccatggtgatgcggttttggcagtacatc
aatgggcgtggatagcggtttgactcacggggatttccaagtctccaccccattgacgtcaatgggagtttgttttggcaccaaaatcaacgg
gactttccaaaatgtcgtaacaactccgccccattgacgcaaatgggcggtaggcgtgtacggtgggaggtctatataagcagagctggttt
agtgaaccgtcag

EGR-1 sequence

acggagggaatagcctttcgattctgggtggtgcattggaagccccaggctctaaaaccc 60
ccaacctactgactggtggccgagtatgcacccgactgctagctaggcagtgtcccaaga 120
accagtagccaaatgtcttggcctcagttttcccggtgacacctggaaagtgaccctgcc 180
attagtagaggctcaggtcagggccccgcctctcctgggcggcctctgccctagcccgcc 240
ctgccgctcctcctctccgcaggctcgctcccacggtccccgaggtgggcgggtgagccc 300
aggatgacggctgtagaaccccggcctgactcgccctcgccccgcgccgggcctgggct 360
tccctagcccagctcgcacccgggggccgtcggagccgccgcgcgcccagctctacgcgc 420
ctggccctccccacgcgggcgtccccgactcccgcgcgcgctcaggctcccagttgggaa 480
ccaaggaggggggaggatgggggggggggtgtgcgccgacccggaaacgccatataaggag 540
caggaaggatcccccgccggaacagaccttatttgggcagcgccttatatggagtggccc 600
aatatggccctgccgcttccggctctgggaggaggggcgagcgggggttggggcgggggc 660
aagctgggaactccaggcgcctggcccgggaggccactgctgctgttccaatactaggct 720
ttccaggagcctgagcgctcgcgatgccggagcgggtcgcagggtggaggtgcccaccac 780
tcttggatgggagggcttcacgtcactccgggtcctcccggccggtccttccatattagg 840
gcttcctgcttcccatatatggccatgtacgtcacggcggaggcgggcccgtgctgttcc 900
agacccttgaaatagaggccgattcggggagtcgcgagagatcccagcgcgcagaacttg 960
gggagccgccgccgcgattcgccgccgccgccagcttccgccgccgcaagatcggcccct 1020
gccccagcctccgcggcagccctgcgtccaccacgggccgcggctaccgccagcctgggg 1080
gcccacctacactccccgcagtgtgcccctgcaccccgcatgtaacccggccaacccccg 1140
gcgagtgtgccctcagtagcttcggccccgggctgcgcccaccacccaacatcagttctc 1200

PAI-1 sequence

aagcttaccatggtaacccctggtcccgttcagccaccaccaccccacccagcacacctc 60
caacctcagccagacaaggttgttgacacaagagagccctcaggggcacagagagagtct 120
ggacacgtggggagtcagccgtgtatcatcggaggcggccgggcacatggcagggatgag 180
ggaaagaccaagagtcctctgttgggcccaagtcctagacagacaaaacctagacaatca 240
cgtggctggctgcatgcctgtggctgttgggctgggcaggaggagggaggggcgctcttt 300
cctggaggtggtccagagcaccgggtggacagccctgggggaaaacttccacgttttgat 360
ggaggttatctttgataactccacagtgacctggttcgccaaaggaaaagcaggcaacgt 420
gagctgtttttttttctccaagctgaacactaggggtcctaggctttttgggtcacccg 480
gcatggcagacagtcaacctggcaggacatccgggagagacagacacaggcagagggcag 540
aaaggtcaagggaggttctcaggccaaggctattggggtttgctcaattgttcctgaatg 600
ctcttacacacgtacacacacagagcagcacacacacacacacacacatgcctcagcaag 660
tcccagagagggaggtgtcgagggggacccgctggctgttcagacggactcccagagcca 720
gtgagtgggtggggctggaacatgagttcatctatttcctgcccacatctggtataaaag 780
gaggcagtggcccacagaggagcacagctgtgtttggctgcagggccaagagcgctgtca 840
agaagacccacacgccccctccagcagctgaattcctgcagctcagcagccgccgccag 900
agcaggacgaaccgccaatcgcaaggcacctctgagaacttcaggatgcagatgtctcca 960
gccctcacctgc 972

beta-lactamase sequence (beta-lactamase is from bp 6-800)
ggtaccgagctcttacgcgtgctagcccgggctcgagatctgcgatctaagtaagcttgg 60
cattccggtactgttggtaaagccaccatgggtcacccagaaacgctggtgaaagtaaaa 120
gatgctgaagatcagttgggtgcacgagtgggttacatcgaactggatctcaacagcggt 180
aagatccttgagagttttcgccccgaagaacgttttccaatgatgagcacttttaaagtt 240
ctgctatgtggcgcggtattatcccgtgttgacgccgggcaagagcaactcggtcgccgc 300
atacactattctcagaatgacttggttgagtactcaccagtcacagaaaagcatcttacg 360
gatggcatgacagtaagagaattatgcagtgctgccataaccatgagtgataacactgcg 420
gccaacttacttctgacaacgatcggaggaccgaaggagctaaccgctttttgcacaac 480
atgggggatcatgtaactcgccttgatcgttgggaaccggagctgaatgaagccatacca 540
aacgacgagcgtgacaccacgatgcctgcagcaatggcaacaacgttgcgcaaactatta 600
actggcgaactacttactctagcttcccggcaacaattaatagactggatggaggcggat 660
aaagttgcaggaccacttctgcgctcggcccttccggctggctggtttattgctgataaa 720
tctggagccggtgagcgtgggtctcgcggtatcattgcagcactggggccagatggtaag 780
ccctcccgtatcgtagttatctacacgacggggagtcaggcaactatggatgaacgaaat 840
agacagatcgctgagataggtgcctcactgattaagcattggtaatctagagtcggggcg 900
gccggccgcttcgagcagacatgataagatacattgatgagtttggacaaaccacaacta 960
gaatgcagtgaaaaaaatgctttatttgtgaaatttgtgatgctattgctttatttgtaa 1020
ccattataagctgcaataaacaagttaacaacaacaattgcattcattttatgtttcagg 1080
ttcaggggggaggtgtgggaggttttttaaagcaagtaaaacctctacaaatgtggtaaaa 1140
tcgataaggatccgtcgaccgatgcccttgagagccttcaacccagtcagctccttccgg 1200
tgggcgcggggcatgactatcgtcgccgcacttatgactgtcttctttatcatgcaactc 1260
gtaggacaggtgccggcagcgctcttccgcttcctcgctcactgactcgctgcgctcggt 1320
cgttcggctgcggcgagcggtatcagctcactcaaaggcggtaatacggttatccacaga 1380
atcaggggataacgcaggaaagaacatgtgagcaaaaggccagcaaaaggccaggaaccg 1440
taaaaaggccgcgttgctggcgttttccataggctccgccccctgacgagcatcacaa 1500
aaatcgacgctcaagtcagaggtggcgaaacccgacaggactataaagataccaggcgtt 1560
tccccctggaagctccctcgtgcgctctcctgttccgaccctgccgcttaccggatacct 1620

gtccgcctttctcccttcgggaagcgtggcgctttctcaatgctcacgctgtaggtatct 1680
cagttcggtgtaggtcgttcgctccaagctgggctgtgtgcacgaacccccgttcagcc 1740
cgaccgctgcgccttatccggtaactatcgtcttgagtccaacccggtaagacacgactt 1800
atcgccactggcagcagccactggtaacaggattagcagagcgaggtatgtaggcggtgc 1860
tacagagttcttgaagtggtggcctaactacggctacactagaaggacagtatttggtat 1920
ctgcgctctgctgaagccagttaccttcggaaaaagagttggtagctcttgatccggcaa 1980
acaaaccaccgctggtagcggtggtttttttgtttgcaagcagcagattacgcgcagaaa 2040
aaaaggatctcaagaagatcctttgatcttttctacggggtctgacgctcagtggaacga 2100
aaactcacgttaagggattttggtcatgagattatcaaaaaggatcttcacctagatcct 2160
tttaaattaaaaatgaagttttaaatcaatctaaagtatatatgagtaaacttggtctga 2220
cagctgcaggggggggggggcgctgaggtctgcctcgtgaagaaggtgttgctgactcat 2280
accaggcctgaatcgccccatcatccagccagaaagtgagggagccacggttgatgagag 2340
ctttgttgtaggtggaccagttggtgattttgaacttttgctttgccacggaacggtctg 2400
cgttgtcgggaagatgcgtgatctgatccttcaactcagcaaaagttcgatttattcaac 2460
aaagccgccgtcccgtcaagtcagcgtaatgctctgccagtgttacaaccaattaaccaa 2520
ttctgattagaaaaactcatcgagcatcaaatgaaactgcaatttattcatatcaggatt 2580
atcaataccatatttttgaaaaagccgtttctgtaatgaaggagaaaactcaccgaggca 2640
gttccataggatggcaagatcctggtatcggtctgcgattccgactcgtccaacatcaat 2700
acaacctattaatttcccctcgtcaaaaataaggttatcaagtgagaaatcaccatgagt 2760
gacgactgaatccggtgagaatggcaaaagcttatgcatttctttccagacttgttcaac 2820
aggccagccattacgctcgtcatcaaaatcactcgcatcaaccaaaccgttattcattcg 2880
tgattgcgcctgagcgagacgaaatacgcgatcgctgttaaaaggacaattacaaacagg 2940
aatcgaatgcaaccggcgcaggaacactgccagcgcatcaacaatattttcacctgaatc 3000
aggatattcttctaatacctggaatgctgttttcccggggatcgcagtggtgagtaacca 3060
tgcatcatcaggagtacggataaaatgcttgatggtcggaagaggcataaattccgtcag 3120
ccagtttagtctgaccatctcatctgtaacatcattggcaacgctacctttgccatgttt 3180
cagaaacaactctggcgcatcgggcttcccatacaatcgatagattgtcgcacctgattg 3240
cccgacattatcgcgagcccatttatacccatataaatcagcatccatgttggaatttaa 3300
tcgcggcctcgagcaagacgtttcccgttgaatatggctcataacacccttgtattact 3360
gtttatgtaagcagacagttttattgttcatgatgatatatttttatcttgtgcaatgta 3420
acatcagagattttgagacacaacgtggctttcccccccccccctgcagactcttccttt 3480
ttcaatattattgaagcatttatcagggttattgtctcatgagcggatacatatttgaat 3540
gtatttagaaaaataaacaaataggggttccgcgcacatttccccgaaaagtgccacctg 3600
acgcgccctgtagcggcgcattaagcgcggcgggtgtggtggttacgcgcagcgtgaccg 3660
ctacacttgccagcgccctagcgcccgctcctttcgctttcttcccttcctttctcgcca 3720
cgttcgccggctttccccgtcaagctctaaatcgggggctcccttagggttccgattta 3780
gtgctttacggcacctcgaccccaaaaaacttgattagggtgatggttcacgtagtgggc 3840
catcgccctgatagacggtttttcgccctttgacgttggagtccacgttctttaatagtg 3900
gactcttgttccaaactggaacaacactcaaccctatctcggtctattcttttgatttat 3960
aagggattttgccgatttcggcctattggttaaaaaatgagctgatttaacaaaaattta 4020
acgcgaattttaacaaaatattaacgtttacaatttcccattcgccattcaggctgcgca 4080
actgttgggaagggcgatcggtgcgggcctcttcgctattacgccagcccaagctaccat 4140
gataagtaagtaatattaaggtacgggaggacttggagcggccgcaataaaatatcttt 4200
attttcattacatctgtgtgttggttttttgtgtgaatcgatagtactaacatacgctct 4260
ccatcaaaacaaaacgaaacaaaacaaactagcaaaataggctgtccccagtgcaagtgc 4320
aggtgccagaacatttctctatcgata 4347

In addition, the policy change occurred in the middle of this study, so while the beta-lactamase virus was the same throughout the study, the source of CCF-2 changed. The only thing that changed about CCF-2, however, is the loading reagents that came with it. I will only go over the CCF-2 that can now be accessed, from Aurora Biotechnologies (San Diego, CA).

The CCF-2 is provided in 200 μg aliquots, with a molecular weight of 1082. This powder should be stored at -20°C, even when reconstituted with DMSO. The DMSO (dimethylsulfoxide) is provided as Solution A by Aurora. This stock should be dessicated and stored at room temperature. Keeping the DMSO anhydrous is extremely important. The reconstitution should bring the concentration of the CCF-2 to 1 mM, thus, adding 185 μl of Solution A to the 185 nmol of CCF-2 should do nicely.

At the time of the experiment, the solution should be thawed, but kept cool. Dilute the CCF-2 in DMSO with Solution B, containing DMSO and 100 mg/ml of Pluronic F-127, which helps permeabilize the cells to the AM ester, and 0.1% Acetic Acid. The concentration at this point should be 100 μM (so the ratio of CCF-2 to Solution B should be 1:9). Finally, dilute the stock in PBS, or other serum-free buffer, by 100-fold. Thus, the final concentration should be 1 μM, although one can use up to 4-5 μM without significant precipitation. As an example, to prepare 1 ml of loading solution, one should place in a microcentrifuge tube 9 μl of Solution B, then add 1 μl of the dissolved CCF-2 in Solution A, and mix. Then, 1 ml PBS should be added to the tube, and then vortexed for at least 10 seconds. This solution is now ready for use. Aurora adds that probenecid (250 mM in NaOH) can also be used. I have always used probenecid at – mM, but it was dissolved in water, so thus did not form a clear solution until diluted into the final loading solution.

Loading of CCF-2 is easy – after preparing the solution, take the cells to be loaded, aspirated the media off the cells, rinse once or twice with PBS to remove the serum, and then place the CCF-2 on the cells. Place the cells in a dark place (under a box, for example) and incubate at room temperature for one to two hours. The cells may be left in the CCF-2 solution for long-term studies; this is extremely useful for magnetic trap studies, because the use of the magnetic trap on beads attached to cells causes the CCF-2 to leak out of the cells. Otherwise, remove the CCF-2 from the cells and place the cells in fresh buffer. Media can also be used at this point. The cye loads poorly at 37°C, and the dye will leak out of the cells quickly at 37°C as well, so keep this in mind.

Using this technique, I have loaded CHO cells, bovine aortic endothelial cells, HASMCs, and Rat hepatocytes (although in the last, it is useful to use 3 μM to get a strong signal). The dye usually lasts 1-2 hours post loading if the dye is removed, up to 6-8 hours if the dye is maintained. The difference between blue and green is most obvious when using a multiple-pass filter (the blue is quite dim), and very obvious when using the two-photon system with 2 channels.

Appendix C: Matlab Programs

There are many Matlab programs and functions written for this project, most notably the cell strain and cell height measurements for the single pole studies. These programs will probably be upgraded or deleted to make way for better functions, as well as a shift to Labview, etc which may be able to process the data better. Further, the actual form of the input data is likely to be different, and since they are not specified here, one should not look at these programs to use them as they are, but to see the approach taken to find an answer. That in fact may be difficult, given that some of these use propriety MATLAB functions which may be obselete by the time you are looking at this, but the general idea should be there. Hopefully you wont find any mistakes, but keep in mind that you are seeing the "current" version of the program, which may have been modified for specific cases. In act, some of these programs still have the input filename specified (especially the csv files).

These first functions were written by Jan Lammerding

Main function mpt.m, which is executed to start the multiple particle tracking.

```
function ud = MPT(action, varargin)
% Multiple Particle Tracking Program with GUI
% requires the MATLAB files: gaussfit.m parabolicfit.m
forthorderfit.m
% Jan Lammerding
% 02/07/2001
% added   1) threshold for cross-correlation,
%         2) invert signal for brighfield for crosscorrelation
%         3) close result windows when exiting program

if nargin<1,
   action='InitializeMPT';
   if nargout>0  % If user wants the UserData, give it to them.
      ud = feval(action,varargin{:});
      return
   end
end

feval(action,varargin{:})
return


%-----------------------------------------------
%
% subfunction: initialize multiple particle tracking (MPT)
%
function udout = InitializeMPT()
% If MPT is already running, bring it to the foreground
```

```
h = findobj(allchild(0), 'tag', 'MPT Program');
if ~isempty(h)
   figure(h(1))
   if nargout>0
      udout = get(h(1), 'UserData');
   end
   return
end

screenD = get(0, 'ScreenDepth');
if screenD>8
   grayres=256;
else
   grayres=128;
end

MPTFig = figure('Color',[0.8 0.8 0.8], ...
   'Colormap', gray(grayres), ...
   'MenuBar','none', ...
   'BusyAction','Queue','Interruptible','off',...
   'Name','Multiple Particle Tracking Program', ...
   'Tag','MPT Program',...
   'Visible','off','Resize','off','HandleVisibility', 'on',...
   'NumberTitle','off', 'IntegerHandle', 'off', ...
   'Position',[350 230 610 460], ...
   'WindowButtonMotionFcn','MPT(''NormalMotionFcn'');',...
   'KeyPressFcn','MPT(''KeyPress'');',...
   'CloseRequestFcn','MPT(''CloseMPT'');');

ud.FigureHandle = MPTFig;
% define Standard Values
ud.Beads=0;
ud.Method=[];
ud.Filter=[];
ud.Field=[];
ud.KernelWidth=[];
ud.KernelHeight=[];
ud.SearchWidth=[];
ud.SearchHeight=[];
ud.KernelPosition=[];
ud.Pathname=pwd;
ud.Filename='MyFile';
ud.Results=[];

% handles for bead markers
ud.h.Rect=[];
ud.h.Label=[];
```

```
% define standard settings
Std.Interruptible = 'off';
Std.BusyAction = 'queue';

% Defaults for image axes
Ax = Std;
Ax.Units = 'Pixels';
Ax.Parent = MPTFig;
Ax.XTick = [];
Ax.YTick = [];
Ax.Box='on';

Img = Std;
Img.CData = [];
%Img.CDataMapping = 'Scaled';

Ctl = Std;
Ctl.Units = 'Pixels';
Ctl.Parent = MPTFig;

Btn=Ctl;
Btn.Parent = MPTFig;
Btn.Style = 'pushbutton';
Btn.Enable = 'off';

Frame = Ctl;
Frame.Style = 'Frame';

Edit = Ctl;
Edit.Style = 'edit';
Edit.HorizontalAlignment = 'right';
Edit.BackgroundColor = 'white';
Edit.ForegroundColor = 'black';

Menu = Ctl;
Menu.Style = 'Popupmenu';

Text = Ctl;
Text.Style = 'text';
Text.HorizontalAlignment = 'left';


% Frames
bgd=[0.7 0.7 0.7];
Frame1 = uicontrol(Frame, ...
   'Position',[455 125 145 320]);
```

```
Frame2 = uicontrol(Frame, ...
   'Position',[155 10 445 100]);
Frame3 = uicontrol(Frame, ...
   'BackgroundColor',bgd,...
   'Position',[ 415 63 175 40 ]);
Frame4 = uicontrol(Frame, ...
   'BackgroundColor',bgd,...
   'Position',[ 415 17 175 40 ]);

% Images
StartImg=200*ones(480,640);
StartImg(220:260,300:340)=250*rand(41,41);
Kernel=ones(20,20);

ud.h.ImageAxes = axes(Ax, ...
   'Position', [35 145 400 300]);
ud.h.ImageImage = image(StartImg, Img,...
   'Parent',ud.h.ImageAxes, ...
   'XData',[1 size(StartImg,2)],'YData',[1 size(StartImg,1)],...
   'ButtonDownFcn','MPT(''PickBead'')'); %, ...
set(ud.h.ImageImage,'XData',[1 640],'YData',[1 480]);
set(ud.h.ImageAxes,'DataAspectRatio',[1 1 1],'TickDir','in')
ud.h.TrackBox = line('XData', [], ...
   'YData', [], ...
   'Parent',ud.h.ImageAxes,...
   'Clipping', 'on', ...
   'Color', 'r', ...
   'LineStyle', '-', ...
   'EraseMode', 'xor',...
   'Visible','off');

udKernelFrame = uicontrol(Frame, ...
   'BackgroundColor',bgd,...
'Position',[54 6 53 16]);
udKernelTitel = uicontrol(Text, ...
      'BackgroundColor',bgd,...
   'Position',[56 8 49 12], ...
   'HorizontalAlignment','center', ...
   'String','Kernel');
ud.h.KernelAxes= axes(Ax, ...
   'Position', [38 24 85 85]);
ud.h.KernelImage= image(Kernel, Img, ...
   'Parent', ud.h.KernelAxes);
set(ud.h.KernelAxes,'PlotBoxAspectRatio',[1 1 1], ...
   'DataAspectRatio',[1 1 1],'XTick',[],'YTick',[],...
   'XLimMode','auto','YLimMode','auto');
ud.h.Cross= line('XData', [18 22 20 20 20], ...
```

```
    'YData', [20 20 20 18 22], ...
    'Clipping', 'on', ...
    'Color', 'r', ...
    'Parent',ud.h.KernelAxes,...
    'LineStyle', '-', ...
    'EraseMode', 'normal',...
    'Visible','off');

% Pushbuttons
ud.h.LoadData = uicontrol(Btn, ...
    'Position',[465 400 125 35], ...
    'Enable','on',...
    'String','Load Frame',...
    'Callback','MPT(''LoadFrame'')');
ud.h.LoadParameters = uicontrol(Btn, ...
    'Position',[465 347 125 35], ...
    'String','Load Parameters', ...
    'Enable','on',...
    'Callback','MPT(''LoadParameters'')');
ud.h.SaveParameters = uicontrol(Btn, ...
    'Position',[465 294 125 35], ...
    'String','Save Parameters',...
    'Callback','MPT(''SaveParameters'')');
ud.h.StartTracking = uicontrol(Btn, ...
    'Position',[465 241 125 35], ...
    'String','Start Tracking',...
    'Callback','MPT(''StartTracking'')');
udhInfo = uicontrol(Btn, ...
    'Position',[465 188 125 35], ...
    'Enable','on',...
    'String','Info',...
    'Callback','MPT(''DisplayInfo'')');
udhQuit = uicontrol(Btn, ...
    'Position',[465 135 125 35], ...
    'String','Quit', ...
    'Enable','on',...
    'Callback','MPT(''CloseMPT'')');
ud.h.Prev = uicontrol(Btn, ...
    'Position',[165 80 115 22], ...
    'String','Prev',...
    'Callback','MPT(''PreviousBead'')');
ud.h.Next = uicontrol(Btn, ...
    'Position',[165 18 115 22], ...
    'String','Next',...
    'Callback','MPT(''NextBead'')');
h1 = uicontrol(Text, ...
    'FontWeight','bold', ...
```

```
    'Position',[165 47 40 26], ...
    'String',['Curr.';'Bead ']);
ud.h.CurrentBead = uicontrol(Edit, ...
    'Position',[205 47 25 26], ...
    'String','1',...
    'Callback','MPT(''ChangeBead'')');
ud.h.Delete = uicontrol(Btn, ...
    'Position',[240 47 40 26], ...
    'String','Delete',...
    'Callback','MPT(''DeleteBead'')');
ud.h.Method = uicontrol(Menu, ...
    'Position',[290 77 115 25], ...
    'String',{'Center of Mass','Gauss','Parabolic','4th Order
Polynomial'}, ...
    'Value',1,...
    'Callback','MPT(''ChangeParameters'')');
ud.h.Filter = uicontrol(Menu, ...
    'Position',[290 46 115 25], ...
    'String',{'No Filter','Threshold Filter'}, ...
    'Value',2,...
    'Callback','MPT(''ChangeParameters'')');
ud.h.Field = uicontrol(Menu, ...
    'Position',[290 15 115 25], ...
    'String',{'Brightfield','Darkfield'}, ...
    'Value',1,...
    'Callback','MPT(''ChangeParameters'')');
h1 = uicontrol(Text, ...
    'BackgroundColor',bgd,...
'Position',[420 72 63 20], ...
    'String','Kernel Size');
h1 = uicontrol(Text, ...
    'BackgroundColor',bgd,...
    'Position',[490 81 33 20], ...
    'String','Width');
h1 = uicontrol(Text, ...
    'BackgroundColor',bgd,...
    'Position',[545 81 33 20], ...
    'String','Height');
ud.h.KernelWidth = uicontrol(Edit, ...
    'Position',[490 67 33 20], ...
    'String','20',...
    'Callback','MPT(''ChangeParameters'')');
ud.h.KernelHeight = uicontrol(Edit, ...
    'Position',[545 67 33 20], ...
    'String','20',...
    'Callback','MPT(''ChangeParameters'')');
h1 = uicontrol(Text, ...
```

```
    'Position',[420 26 63 20], ...
    'BackgroundColor',bgd,...
    'String','Search Area');
h1 = uicontrol(Text, ...
    'Position',[545 35 33 20], ...
    'BackgroundColor',bgd,...
    'String','Height');
h1 = uicontrol(Text, ...
    'Position',[490 35 33 20], ...
    'BackgroundColor',bgd,...
    'String','Width');
ud.h.SearchHeight = uicontrol(Edit, ...
    'Position',[545 21 33 20], ...
    'String','40',...
    'Callback','MPT(''ChangeParameters'')');
ud.h.SearchWidth = uicontrol(Edit, ...
    'Position',[490 21 33 20], ...
    'String','30',...
    'Callback','MPT(''ChangeParameters'')');
set(MPTFig, 'Userdata', ud);
%set(MPTFig, 'visible','on','HandleVisibility','callback');
set(MPTFig, 'visible','on');

if nargout>0
   udout = ud;
end
return



% --------------------------------
% my own subfunctions

%%  Sub-Function - NormalMotionFcn
%%
function NormalMotionFcn
% Set the cursor to a Cross-Hair when above the Original image,
and back
% to an arrow when not.
% This is the normal motion function for the window when we are
not in
% a MyGetline selection state.
DemoFig = gcbf;
ud = get(DemoFig, 'Userdata');
pos = get(ud.h.ImageAxes, 'Position');
pt = get(DemoFig, 'CurrentPoint');
```

```
x = pt(1,1);
y = pt(1,2);
if (x>pos(1) & x<pos(1)+pos(3) & y>pos(2) & y<pos(2)+pos(4))
   %set(DemoFig, 'Pointer', 'cross');
   set(DemoFig,'Pointer','crosshair');
   % follow mouse with rectangle
   pt2 = get(ud.h.ImageAxes, 'CurrentPoint');
   KX=str2num(get(ud.h.KernelWidth,'String'));
   KY=str2num(get(ud.h.KernelHeight,'String'));
   KernelX=pt2(1,1);
   KernelY=pt2(1,2);
   X=[KernelX-KX/2 KernelX+KX/2 KernelX+KX/2 KernelX-KX/2
KernelX-KX/2];
   Y=[KernelY-KY/2 KernelY-KY/2 KernelY+KY/2 KernelY+KY/2
KernelY-KY/2];
   set([ud.h.TrackBox], 'XData', X, 'YData', Y);
   set([ud.h.TrackBox], 'Visible','on');
else
   set(DemoFig, 'Pointer', 'arrow');
   % hide box
   set([ud.h.TrackBox],'Visible','off')
end


%% Sub-Function - CloseMPT
%%
function CloseMPT
% Close request function for the MPT program
% User-defined close request function
% to display a question dialog box
selection = questdlg('Do you really want to quit ?',...
   'Quit MPT Request',...
   'Yes','No','Yes');
%selection = 'Yes';
switch selection,
case 'Yes',
   delete(gcf)
   for i=1:4
      h = findobj(allchild(0), 'tag', ['MPT Results'
num2str(i)]);
      if ~isempty(h)      % close Result windows
         close(h)
      end
   end
case 'No'
   return
end
```

```
%%%
%%%  Sub-Function - PickBead
%%%

function PickBead
DemoFig = gcbf;
ud = get(DemoFig, 'UserData');

pt = round(get(gca, 'CurrentPoint'));
N=str2num(get(ud.h.CurrentBead,'String'));
Beads=ud.Beads;
KX=str2num(get(ud.h.KernelWidth,'String'));
KY=str2num(get(ud.h.KernelHeight,'String'));

KernelX=pt(1,1);
KernelY=pt(1,2);
RectX=[KernelX-KX/2 KernelX+KX/2 KernelX+KX/2 KernelX-KX/2
KernelX-KX/2];
RectY=[KernelY-KY/2 KernelY-KY/2 KernelY+KY/2 KernelY+KY/2
KernelY-KY/2];

% check if bead exists
if N>ud.Beads       % new bead
   ud.Beads=N;
else              % erase old bead and overwrite properties
   delete(ud.h.Label(N));
   delete(ud.h.Rect(N));
end

% Initialize the rectangles to mark beads
ud.h.Rect(N) = line('XData', RectX, ...
   'YData', RectY, ...
   'Parent', ud.h.ImageAxes, ...
   'Clipping', 'on', ...
   'Color', 'b', ...
   'LineStyle', '-', ...
   'EraseMode', 'normal');       % change this back to xor and
use 'k' as color
%ud.h.Label(N) =
text(RectX(3)+2,RectY(3),num2str(N),'EraseMode','xor');
ud.h.Label(N) = text(RectX(3)+2,RectY(3),num2str(N), ...
   'Parent',ud.h.ImageAxes','EraseMode','normal','color','b');
%set(ud.h.Label(N),'Color','b')
ud.Method(N)=get(ud.h.Method,'Value');
```

```
ud.Filter(N)=get(ud.h.Filter,'Value');
ud.Field(N)=get(ud.h.Field,'Value');
ud.KernelWidth(N)=KX;
ud.KernelHeight(N)=KY;
ud.SearchWidth(N)=str2num(get(ud.h.SearchWidth,'String'));
ud.SearchHeight(N)=str2num(get(ud.h.SearchHeight,'String'));
ud.KernelPosition(1:2,N)=[KernelX; KernelY];

% update userdata:
set(ud.h.TrackBox,'XData',get(ud.h.TrackBox,'XData')-1000);    %
to avoid overlapping !
set(ud.h.CurrentBead,'String',num2str(N+1));
set([ud.h.Prev ud.h.SaveParameters
ud.h.StartTracking],'Enable','on')
set([ud.h.Next ud.h.Delete],'Enable','off');
set(DemoFig, 'UserData', ud);
UpdateKernel



%%
%% Sub-Function LoadFrame
function LoadFrame
DemoFig = gcbf;
ud = get(DemoFig, 'UserData');
[filename, pathname]=uigetfile('*.bmp','Load 1st Frame');
if filename
   set(DemoFig,'Pointer','watch')
   frame=[];
   file=fullfile(pathname,filename);
   frame=imread(file);
   % update Userdata
   img = double(frame);
   ud.Pathname=pathname;
   ud.Filename=filename;
   set(ud.h.ImageImage, 'Cdata', img,...
      'XData',[1 size(frame,2)],'YData',[1 size(frame,1)]);
  set(ud.h.ImageAxes,'XLim',[1 size(frame,2)],'YLim',[1
size(frame,1)]);
   set(DemoFig,'UserData',ud);
   UpdateNumbers
   UpdatePopup
   UpdateKernel
   NormalMotionFcn
end
```

```
%%
%% Sub-function SaveParameters
function SaveParameters
DemoFig = gcbf;
ud = get(DemoFig, 'UserData');
oldDir=cd;   % remember old directory
cd(ud.Pathname);
[path, name, ext, ver]=fileparts(ud.Filename);
initfile=[name '_parameters' '.mat'];
[filename, pathname]=uiputfile(initfile,'Save Parameters');
%reset directory to old directory:
cd(oldDir);
if filename
   file=fullfile(pathname,filename);
   % prepare filestructure
   data=ud; data.FigureHandle=[]; data.h=[]; data.Results=[];
   save(file,'data');
end


%%
%% Sub-function LoadParameters
function LoadParameters
DemoFig = gcbf;
ud = get(DemoFig, 'UserData');
oldDir=cd;
cd(ud.Pathname);
[filename, pathname]=uigetfile('*.mat','Load Parameters');
cd(oldDir);
if filename
   set(DemoFig,'Pointer','watch')
   data=[];
   file=fullfile(pathname,filename);
   load(file)
   % erase old bead markers
   for i=1:ud.Beads
      delete(ud.h.Label(i));
      delete(ud.h.Rect(i));
   end
   ud.h.Rect=[];
   ud.h.Label=[];

   % update Userdata
   data.h=ud.h; data.FigureHandle=ud.FigureHandle;      % keep
Figurehande and guicontrols
```

```
    ud=data;
    set(DemoFig,'UserData',ud);
    set(ud.h.CurrentBead,'String','1')
    % update enable buttons
    set([ud.h.Next ud.h.Delete ud.h.StartTracking
ud.h.SaveParameters],'Enable','on');
    set(ud.h.Prev,'Enable','off')
    if ud.Beads<=1
       set(ud.h.Next,'Enable','off')
    end
    % update kernels
    for i=1:ud.Beads
       KernelX=ud.KernelPosition(1,i);
       KernelY=ud.KernelPosition(2,i);
       KX=ud.KernelWidth(1,i);
       KY=ud.KernelHeight(1,i);
       RectX=[KernelX-KX/2 KernelX+KX/2 KernelX+KX/2 KernelX-KX/2
KernelX-KX/2];
       RectY=[KernelY-KY/2 KernelY-KY/2 KernelY+KY/2 KernelY+KY/2
KernelY-KY/2];
       ud.h.Rect(i) = line('XData', RectX, ...
          'YData', RectY, ...
          'Clipping', 'on', ...
          'Parent', ud.h.ImageAxes, ...
          'Color', 'b', ...
          'LineStyle', '-', ...
          'EraseMode', 'normal');   % this used to be xor and
color 'k'
       ud.h.Label(i) = text(RectX(3)+2,RectY(3),num2str(i), ...
          'Parent', ud.h.ImageAxes, 'EraseMode','normal');
       set(ud.h.Label(i),'Color','b')
    end
    set(DemoFig,'UserData',ud);
    UpdateNumbers
    UpdatePopup
    UpdateKernel
    NormalMotionFcn
end

%%
%% Sub-Function DisplayInfo
function DisplayInfo
str={'Getting started' ...
       ['Load the first frame of the sequence you want to perform
the multiple   '
       'particle tracking on. Set the parameters (Centroid
determination method,'
```

```
      'filter, etc.) to the appropiate settings and then select
the beads you  '
      'want to track by clicking on them with the left mouse
button. You can   '
      'modify the parameters for each bead by using the <Prev>
or <Next> button'
      'to go to the bead and then adjust the parameters. The
kernel image will '
      'be updated immediately.
'
      'When done, save the current parameters (Kernel positions
and settings)  '
      'and press <Start Tracking> to begin tracking. You will be
prompted to   '
      'enter the file to which the results are save. If you hit
<cancel>, the  '
      'results will not be saved.
'];...
      'Parameters' ...
      ['The following parameters can be selected for each bead
'
      '
'
      'Center of Mass:  The centroid position is calculated
based on the center'
      '                 of mass (the intensity). This is the
fastest and most  '
      '                 robust algorithm, but not the most
accurate on.        '
      'Gauss:           Fits 2-dimensional Gauss-distribution to
kernel        '
      '                 intensity to determine the center
location based on    '
      '                 iterative least-square fit.
'
      'Parabolic:       Fits 2nd order polynomial to kernel
intensity map to   '
      '                 determine center location based on least
square fit.   '
      '4th Order Poly:  Fits 4th order polynomial to kernel
intensity map to   '
      '                 determine center location based on least
square fit.   '
      '
'
      'Kernel size:     The kernel size in pixels. Kernels are
centered around '
```

```
      '                    the point that was selected with the
mouse.              '
      'Search area:        Area for which the cross-correlation is
performed to    '
      '                    identify the matching kernel in the
following frame.    '
      '                    The search area is centered around the
kernel.          '
      '
'];...
      'File format' ...
      ['Image file:         Frames should be grayscale images of
type ".bmp", with '
      '                    intensity values ranging from 0 (black)
to 255 (white).'
      'Parameter file:     File thatcontains the kernel positions
and settings.    '
      '                    This is a MATLAB ".mat" file.
'
      'Result file:        Results are saved as comma-separated-
value (*.csv)      '
      '                    files. Each bead is represented by a
pair of columns.   '
      '                    The first column contains the x-position
for the first '
      '                    bead, the second column the y-position.
Each row        '
      '                    represents the position for one frame.
']};
helpwin(str,'Getting started','Multiple Particle Tracking
Program')


%%
%% Sub-function FindCenter
function
CenterPosition=FindCenter(KernelImg,method,field,filter)
% N: Bead Number
% KernelImg: bitmap of kernel
% method: 1: center of mass, 2: gauss, 3: parabolic, 4: 4th
order polyn
% field: 1: brightfield 2: darkfield
% filter: 1: no filter, 2: threshold filter
% center is being expressed relative to kernel (topleft=1,1)
% requires the files gaussfit.m, parabolicfit.m, and
forthorderfit.m
```

```
%%
if field==1                          %  invert image for bright field
images
   KernelData=max(max(KernelImg))-KernelImg;
else
   KernelData=KernelImg;
end
if filter==2                      % Threshold filter
   T=mean(mean(KernelData));        % use mean as Threshold
   KernelData(KernelData<T)=0;      % set values below threshold
to zero
end

% set iteration tol (1e-6) and max iteration (1000):
opt=zeros(1,14); opt(1:3)=[0 1e-6 1e-6]; opt(14)=1000;
% use estimate for center:
[h w]=size(KernelData);             % determine size of kernel
%%switch ud.Method(N)
switch method
case 1
   % CENTER OF MASS FIT
   [x,y]=meshgrid(1:w,1:h);
   xc=sum(sum(x.*KernelData))/(sum(sum(KernelData)+eps)); %
compute center of intensity
   yc=sum(sum(y.*KernelData))/(sum(sum(KernelData)+eps));
case 2
   % GAUSSIAN FIT
   C0=[w/2 h/2 1 max(max(KernelData))/1.995];     % start values
for iteration
   center=fmins('gaussfit',C0,opt,[],KernelData);
   xc=center(1);
   yc=center(2);
case 3
   % PARABOLIC FIT
   C0=[w/2 h/2 1 max(max(KernelData))];
   center=fmins('parabolicfit',C0,opt,[],KernelData);
   xc=center(1);
   yc=center(2);
case 4
   %4th ORDER FIT
   C0=[w/2 h/2 1 1 max(max(KernelData))];
   center=fmins('forthorderfit',C0,opt,[],KernelData);
   xc=center(1);
   yc=center(2);
otherwise                  % invalid method selection
   disp('invalid method selection')
   xc=-1;
```

```
   yc=-1;
end
if (xc<1 | xc>w | yc<1 | yc>h)      % return -1,-1 in case of
invalid results
   xc=-1;
   yc=-1;
end
CenterPosition=[xc; yc];


%%
%% Sub-function KeyPress
function KeyPress
DemoFig = gcbf;
ud = get(DemoFig, 'UserData');
key = real(get(DemoFig, 'CurrentCharacter'));
if isempty(key), % switch statement was triggering error in
Unix, the
   return;        % "Shift" key was causing the variable key to
be []
end
switch key
case {8, 127}  % delete and backspace keys
   PreviousBead      % same as prev-bead
case {13, 3}    % enter and return keys
   NextBead
case 27       % escape key
   CloseMPT       %??
end


%%
%% Sub-Function PreviousBead
function PreviousBead
DemoFig = gcbf;
ud = get(DemoFig, 'UserData');
N=str2num(get(ud.h.CurrentBead,'string'))-1;
if N>=1    % make sure that current bead>=1
   set(ud.h.CurrentBead,'String',num2str(N));
   % if N<ud.Beads
   % set([ud.h.Label(N+1) ud.h.Rect(N+1)],'Color','b');
   % end
   %set([ud.h.Label(N) ud.h.Rect(N)],'Color','r');
   set([ud.h.Next ud.h.Delete],'Enable','on')
   UpdatePopup
   UpdateNumbers
   UpdateKernel
```

```
end
if N==1    % disable prev-button once bead #1 is reached
   set(ud.h.Prev,'Enable','off');
end


%%
%% Sub-Function PreviousBead
function NextBead
DemoFig = gcbf;
ud = get(DemoFig, 'UserData');
N=str2num(get(ud.h.CurrentBead,'string'))+1; %increase
beadnumber by 1
if N<=ud.Beads+1  % make sure that current bead<total beads
   set(ud.h.CurrentBead,'String',num2str(N));
   % set([ud.h.Label(N-1) ud.h.Rect(N-1)],'Color','b');
   % set([ud.h.Label(N) ud.h.Rect(N)],'Color','r');
   set(ud.h.Prev,'Enable','on');
   % highlight selected kernel
   UpdatePopup
   UpdateNumbers
   UpdateKernel
end
if (N==ud.Beads+1)     % disable next-button once new bead
(last+1) is reached
   set([ud.h.Next ud.h.Delete],'Enable','off');
end


%%
%% Sub-function UpdateKernel
function UpdateKernel
DemoFig = gcbf;
ud = get(DemoFig, 'UserData');
N=str2num(get(ud.h.CurrentBead,'string'));
if N<=ud.Beads      % only display kernel if bead has been
picked
   KernelX=ud.KernelPosition(1,N);
   KernelY=ud.KernelPosition(2,N);
   KX=ud.KernelWidth(N);
   KY=ud.KernelHeight(N);
   FrameImg=get(ud.h.ImageImage,'Cdata');
   [maxY,maxX]=size(FrameImg);      % determine max values from
frame size
   LeftX=max([round(KernelX-KX/2) 1]);
   RightX=min([round(KernelX+KX/2) maxX]);
   TopY=max([1 round(KernelY-KY/2)]);
```

```
   BottomY=min([round(KernelY+KY/2) maxY]);
   KernelImg=FrameImg(TopY:BottomY,LeftX:RightX);
else
   KX=str2num(get(ud.h.KernelWidth,'string'));
   KY=str2num(get(ud.h.KernelHeight,'string'));
   KernelImg=ones(KY,KX);
   set(ud.h.Cross,'Visible','off');

end
[h,w]=size(KernelImg);
set(ud.h.KernelImage, 'Cdata', KernelImg,'XData',[1
w],'YData',[1 h]);

% mark centroid position
if N<=ud.Beads
   %function
CenterPosition=FindCenter(KernelImg,method,field,filter)

C=FindCenter(KernelImg,ud.Method(N),ud.Field(N),ud.Filter(N));
   if C~=[-1; -1] % in case we found a center
      %C=[h/2; w/2];     % center position
      s=2;              % size of centroid marker
      set(ud.h.Cross,'XData', [C(1)-s C(1)+s C(1) C(1) C(1)],
...
         'YData', [C(2) C(2) C(2) C(2)-s C(2)+s], ...
         'Visible','on');
   else
      set(ud.h.Cross,'Visible','off');
      %nocenter=text(w/4,h/2,['no center'; '  found
'],'Color','r','Parent',ud.KernelAxes)
   end
end



%%
%% Sub-function UpdatePopup
function UpdatePopup
DemoFig = gcbf;
ud = get(DemoFig, 'UserData');
N=str2num(get(ud.h.CurrentBead,'string'));
if N<=ud.Beads      % only update Popups if bead has been picked
   set(ud.h.Method,'Value',ud.Method(N));
   set(ud.h.Filter,'Value',ud.Filter(N));
   set(ud.h.Field,'Value',ud.Field(N));
end
```

```
%%
%% Sub-function UpdateNumbers
function UpdateNumbers
DemoFig = gcbf;
ud = get(DemoFig, 'UserData');
N=str2num(get(ud.h.CurrentBead,'string'));
if N<=ud.Beads      % only update Numbers if bead has been
picked
   set(ud.h.KernelWidth,'String',num2str(ud.KernelWidth(N)));
   set(ud.h.KernelHeight,'String',num2str(ud.KernelHeight(N)));
   set(ud.h.SearchWidth,'String',num2str(ud.SearchWidth(N)));
   set(ud.h.SearchHeight,'String',num2str(ud.SearchHeight(N)));
end


%%
%% Sub-function ChangeBead
function ChangeBead
DemoFig = gcbf;
ud = get(DemoFig, 'UserData');
N=str2num(get(ud.h.CurrentBead,'string'));
N=median([1 N ud.Beads+1]);   % make sure that bead# is in
allowed range
set(ud.h.CurrentBead,'String',num2str(N));
set([ud.h.Prev ud.h.Next ud.h.Delete],'Enable','on');
if N==1;
   set(ud.h.Prev,'Enable','off');
end
if N==ud.Beads+1;
   set([ud.h.Next ud.h.Delete],'Enable','off');
end
UpdatePopup
UpdateNumbers
UpdateKernel      % update Kernel


%%
%% Sub-function ChangeParameters
function ChangeParameters
DemoFig = gcbf;
ud = get(DemoFig, 'UserData');
N=str2num(get(ud.h.CurrentBead,'string'));
if N<=ud.Beads
   ud.Method(N)=get(ud.h.Method,'Value');
   ud.Filter(N)=get(ud.h.Filter,'Value');
   ud.Field(N)=get(ud.h.Field,'Value');
```

```
    ud.KernelWidth(N)=str2num(get(ud.h.KernelWidth,'String'));
    ud.KernelHeight(N)=str2num(get(ud.h.KernelHeight,'String'));
    ud.SearchWidth(N)=str2num(get(ud.h.SearchWidth,'String'));
    ud.SearchHeight(N)=str2num(get(ud.h.SearchHeight,'String'));
    % update kernelmarker rectangle
    KernelX=ud.KernelPosition(1,N);
    KernelY=ud.KernelPosition(2,N);
    KX=ud.KernelWidth(N);
    KY=ud.KernelHeight(N);
    RectX=[KernelX-KX/2 KernelX+KX/2 KernelX+KX/2 KernelX-KX/2
KernelX-KX/2];
    RectY=[KernelY-KY/2 KernelY-KY/2 KernelY+KY/2 KernelY+KY/2
KernelY-KY/2];
    set(ud.h.Rect(N),'XData',RectX,'YData',RectY);
    set(ud.h.Label(N),'Position',[RectX(3)+2, RectY(3)]);

    % update label positions
    set(DemoFig,'UserData',ud)
    UpdateKernel
end


%%
%% Sub-function DeleteBead
function DeleteBead
DemoFig = gcbf;
ud = get(DemoFig, 'UserData');
N=str2num(get(ud.h.CurrentBead,'string'));
if N<=ud.Beads
    ud.Beads=ud.Beads-1;
    ud.Method=[ud.Method(1:N-1) ud.Method(N+1:end)];
    ud.Filter=[ud.Filter(1:N-1) ud.Filter(N+1:end)];
    ud.Field=[ud.Field(1:N-1) ud.Field(N+1:end)];
    ud.KernelWidth=[ud.KernelWidth(1:N-1)
ud.KernelWidth(N+1:end)];
    ud.KernelHeight=[ud.KernelHeight(1:N-1)
ud.KernelHeight(N+1:end)];
    ud.SearchWidth=[ud.SearchWidth(1:N-1)
ud.SearchWidth(N+1:end)];
    ud.SearchHeight=[ud.SearchHeight(1:N-1)
ud.SearchHeight(N+1:end)];
    ud.KernelPosition=[ud.KernelPosition(:,1:N-1)
ud.KernelPosition(:,N+1:end)];
    delete(ud.h.Rect(N));
    delete(ud.h.Label(N));
    ud.h.Rect=[ud.h.Rect(1:N-1) ud.h.Rect(N+1:end)];
    ud.h.Label=[ud.h.Label(1:N-1) ud.h.Label(N+1:end)];
```

```
    set(DemoFig,'UserData',ud)
    if N>ud.Beads;   %in case we deleted the most recent bead
       set(ud.h.CurrentBead,'String',num2str(max([1 ud.Beads])));
    end
    if ud.Beads==0;
       set([ud.h.Delete ud.h.Next],'Enable','off')
    end
    if ud.Beads==1;
       set(ud.h.Prev,'Enable','off')
    end
    % update Labels
    for i=N:ud.Beads
       set(ud.h.Label(i),'String',num2str(i));
    end
    UpdateKernel
    UpdateNumbers
    UpdatePopup
end


%%
%% Sub-function FindNextFile
function [filename,num]=FindNextFile(currfile)
[path,fnamsh,ext]=fileparts(currfile);
%determine current file number
i=1;
%while str2num(fnamsh(end-i:end))
while length(str2num(fnamsh(end-i:end)))
   i=i+1;
end
num=str2num(fnamsh(end-i+1:end));
if num    % only perform analysis if file contains number in the
filename
   % determine the following number
   n=num+1;
   N=length(num2str(n));
   nextfile1=[fnamsh(1:end-N) num2str(n) ext];
   if mod(log10(n),1)
      nextfile2=nextfile1;
   else
      nextfile2=[fnamsh(1:end-N+1) num2str(n) ext];
   end
   if exist(fullfile(path,nextfile1))==2
      filename=fullfile(path,nextfile1);
   elseif exist(fullfile(path,nextfile2))==2
      filename=fullfile(path,nextfile2);
   else
```

```
      filename='-1';
   end
else
   filename='-1';
   num=-1;
end


%%
%% Sub-function CountFrames
function Frames=CountFrames(filename,pathname)
n=0;
nextname=fullfile(pathname,filename);
while (~strcmp(nextname,'-1') & n<10000)
   n=n+1;
   prevname=nextname;
   nextname=FindNextFile(prevname);
end
Frames=n;


%%
%% ------------------------------
%% Sub-Function StartTracking
function StartTracking
DemoFig = gcbf;
ud = get(DemoFig, 'UserData');
% Select File to save Results to
oldDir=cd;   % remember old directory
cd(ud.Pathname);
[path, name, ext, ver]=fileparts(ud.Filename);
initfile=[name '_Results' '.csv'];
[filename, pathname]=uiputfile(initfile,'Save Results to');
%reset directory to old directory:
cd(oldDir);
%if filename
set(DemoFig,'Pointer','Watch')   % set pointer to hour-glass
ud.Frames=CountFrames(ud.Filename, ud.Pathname);       % get
number of frames
if ud.Frames>1
   ud.Results=[]; % clear old results
   set(DemoFig,'UserData',ud)
   ParticleTracking    % perform particleTracking
   % get results from UserData
   if filename         % save results if user selected filename
      ud = get(DemoFig, 'UserData');
      % prepare filestructure
```

```
      ResultData=[];      % might change this into correct
structure !!!!
      ResultData=ud.Results;
      file=fullfile(pathname,filename);
      csvwrite(file,ResultData);
   end
   DisplayResults
else
   disp('Warning: need more than one Frame')
end
NormalMotionFcn      % reset pointer
%end


%%
%% Sub-Function ParticleTracking
function ParticleTracking
DemoFig = gcbf;
ud = get(DemoFig, 'UserData');

NFrames=ud.Frames;              % number of frames
filename=fullfile(ud.Pathname,ud.Filename);
%ext='.bmp';            % extension for image type
Nbead=ud.Beads;                 % number of beads

% OPEN 1st IMAGE
currentFrame=imread(filename);

kernels=[];     % structure to store kernel images
LeftX=[];
TopY=[];

FrameImg=get(ud.h.ImageImage,'Cdata');
[maxY,maxX]=size(FrameImg);    % determine max values from frame
size
for N=1:Nbead
   % store kernel data
   KernelX=ud.KernelPosition(1,N);
   KernelY=ud.KernelPosition(2,N);
   KX=ud.KernelWidth(N);
   KY=ud.KernelHeight(N);
   LeftX(N)=max([round(KernelX-KX/2) 1]);
   RightX=min([round(KernelX+KX/2) maxX]);
   TopY(N)=max([1 round(KernelY-KY/2)]);
   BottomY=min([round(KernelY+KY/2) maxY]);
   %KernelImg=FrameImg(TopY:BottomY,LeftX:RightX);
   kernels{N}=FrameImg(TopY(N):BottomY,LeftX(N):RightX);
```

```
end
% store kernels for later comparison
ud.h.firstKernels=kernels;

% INITIALIZE RESULT VARIABLES
center=zeros(NFrames,2*Nbead);
ud.h.CrosscorrelationResults=zeros(NFrames-1,Nbead);

for N=1:Nbead
   % COMPUTE CENTER OF BEAD
   kernel=kernels{N};
   offset=[LeftX(N)-1; TopY(N)-1];

KernelCenter=FindCenter(kernel,ud.Method(N),ud.Field(N),ud.Filte
r(N))+offset;
   center(1,2*N-1:2*N)=KernelCenter.';        % store first
position
   % calculate starting point for cross correlation
   StartX(N)=LeftX(N)-round(ud.SearchWidth(N)/2);       %
starting point x
   StartY(N)=TopY(N)-round(ud.SearchHeight(N)/2);       %
starting point y
end

disp('Performing particle tracking, please wait.')
disp(char(['Frame: ' num2str(1) ' out of ' num2str(NFrames)]))
tic  % start measuring computation time

% PERFORM PARTICLE TRACKING FOR IMAGES 2-NFrames
for n=2:NFrames
   disp(char(['Frame: ' num2str(n) ' out of '
num2str(NFrames)]))
   % open next image
   filename=FindNextFile(filename);
   currentFrame=imread(filename);
   for N=1:Nbead
      kernel=double(kernels{N});
      if ud.Field(N)==1     % in case of Brightfield
         kernel=255-kernel;    % invert kernel intensity
      end
      avg1=mean(mean(kernel));      % compute mean intensity of
kernel

      % added on 2/6/01
      if ud.Filter(N)==2                    % Threshold filter
         T=avg1;       % use mean as Threshold
```

```
         kernel(kernel<T)=0;     % set values below threshold to
zero
      end

      % CROSS-CORRELATION

CrossCorrelation=zeros(ud.SearchHeight(N),ud.SearchWidth(N));
      % compute cross correlation c for every point in search
area
      for i=1:ud.SearchWidth(N)
         for j=1:ud.SearchHeight(N)
            Xl=StartX(N)+i;         % left Corner of cross-
correlation window
            Xr=Xl+size(kernel,2)-1;   % right corner of cross-
correlation window
            Yt=StartY(N)+j;         % top corner of cross-
correlation window
            Yb=Yt+size(kernel,1)-1;   % bottom corner of cross-
correlation window
            % WARNING!!!!!
            % make sure that index does not exceed dimensions of
frame!
            if (Xl>=1 & Xr<=maxX & Yt>=1 & Yb<=maxY)
               testKernel=double(currentFrame(Yt:Yb,Xl:Xr));
               avg2=mean(mean(testKernel));
               if ud.Field(N)==1        % invert signal for
brightfield
                  testKernel=255-testKernel;
                  avg2=255-avg2;
               end

               if ud.Filter(N)==2                    % Threshold
filter
                  T=avg2;        % use mean as Threshold
                  testKernel(testKernel<T)=0;     % set values
below threshold to zero
               end


               CrossCorrelation(j,i)=sum(sum((testKernel-
avg2).*(kernel-avg1)));
            else
               CrossCorrelation(j,i)=NaN;
            end
         end
      end
```

```
      % determine bead center:
      % find correlation maximum
      [i,j]=find(CrossCorrelation==max(max(CrossCorrelation)));
      if (length(i)==1 & length(j)==1)     % check if there is a
unique peak
         Xleft=StartX(N)+j;                        % compute
matching kernel x-position
         Ytop=StartY(N)+i;                         % compute
matching kernel y-position
         % store peak cross-correlation result
      else
         disp(char(['Warning: Could not find unique correlation
peak for bead ' ...
               num2str(N)]))
         Xleft=max([1 StartX(N)]);
         Ytop=max([1 StartY(N)]);
      end
      maxCorrelation=sum(sum((kernel-mean(mean(kernel))).^2));
      ud.h.CrosscorrelationResults(n-
1,N)=max(max(CrossCorrelation))/maxCorrelation;


      % matching kernel from best cross-correlation fit
      matchedKernel=currentFrame(Ytop:Ytop+ud.KernelHeight(N),
...
         Xleft:Xleft+ud.KernelWidth(N));
      offset=[Xleft-1; Ytop-1];
      newCenter=FindCenter(double(matchedKernel), ...
         ud.Method(N),ud.Field(N),ud.Filter(N))+offset;

      % update Sx,Sy, kernel
      StartX(N)=Xleft-round(ud.SearchWidth(N)/2);      %
starting point x
      StartY(N)=Ytop-round(ud.SearchHeight(N)/2);      %
starting point y
      kernels{N} = matchedKernel;     % update kernel

      % store results
      center(n,2*N-1:2*N)=newCenter.';
   end
end

toc  % display calculation time
% store results
ud.h.lastFile=filename;
ud.h.lastKernels=kernels;
ud.Results=center;
```

```
set(DemoFig,'UserData',ud);


%%
%% Sub-function DisplayResults
function DisplayResults
   std.Color=[0.8 0.8 0.8];
   std.MenuBar='none';
   std.NumberTitle='off';
   std.BusyAction='queue';
   std.Interruptible='off';
   %std.Visible='off';
   std.Resize='on';
   std.HandleVisibility='on';
   std.IntegerHandle='off';
   % check if windows already exist
h = findobj(allchild(0), 'tag', 'MPT Results1');
if ~isempty(h)
   MPTResults1=figure(h(1));
   %set(MPTResults1,'Visible','off')
else
   MPTResults1 = figure(std, 'Name','MPT Results 1: First & Last
Frame', ...
      'Tag','MPT Results1');
end
h = findobj(allchild(0), 'tag', 'MPT Results2');
if ~isempty(h)
   MPTResults2=figure(h(1));
   %set(MPTResults2,'Visible','off')
else
   MPTResults2 = figure(std, 'Name','MPT Results 2: Kernel
Information', ...
      'Tag','MPT Results2');
end
h = findobj(allchild(0), 'tag', 'MPT Results3');
if ~isempty(h)
   MPTResults3=figure(h(1));
   %set(MPTResults3,'Visible','off')
else
   MPTResults3 = figure(std, 'Name','MPT Results 3: Cross-
Correlation Results', ...
      'Tag','MPT Results3');
end
h = findobj(allchild(0), 'tag', 'MPT Results4');
if ~isempty(h)
   MPTResults4=figure(h(1));
   %set(MPTResults4,'Visible','off')
```

```
else
   MPTResults4 = figure(std, 'Name','MPT Results 4: Centroid
Positions', ...
      'Tag','MPT Results4');
end


% access results
DemoFig = gcbf;
ud = get(DemoFig, 'UserData');
center=ud.Results;
CrossCorrelation=ud.h.CrosscorrelationResults;
Nbeads=ud.Beads;
NFrames=ud.Frames;
firstFile=fullfile(ud.Pathname,ud.Filename);
lastFile=ud.h.lastFile;


% DISPLAY first and last IMAGE
firstFrame=imread(firstFile);
lastFrame=imread(lastFile);
figure(MPTResults1)
subplot(2,1,1)
imagesc(firstFrame)
colormap(gray)
axis('image')
title('First Frame')
for N=1:Nbeads
   text(center(1,N*2-1),center(1,N*2),num2str(N),'Color','r')
end
subplot(2,1,2)
imagesc(lastFrame)
colormap(gray)
axis('image')
title('Last Frame')
for N=1:Nbeads
   text(center(end,N*2-
1),center(end,N*2),num2str(N),'Color','r')
end


% DISPLAY KERNEL
figure(MPTResults2)
clf
for n=1:Nbeads
   firstKernel=ud.h.firstKernels{n};     % retrieve kernel
information from kernels
```

```
    lastKernel=ud.h.lastKernels{n};
    subplot(2,Nbeads,n)
    imagesc(firstKernel)
    axis('image'); title(char(['Kernel ' num2str(n)]))
    colormap(gray)
    subplot(2,Nbeads,Nbeads+n)
    imagesc(lastKernel)
    axis('image'); title(char(['Kernel ' num2str(n)]))
    colormap(gray)
end
subplot(2,Nbeads,round(Nbeads/2))
xlabel('First Frame')
subplot(2,Nbeads,round(Nbeads*3/2))
xlabel('Last Frame')

% PLOT CROSS-CORRELATION PEAK RESULTS
figure(MPTResults3)
steps=[1:NFrames-1];
for N=1:Nbeads
    subplot(Nbeads,1,N)
    plot(steps,CrossCorrelation(:,N))
    text(1.2,0.1,['Bead ' num2str(N)])
    axis([1 NFrames-1 0 1.1])
    %xlabel('step'); ylabel('peak cross-correlation')
end
subplot(Nbeads,1,Nbeads); xlabel('step')
subplot(Nbeads,1,round(Nbeads/2)); ylabel('peak cross-
correlation')

figure(MPTResults4)
clf
frame=[1:NFrames];
subplot(2,1,1)
hold on
for N=1:Nbeads
    plot(frame,center(:,2*N-1),'bo',frame,center(:,2*N-1),'r:')
    text(frame(end),center(end,2*N-1),['Bead ' num2str(N)]);
end
hold off
title('Bead Center x-position')
xlabel('frame')
ylabel('pixel')

subplot(2,1,2)
hold on
for N=1:Nbeads
    plot(frame,center(:,2*N),'bo',frame,center(:,2*N),'r:')
```

```
   text(frame(end),center(end,2*N),['Bead ' num2str(N)]);
end
hold off
title('Bead Center y-position')
xlabel('frame')
ylabel('pixel')

figure(MPTResults1)
```

Function parabolicfit.m

```
function err2=parabolicfit(C,K)
% fit the following equation to kernel K and compute sum of
error ^2
% z=C(4)-C(3)*(x.^2+y.^2);
% where x=X-C(1), y=Y-C(2)
% used for centroid2


xc=C(1);
yc=C(2);
[h w]=size(K);
[x y]=meshgrid(1:w,1:h);
x=x-xc;
y=y-yc;


% parabolic fit
% format for C:
%C=[x-center, y-center, radius*, max]
z=C(4)-C(3)*(x.^2+y.^2);

err2=sum(sum((K-z).^2));
```

Function numdiff.m

```
function diff=numdiff(f,h)
% numerical differentiation with order of error h^2 for interior
points
% taken from numerical analysis book (burden & faires)
% input arguments:
% f=column vector containing function points
% h=spacing between function points
% Jan Lammerding
% 11/14/2000
```

```
[n,p] = size(f);
if n==1; % convert to column vector
   f=f.';
   n=p;
end

g  = zeros(size(f)); % case of singleton dimension

% Take forward differences on left and right edges
%if n > 1
   %g(1) = (f(2) - f(1))/h
   %g(n) = (f(n) - f(n-1))/h;
   % better approach: order h^2
   %g(1)=(-1.5*f(1)+2*f(2)-0.5*f(3))./h;
   %g(n)=(1.5*f(n)-2*f(n-1)+0.5*f(n-2))./h;
%end


% Take centered differences h^2 on next to edge points
%if n > 2
   %g(2:n-1) = (f(3:n)-f(1:n-2))./(2*h);
   %g(2)=(f(3)-f(1))./(2*h);
   %g(n-1)=(f(n)-f(n-2))./(2*h);
%end

% use 5 point (O(h^2) method for points on edges
if n>6
   g(1:2)=(-25*f(1:2)+48*f(2:3)-36*f(3:4)+16*f(4:5)-
3*f(5:6))./(12*h);
   g(n-1:n)=(3*f(n-5:n-4)-16*f(n-4:n-3)+36*f(n-3:n-2)-48*f(n-
2:n-1)+25*f(n-1:n))./(12*h);
end

% use centered h^4 method for interior points
if n > 5
   g(3:n-2)=(8*f(4:n-1)-8*f(2:n-3)+f(1:n-4)-f(5:n))./(12*h);
end

diff=g;
```

Function gaussfit.m

```
function err2=gaussfit(C,K)
% fit the following equation to kernel K and compute sum of
error ^2
% z=C(4)*1/(sigma*sqrt(2*pi)).*exp(-(x.^2+y.^2)/(2*sigma^2));
% where x=X-C(1), y=Y-C(2), sigma=C(3)
```

```
% used for centroid2

xc=C(1);
yc=C(2);
[h w]=size(K);
[x y]=meshgrid(1:w,1:h);
x=x-xc;
y=y-yc;

% gaussian fit:
% format for C:
% C=[x-center, y-center, sigma, amplitude]
sigma=C(3);
z=C(4)*1/(sigma*sqrt(2*pi)).*exp(-(x.^2+y.^2)/(2*sigma^2));

% compute sum of squared error
err2=sum(sum((K-z).^2));
```

Function forthorderfit.m (Fourth order fitting)

```
function err2=forthorderfit(C,K)
% fit the following equation to kernel and compute sum of error
^2
% z=C(5)-C(4)*(x.^2+y.^2)-C(3)*(x.^4+y.^4);
% where x=X-C(1), y=Y-C(2)
% used for centroid2

xc=C(1);
yc=C(2);
[h w]=size(K);
[x y]=meshgrid(1:w,1:h);
x=x-xc;
y=y-yc;

% 4th order fit
% format for C:
% C=[x-center, y-center, radius1*, radius2*, max]
z=C(5)-C(4)*(x.^2+y.^2)-C(3)*(x.^4+y.^4);


err2=sum(sum((K-z).^2));
```

Calibration routine calibration.m

```
% Program for force calibration of the single pole magnetic trap
% reads bead coordinates in csv-file format,
```

```
% smoothes curves,
% takes derivative and computes force vs distance relationship
% uses curvefitting to determine velocity

% Author: Jan Lammerding
% Date: 11/22/00
% difference to calibration4: regression for force instead of
velocity
% includes global regression for force/distance relation
% simplified version, but smoothes x and y positions separately
% displays force as vectors
% last edited 1/16/01

% requires file errforce1

clear

scale=0.228;            % scale [micron/pixel]
frames=30;                 % 30 [frames per second]
rho=0.974;                 % density [g/ml]
kv=12500;               % kinematic viscosity
[centistokes]=[mm^2/s]
D=4.5;                  % bead diameter [microns]
c=3*pi*D*rho*kv*1e-6;     %constant to convert velocity to force,
% according to stokes law: F=c*v  [nN]


%
% open dialog box to load file
[filename pathname]=uigetfile('*.csv','Open File with
Coordinates');


if filename
% read data from file
data=csvread(fullfile(pathname,filename));
else
   error('Must select valid file!')
end

% determine number of beads (each bead takes up two columns)
[rows columns]=size(data);
n=columns/2;

% create beadlegend
beadlegend=[];
for i=1:n
```

```
   beadlegend=char([beadlegend; 'bead ', num2str(i)]);
end

% extract bead coordinates from data
for i=1:n
   beadx(:,i)=data(:,i*2-1);
   beady(:,i)=data(:,i*2);
end

% select end points from plot of data

figure(1)
for i=1:n
   button=0;
   while ~button
      clf
      plot(beadx(:,i),beady(:,i),'+')
      title(['Bead ' num2str(i) ': Pick end point with mouse,
then hit any key'])
      [x,y]=ginput(1);
%      x=581;
 %     y=287;
      endN(i)=pairs(x+j*y,beadx(:,i)+j*beady(:,i));
      endx(i)=beadx(endN(i),i);
      endy(i)=beady(endN(i),i);
      hold on
      plot(endx(i),endy(i),'ro')
      hold off
      button=waitforbuttonpress;
   end
end
close(1)

% truncate vectors at end point
maxN=max(endN);          % max frame# for slowest bead to reach
final position
time=([1:maxN]./frames).';  %time vector [s]
bx=zeros(maxN,n);
bx=zeros(maxN,n);


% prompt user for smoothing window size
w=inputdlg('Please enter size w/2 of smoothing
window','Calibration Program',1,{'2'});
w=str2num(w{1});
% w=input('Please enter size w/2 of smoothing window (default
2): ');
```

```
if (~length(w) | w<1)     % use default for missing or invalid
input
   w=2;
end

for i=1:n
   bx(:,i)=ones(maxN,1)*endx(i); % fill end of vectors with end
point
   by(:,i)=ones(maxN,1)*endy(i);

   % smooth positions

bx(1:endN(i),i)=regrsmooth(time(1:endN(i)),beadx(1:endN(i),i),w)
;

by(1:endN(i),i)=regrsmooth(time(1:endN(i)),beady(1:endN(i),i),w)
;
end


figure(2)
clf
subplot(2,1,1)
plot(beadx,beady,'+')
axis equal
axis([0 640 0 480])
title('original plot:')
xlabel('x [pixel]')
ylabel('y [pixel]')
legend(beadlegend,-1)

subplot(2,1,2)
plot(bx,by,'+')
axis equal
axis([0 640 0 480])
title('truncated plot:')
xlabel('x [pixel]')
ylabel('y [pixel]')
legend(beadlegend,-1)

% pause
% erase unnessary variables
% clear data
% clear beadx beady
clear d dist
clear v vel
```

```
% compute distance from end point in microns
for i=1:n
   d=sqrt((bx(:,i)-endx(i)).^2+(by(:,i)-endy(i)));
   dist(:,i)=d*scale;     % convert into microns and store result
end

figure(3)
clf
plot(time,dist)
xlabel('time [sec]')
ylabel('distance [micron]')
legend(beadlegend,0)

distance=[];
velocity=[];
rawvel=[];
Vx=[];
Vy=[];

for i=1:n

   %use distance from smoothed positions
   sdist=dist(:,i);

   % SMOOTH DISTANCE
   % method 3: using piecewise linear regression
   sdist3=regrsmooth(time,dist(:,i),w);


   % COMPUTE VELOCITY
   % raw data:
   vel0=numdiff(sdist,1/frames);

   % method 3: used smoothed (3) distance
   vel3=numdiff(sdist3,1/frames);

   % and use step for step in x and y component
   vx=numdiff(bx(:,i),1/frames)*scale;
   vy=numdiff(by(:,i),1/frames)*scale;
   v=sqrt(vx.^2+vy.^2);


   % save results:
   cut=2;                              % ignore first and last
measurements
   distance(:,i)=sdist3(cut:end-cut);    % distance from pole
   velocity(:,i)=-vel3(cut:end-cut);       % velocity of bead
```

```
   rawvel(:,i)=-vel0(cut:end-cut);       % velocity based on raw
data
   Vx(:,i)=vx(cut:end-cut);             % currently not used
   Vy(:,i)=vy(cut:end-cut);

end

%COMPUTE FORCE
force=c*velocity;


figure(4);
clf
plot(distance, velocity, distance, rawvel,'y+')
title('velocity profile')
xlabel('distance [microns]')
ylabel('velocity [micron/s]')
legend(beadlegend,-1)


figure(5);
clf
plot(distance,force)
title('force profile')
xlabel('distance [microns]')
ylabel('force [nN]')
legend(beadlegend,-1)
grid on
df=[distance,force];
% output filename here
csvwrite('lo02aa.csv',df);

% Allow user to ignore one outlier for global regression
outlier=inputdlg('Enter outlier you wish to ignore','Calibration
Program',1,{'0'});
outlier=str2num(outlier{1});
%outlier=input('\nEnter outlier you wish to ignore (default 0):
');
if (~length(outlier) | outlier <1 | outlier>n)
   disp('No outliers! Consider entire data!')
   outlier=0;
end

% global regression for velocity
figure(6)
global raw_dist raw_force
tol_end=5;
```

```
tol_start=2;
acc_dist=[];
acc_force=[];
opt=zeros(1,14); opt(1:3)=[0 1e-4 1e-4]; opt(14)=10000;

for i=1:n;      % for each bead
   %clear raw_dist raw_vel svel
   raw_dist=[]; raw_force=[]; sforce=[];

   start_d=mean(distance(1:10,i));

   raw_dist=distance(distance(:,i)>tol_end &
distance(:,i)<start_d-tol_start,i);
   raw_force=force(distance(:,i)>tol_end &
distance(:,i)<start_d-tol_start,i);

   % store all values for global regression
   if i~=outlier    % exclude bead 3
     acc_dist=[acc_dist; raw_dist];
     acc_force=[acc_force; raw_force];
   end

   c1(i,:)=fmins('errforce1',[150 0 1],opt);
   sforce=c1(i,1)./((distance(:,i)+c1(i,2)).^c1(i,3));

   subplot(n,1,i)
   plot(distance(:,i),-
c*numdiff(distance(:,i),1/frames),'y+',distance(:,i),sforce)
   legend(char(['Bead ' num2str(i)]),'regression',-1);
   ylabel('force [nN]')
   axis([0 max(max(distance)) 0 max(sforce)])
   %axis tight
end
xlabel('distance [\mum]')
disp('Curve fitting')
disp('fitted the following equation to the data')
disp('force=a/(distance+b)^n')
disp('coefficients for individual curve fit:')
disp('a              b              n')
disp(c1)

% for all beads at once:
raw_dist=[];
raw_dist=acc_dist;
raw_force=[];
raw_force=acc_force;
c2=fmins('errforce1',[150 0 1],opt);
```

```
dis=linspace(0, max(max(distance)),100);
gsforce=c2(1)./((dis+c2(2)).^c2(3));

figure(7)
%plot(distance,force,'y+',dis,gsforce)     % plots all data
points
plot(acc_dist,acc_force,'y+',dis,gsforce)  % plots data points
considered for regression
title('Global regression for force vs distance')
xlabel('distance [\mum]')
ylabel('force [nN]')
grid on
legend('Data Points used for Regression','Regression')
disp('Coefficients for global curve fit:')
disp('a              b              n')
disp(c2)
```

Function errforce1.m

```
function err=errforce1(lambda)
% function has form force=lambda1/(d+lambda2)^n
global raw_force raw_dist

d = raw_dist;
y = raw_force;
z=lambda(1)./((d+lambda(2)).^lambda(3));

err = norm(z-y);
```

MATLAB programs used for data analysis (Hayden Huang)

Program used to find the kappa and mu-star by minimizing the error of the data to the function. kmsearch.m

```
% program to fit kappa and mu-star to real cell strain data
clear;
% syntax for error function: function sig=cserr(mu2, kap2);
final=zeros(10,2);
gss=zeros(10,2);
guess=[.004,150000];
tic;
for i=1:10
   gss(i,:)=guess;
   final(i,:)=fminsearch('cserr',guess);
   guess(1)=guess(1)*(0.5+rand)^2;
```

```
    guess(2)=guess(2)*(0.5+rand)^2;
end
toc
```

Function cserr.m used to find the error of the data point to the theoretical model based on current guesses for kappa and mu-star.

```
% function to read data and generate an error term for use in
minimization
function sig=cserr(x);
% input file here
a=csvread('ecs.csv');

% first column is r, then theta, then force, then measured dx
[ind1,ind2]=size(a);
% ind1 = number of data points
% ind2 should be 4
sumerr=0;
for i=1:ind1
    % function cstrain syntax:   dx=cstrain(f,r,theta,kap,mu);
    tdx=cstrain(a(i,3),a(i,1),a(i,2),x(2),x(1));
    sumerr=sumerr+(tdx-a(i,4))*(tdx-a(i,4));
end
sig=sumerr;
```

Function cstrain.m used to find, based on a given kappa and mu-star,

```
%function made by A.A.B. in PRE: model for cell deformation

function dx=cstrain(f,r,theta,kap,mu);
pois=0.5;
kap1=sqrt(0.5*(1-pois));
coeff=(f/(2*pi*mu));
a=0.5*besselk(0,kap*r)+0.25*(1-pois)*besselk(0,kap1*kap*r);
coeff2=-cos(2*theta);
b=(1/(kap*r))*besselk(1,kap*r)-
(kap1/(kap*r))*besselk(1,kap*kap1*r);
c=0.5*besselk(0,kap*r)-0.25*(1-pois)*besselk(0,kap*kap1*r);
fin=coeff*(a+coeff2*(b+c));
dx=fin;
```

Program calfin.m used to take the csv calibration data from calibration.m and turn it into a clean plot. Will take averages and standard deviations every 5 microns from given input files.

```
% quick small m-file to organize the calibration data files
% and take the averages and stdevs of the data.

clear;
```

```
% input the beginning and end distances.  Note that 0 = mag trap
tip.
begin=10;
fin=100;
%the step default is 5 microns

a1=csvread('f20.csv');
a2=csvread('f20a.csv');
a3=csvread('f20b.csv');
a4=csvread('f20c.csv');
a5=csvread('f20d.csv');
a6=csvread('f20ca.csv');
% combine into one long array
af=[a1;a2;a3;a4;a5;a6];
sz=size(af);
sz1=sz(1);
aff=sortrows(af);
note=floor((fin-begin)/5);
fforc=zeros(note, 1);
fstd=zeros(note, 1);
% find mean values
for j=1:note
   num=0;
   for i=1:sz1
      if aff(i,1)>10+5*(j-1)
         if aff(i,1)<10+5*j
            fforc(j)=fforc(j)+aff(i,2);
            num=num+1;
         end
      end
   end
   fforc(j)=fforc(j)/num;
end
% find standard deviations
for j=1:note
   num=0;
   for i=1:sz1
      if aff(i,1)>10+5*(j-1)
         if aff(i,1)<10+5*j
            fstd(j)=fstd(j)+(aff(i,2)-fforc(j))^2;
            num=num+1;
         end
      end
   end
   fstd(j)=sqrt(fstd(j)/num);
end
%output to file!
```

```
dist=[begin+2.5:5:fin-2.5];
ff=[dist',fforc,fstd];
csvwrite('f20g.csv',ff);
```

MATLAB function cellheight.m used to get average cell height (and standard deviation) from a text-file with all the pixel counts, using a 25%-from-base estimate for cell height.

```
% file to get average cell heights
clear;

numsli=input('Enter the number of slices per block: ');
numblo=input('Enter the number of blocks: ');

% data inout here, input filename.
% assume 3 column structure, z-section, num valid pixels, and
average intensity
fid=fopen('293ha.txt','r');
a=fscanf(fid,'%lg, %lg, %lg');
fclose(fid);
ind=floor(size(a)/3);
% quick check
if numsli*numblo~=ind
   z=input('input problem, file size is wrong');
   pause
end
dat=zeros(ind(1),3);
j=1;
for i=1:ind(1)
   dat(i,1)=a(j);
   dat(i,2)=a(j+1);
   dat(i,3)=a(j+2);
   j=j+3;
end

% dat now contains all the info in one long column.
% Now, analyze each block for a cell height

heit=zeros(numblo,1);
for i=1:numblo
% workmat is a matrix from dat that contains only one block of
info
   startind=1+(i-1)*numsli;
   workmat=dat(startind:startind+numsli-1,:);
   minval=min(workmat(:,2));
   maxval=max(workmat(:,2));
   % height will be taken from the 25% rise on both sides
```

```
    % that is, if the amplitude is 1, the height is from when
    % the value first crosses 0.25 to when the valuse crosses
    % 0.25 again on its way down.
    ampl=0.25*(maxval-minval)+minval;
    holder=0;
    for j=1:numsli
       if holder==0
          if workmat(j,2)>ampl
             startht=j;
             holder=1;
          end
       else
          if workmat(j,2)<ampl
             endht=j;
             holder=0;
          end
       end
    end
    heit(i)=0.154*(endht-startht);
end
% for certain files, I need to omit some data due to
instrumetation
% problems, so there is some data elimination in the analysis
avght=mean(heit(1:100))
stht=std(heit(1:100))
```

Appendix D: Virus generation protocol

The virus protocol here is adapted from the protocol taken from the PNAS paper by T. He et al and the web page they created to assist in the generation. I have downloaded the original web page (www.coloncancer.org) and have added comments and changes I made.

A Simplified System for Rapid Generation of Recombinant Adenoviruses

A Practical Guide for using the AdEasy System

Tong-Chuan He, Kenneth W. Kinzler, and Bert Vogelstein
Howard Hughes Medical Institute
and Molecular Genetics Laboratory
Johns Hopkins Oncology Center
424 North Bond Street
Baltimore, MD 21231, USA
Tel: (410)955-8886
Fax: (410)955-0548
e-mail: tche@welchlink.welch.jhu.edu

Last update: April, 1998

Contents

I. Introduction
II. General Considerations
III.Generation of Recombinants in Bacterial Cells
IV. Viral Production in 293 or 911 Cells
V. Preparation of High Titer Viral Stocks
VI. Appendices

I. Introduction

Summary

Recombinant adenoviruses provide a versatile system for gene expression studies and therapeutic applications. We here report a strategy which simplifies the generation and production of such viruses. A recombinant adenoviral plasmid is generated with a minimum of enzymatic manipulations, employing homologous recombination in bacteria rather than in eucaryotic cells. Following transfections of such plasmids into a mammalian packaging cell line, viral production is conveniently followed with the aid of

green fluorescent protein, encoded by a gene incorporated into the viral backbone. Homogeneous viruses can be obtained from this procedure without plaque purification. This system should expedite the process of generating and testing recombinant adenoviruses for a variety of purposes.

Outline of the AdEasy system

Schematic Outline of the AdEasy System. The gene of interest is first cloned into a shuttle vector, e.g. pAdTrack-CMV. The resultant plasmid is linearized by digesting with restriction endonuclease Pme I, and subsequently cotransformed into E. coli. BJ5183 cells with an adenoviral backbone plasmid, e.g. pAdEasy-1,. Recombinants are selected for kanamycin resistance, and recombination confirmed by restriction endonuclease analyses. Finally, the linearized recombinant plasmid is transfected into adenovirus packaging cell lines, e.g. 293 cells. Recombinant adenoviruses are typically generated within 7 to 12 days. The "left arm" and "right arm" represent the regions mediating homologous recombination between the shuttle vector and the adenoviral backbone vector. An: polyadenylation site; Bm: BamHI, RI: EcoRI; LITR: left-hand ITR and packaging signal; RITR: right-hand ITR; Sp: SpeI.

II. General Considerations

1. Because PmeI and PacI sites are designed to linearize the final constructs for transformation and transfections, avoid using these sites in you inserts. (If you absolutely cannot avoid Pme1 and Pac1 sites, you can still use these vectors, but with more difficulty (employing partial digestions or digestion with EcoRI and recA-assisted restriction endonuclease (RARE) cleavage).
2. Avoid cloning elements that are present more than once in the vector (e.g., CMV promoters) in head-to-head orientations.
3. Except for pAdEasy-1 and pAdEasy-2, all other constructs (including recombinant adenoviral plasmids) confer resistance to **kanamycin** (***NOT ampicilin***).
4. High competence of BJ5183 cells is important to obtain homologous recombinants because these cells have relative low transformation efficiency. Therefore it is important to carefully follow the protocol for preparation of these cells.
5. Purification of plasmid DNAs: Standard CsCl gradient purification for all plasmid DNAs used in the experiments is recommended, though miniprep DNAs made by commercial kits (e.g. Nucleobond) are also acceptable.
6. References:

T.-C. He, et al (1998) PNAS 95: 2509-2514.
H. Hermeking, et al (1997) Molecular Cell 1:3-11.

III.Generation of Recombinants in Bacterial Cells

1. Prepare electrocompetent BJ5183 cells in 20 µl/tube aliquotes (see **Appendex A and B**).

2. Linearize the shuttle plasmids with PmeI. Usually one-fifth of a miniprep is sufficient. After digestion, DNAs are phenol-chloroform extracted, ethanol precipitated, and resuspended in 6.0 μl H_2O.
3. Co-transform PmeI-digested shuttle plasmid with 1.0 μl adenoviral backbone vector (100 ng/ml). Twenty ul of electrocompetent *E. coli* BJ5183 cells were added and electroporation was performed in 2.0 mm cuvettes at 2,500V, 200 Ohms, and 25 μFD in a Bio-Rad Gene Pulser electroporator. Resuspend transformation mix in 500 μl L-broth, and incubate at 37°C for 15-20 min. Plate on 4 to 5 LB/kan plates, and grow at 37°C overnight (16-20 hrs).
4. Pick up 10 to 20 smallest colonies, and grow them in 2 ml L-broth containing 25 μg/ml kanamycin for 10-15 hours.
5. Perform minipreps using the conventional alkaline lysis method, and check the sizes of supercoiled plasmids by running one-fifth of a miniprep on 1% agarose gel.
6. Restriciont digest DNA from clones with PacI. Candidate clones usually yield a large fragment (near 30 kb), plus a smaller fragment of 3.0kb or 4.5kb.
7. Re-transform the correct recombinant plasmids into DH10B (or your favorite plasmid propagation strain). Plasmids are purified by CsCl -banding (see **Appendix D**) or using commercially available purification kits.

IV. Viral Production in 293 or 911 Cells

1. 293 cells (E1-transformed human embryonic kidney cells) or 911 cells (E1-transformed human embryonic retinal cells) in one or two T-25 flasks at 2 x 10^6 cells per flask ~24 hours prior to transfection. The confluency should be about 50% to 70% at the time of transfection.
2. On the day of transfection, digest recommbinant adenovial plasmids with PacI (usually 4 μg DNA is needed to transfect one T-25 flask). Ethanol precipitate the plasmids and resuspend in 20 μl of sterile H_2O. <Note: I used chloroform-phenol extraction, which works as well>
3. Perform a standard Lipofectamine transfection according to manufacture's manual. Mix 4 μg of PacI-digested plasmid and 20 μl of Lipofectamine (GIBCO BRL) for each T-25 in 500 μl of OptiMem I medium, and incubate at room temperature for 15-30 min. <Note: I used Lipofectin – ultimately, since 293 cells are very easily transfected, the actual reagent is not that important>
4. While waiting, remove growth medium from recipient cells and wash them once with 4 ml serum-free medium (e.g. plain DMEM, or Hank's). Add 2.5 ml OptiMem I per T-25 flask. Return to 37°C CO_2 incubator for ~10 min.
5. Add Lipofectamine-DNA mix to the flasks, and return to 37°C CO_2 incubator. <Note: the actual technique used for Lipofectin varies. For my case, I prepared everything out of the flask, and then aspirated the media off the cells and placed the transfection solution on the cells>
6. Remove medium containing Lipofectamin-DNA mix four hours later, and add 6 ml fresh complete DMEM (10% FBS, 1% Pen/Strep). Do not change the lipo/DNA medium if a significant amount of floating cells are observed; sometimes this happens with 293 cells and doesn't necessarily indicate a problem. If lots of floating cells are seen, add 6.0 ml complete DMEM to each flask and incubate at 37°C overnight. Change medium

next morning. <Note: it is also ok to simply add DMEM+FCS to the mixture even if the cells look fine. FBS and FCS are the same thing>
7. Transfections and viral productions can monitored by GFP expression if pAdTrack-based vectors are used. No obvious plaques or CPE are easily observed by standard microscopy up to 2 weeks post transfection in most cases. However, plaques are always observed under fluorescence using the GFP marker. <Note: do not change media in this period. Cells will become very confluent over this period, so it is important to have the cells at less than full confluence at the time of transfection. Plaques are obvious if you know what to look for. Be sure there are rounded up cells around a small clear (cell-free) region. There are normally lots of cell-free regions, but the key is the rounded up cells. Sometimes there will be detachment uniformly, and not in small regions, this is ok. The second infection should have the plaques.
8. Scrape cells off flasks with a rubber policeman (not trypsin) at 7 to 10 days post-transfection and transfer to 50 ml conical tubes. Spin cells in a benchtop centrifuge and resuspend pellet in 2.0 ml HBSS or sterile PBS. Freeze cells in dry ice/methanol bath, and thaw in a 37°C water bath. Vortex vigorously. Repeat freeze/thaw/vortex for 3 more cycles (four cycles total). Do not let virus supernatants warm up. Spin samples briefly and store supernatant at -20°C. <Note: it is not unusual to keep cells longer than 7-10 days.>
9. Infect two 50% to 70% confleunt T-25 flasks of 911 or 293 cells using 30-50% of the above viral supernatants for each flask. CPE or cell lysis should become evident at 2 to 3 days post infection. Productive infections easily observed with the AdTrack vectors.
10. Collect viruses when a third to half of the cells are detached, usually 3 to 5 days post infection. Presence of the recombinant adenoviruses can be confirmed by Western blot and/or PCR (for PCR, take 5 µl virus sup plus 10 µl PCR-grade Protease K at 55°C for 1 hour, then boil samples for 5 min. spin briefly, use 1 to 2 µl for PCR).
11. Scrape cells off and prepare viral supernatants as described in **step 8** above. You should have at least 10^7 infectious particles/ml at this stage, and often much more. Each round of amplification should give at least 10-fold more virus than present in the previous round.
12. To amplify further, repeat the infection of cells using 30-50% of the viral supernatant from **step 11**, using T75 flasks instead of T25 flasks. Titers can be measured at any time, which is particularly easy with AD-Track vectors. Simply infect 293 cells with various dilutions of viral supernatant and see how many are green 18 hours later. Without AdTrack, viruses can be plaque titered or titered by limiting dilution using standard methods; we find these methods much less simple and quantitative than that employing the GFP marker, but these have to be used if GFP is not present.
<Supernatants with virus can be stored at –20°C, and unfortunately, the propogation is mostly empirical>

V. Preparation of High Titer Viral Stocks

1. Plate 911 or 293 cells in T-75 flasks to be 90% confluent at time of infection (about $1x10^7$ cells/T-75). Usually, fifteen to twenty T-75 flasks are sufficient to make a high titer stock. <Note I usually use 10 T150 flasks minimum to get a decent yield>
2. Infect cells with virus sup at a multiplicity of infection (MOI) of 5 to 10 PFU per cell. When all cells have rounded up and about half of the cells are detatched (usually at 3 to

4 days post infection), harvest and combine all flasks. Spin 5 min in a benchtop centrifuge (~500 g), and remove the supernatant. <Supernatant can be stored for future infections>
3. Resupend pellet in 8.0 ml sterile PBS. Perform four cycles of freeze/thaw/vortex. Centrifuge lysate in Sorvall HS4 rotor at 6000 rpm (7000 g) 4°C for 5 min. <Vortex is brief, about 10 seconds per sample. Be sure to monitor the freezing and thawing – best to use minimum amount of time necessary to achieve a new state. That is, do not leave thawed for too long, nor frozen for too long. Sometimes, the color of the pellet will change, especially if some of the media is left behind. This is not a problem>
4. Weigh 4.4 grams of CsCl in a 50-ml conical tube, transfer 8.0 mls of clear virus sup to the tube, and mix well by vortexing. Transfer the CsCl solution (about 10 ml, density of 1.35 g/ml) to a 12 ml polyallomer tube for SW41 rotor. Overlay with 2 ml mineral oil. Prepare a balance tube. Spin the gradient in SW41 rotor at 32,000 rpm, 10°C, for 18 to 24 hours. <Need high-speed centrifuge for this – make sure tubes are balanced correctly. Usually, inbalanced tubes can be corrected by varying the amount of mineral oil>
5. Collect virus fraction (about 0.5 to 1.0 ml) with a 3cc syringe and an 18g needle. Mix with equal volume 2X Storage Buffer (2X Storage Buffer = 10 mM Tris, pH 8.0, 100 mM NaCl, 0.1% BSA, and 50% glycerol, filter sterilized). Store virus stocks at -20°C. <This is probably the most tricky step – normally people say that you need to puncture the tube from the bottom, but this is very difficult (not to mention potentially dangerous) so I usually go from the top. The band should be visible about 1-2 cm below the top surface. The band is extremely fluid and is usually a ghostly white color. The very top surface has cell debris and undesirable material. Be careful when inserting the needle to simply puncture the top, and not collect any debris. This can be aided further by collecting some air in the syringe prior to insertion, and then after inserting the needle between the top layer and the viral band, ejecting the air carefully>
6. Check viral titer by GFP (preferred) of by plaque assays (**see below**) or by immunohistochemical staining, or simply read OD at 260 nm. To read OD, add 15 µl virus to 15 µl blank solution (Blank Solution = 1.35g/ml CsCl mixed with equal vol 2X Storage Buffer) plus 100 µl TE/0.1% SDS; vortex 30 seconds, centrifuge 5 min. measure A260. One A260 unit contains ~1012 viral particles (particles:infectious particles =~20:1). <These techniques are not reliable, according to He himself. Usually I use am empirical method – simply infect the target cells with varying amounts of GFP virus, and see what the minimum amount is that is required to infect all the cells. Then, for viruses that do not have GFP, simply infect cells with GFP and the "invisible" virus in a 24-well plate and compare the rate of plaque formations>

VI. APPENDICES

A. Protocol for making electrocompetent bacteria cells

1) Use a fresh colony or frozen stock of DH10B cells to inoculate 10 ml of LB medium in a 50 ml tube. Grow cells in a rotator overnight at 37°C.
2) Dilute 1 ml of cells into 1000 ml of LB medium in eight 1 liter flasks (125 ml each). Grow for 4 to 5 hour with vigorous aeration at 37°C, until A_{550} is ~0.8.
3) Collect cells in four 250 ml conical centrifuge tubes and incubate on ice for 10 minutes to 1 hour. (The longer the cells are incubated the higher the competency.)
4) Pellet cells by centrifuging at 3,000 rpm (2,600 g) at 4°C for 10 min.

5) Wash the cell pellet by resuspending in 1000 ml of sterilized, ice-cold WB (WB = 10% ultra pure glycerol, 90% distilled water, v/v)
6) Centrifuge the cell suspension at 3,000 rpm (2500 g) for 30 min.
7) Repeat steps 5 and 6.
8) Pour off the supernate roughly, gently pipet most of supernate off, leaving about 20 ml, transfer the cell suspension to a 50 ml tube. Spin at 3,000 rpm x 10 min, and pipet all but 5 ml of the supernate out.
9) Resuspend cell pellet in the WB remaining in the tube. Aliquot 20 ul per tube and store at -80°C.
<I tried making this bacteria, and succeeded in getting bacteria that were highly competent for standard transformations, but not for viral electroporation. I ultimately used bacteria from the Expermental MedicineDivision, since they had experience making viruses with this protocol as well. A brief note is that bacteria should be at much less than 0.8 OD – you want the bacteria at low density>

B. Checking Competency of Electrocompetent Cells

Purified plasmid DNA (10 ng/ul) 1 µl
DH10B competent cells 20 µl
1) Transform cells with Bio-Rad gene pulser (200 Ohms/25µF/ 2.5 KV).
2) Add 1 ml of L-Broth at room temperature.
3) Shake cells at 37°C for 1 hour in 50 ml tube.
4) Make 100-fold and 1000-fold serial dilutions of the cells in L-Broth.
5) Plate 100 ul of diluted cells on L-agar with 100 ug/ml ampiciliin.
6) Incubate overnight @ 37°C. Titer should be >10^8 colonies/ug, and we often achieve 10^9 colonies/ug.
<I did not do this at all>

C. Plaque Assay for Purification and Titration of rAdenoviruses

Note: this only needs to be done for adenoviruses without GFP marker. In those which include GFP marker, titration of infectious units (i.e., those resulting in expression of GFP) is simply determined by fluorescence microscopy of your favorite cell type.
1. Remove all but 2 ml per well of medium from 6-well plates containing 80% to 90% confluent 911 or 293 cells. Infect with appropriately diluted virus for 3 to 6 hours. Infect cells with 6 different dilution titers (e.g. 10^{-3} to 10^{-8} µl/well).
2. Prepare the overlay agar as following: autoclave 100 ml of 2.8% Bacto-Agar (Difco) and keep warm at 45°C water bath. For 100 ml overlay:
Stock Conc. Final Conc. ml/100ml overlay
2 X BEM (GIBCO) 2 X 1X 50.0
HEPES 1.0M 20.0mM 2.0
MgCl2 1.0M 12.5mM 1.25
FBS 100.0% 10.0% 10.0
Pen/Strep 100 X 1 X 1.0
mix well and incubate at 37°C bath.
Bacto-Agar 2.8% 1.0% 36.0

Mix well and swirl at 37°C water bath, add 4 ml/well for 6-well plate.
Note: If you want to melt 2.8% agar stock, microwave or heat it in boiling water bath. Prepare 50 ml overlay at a time. To prevent the pre-drying of agar before plaque formation, it is important to add sterile PBS or Hank's medium in the space between wells, and wrap the plates with SaraWrap.
3. Return the plates to 37°C CO_2 incubator. On days 5 - 7, overlay 2 to 3 ml agar containing nuetral red (from 100x stock, available from GIBCO-BRL) to each well. Plaques should be visible 16-30hrs after the neutral red overlay. (In general, plaques should form in 911 cells in 4 or 5 days and in 293 cells after 5-7 days).
4. Pick 5 to 10 well-isolated plaques for each recombinant by punching out agar plugs with a sterile pasteur pipet. Store agar plugs in 200µl HBSS medium. Perform freeze/thaw/vortex cycle 4 times. Spin samples briefly.
5. Infect one well of 6-well plate of 911 or 293 cells (about 80-90% confluency at time of infection) with 50-70% virus sup of each plaque for 3 to 5 days (depending on the titer of individual plaque). Presence of recombinant virus can be confirmed by Western blot or PCR.
6. Collect viral supernatant using four cycles of freezing/thawing, as described earlier in this guide. The virus sup can be used to further infect T-25, and then T-75 flasks, for large scale preparation.
<I tried this assay, as did some other people in the lab, but no one ever got it to work>

D. CsCl Banding of Plasmid DNA

1. Collect 400 ml cultures (from one 1L flask) in 500 ml centrifuge containers in Sorvall GS3 rotor (holds up to six 500 ml containers). Spin @ 6k (for 10 min @ 4°C in Sorvall centrifuge.
Alternative: use 250 ml conical tubes, cf. 3000 RPM (2500 g) in IEC at 4 degrees for 15 minutes and follow "Wizard Protocol" for alkaline lysis and isopropanol precipitation steps..
2. Resuspend pellets in 7.5 ml BDI (50 mM glucose, 25 mM Tris pH 8.0, 10 mM EDTA stored @ 4 oC; made as follows: 4.5 gm glucose, 12.5 ml 1 M Tris pH 8.5, 25 ml 0.2M EDTA, 460 ml H2O, pH 8.05).
3. Transfer resuspended pellets to 50ml polypropylene tubes. Add 2.5 ml 20 mg/ml lysozyme in BDI. Vortex and sit @ RT for 5 min.
4.Add 20 ml BDII (made fresh) (= 0.125N NaOH/1% SDS; make this by combining 1 ml 50% NaOH, 10 ml 10%SDS, and 89 ml H_2O). Invert tubes gently and sit on ice for 10 min.
5. Add 15 ml BDIII (3M K+, 5M Acetate pH 4.8; made as follows: 147.3 g K.Acetate, 57.5 ml Acetic Acid, H_2O to 500 ml, pH should be ~4.8). Invert sharply several times and incubate on ice for 10 min. Spin in HS4 for 45 min at 7000 rpm.
6. Transfer 21 ml of supernatant to each of two 50 ml polypropylene tubes containing 14 ml isopropanol. Mix and let sit @RT for 5 min. Spin in HS4 rotor for 15 min @ 4.2 K rpm (4800 g) at 4°C.
7. Wash pellet with 70% ethanol. Remove last dregs of ethanol with pipet tip. Dissolve pellets in a total of 8.3 ml LoTE (4 ml per pellet).

8. Weigh 8.8 gm CsCl (Ultrapure) in weigh boat and put into a centrifuge tube. Add exactly 8 ml DNA solution. Density should be 1.57 - 1.60, but you generally do not need to measure this if you have weighed and pipetted out DNA carefully.
9. Add 800 ul 1 mg/ml ethidium bromide in TE.
10. Transfer solution to Ti 70 or Ti 50 ultracentrifuge tubes (both SETON 6041). screw on collars, put tops on. Tighten with screwdriver.
11. Opposite tubes should weigh within 100 mg of each other.
12. Place in Ti 70 rotor and spin @ least 16 (--> 20 hr) @ 50.000 rpm (brake @ 800rpm) @ 20°C.
Alternatively, you can use a Ti 50 rotor and spin at 48 K for the same amount of time.
13. Prepare 2 syringes (3 cc) with 1" 22 gauge needles for each prep. Label syringes so you won't mix them up.
14. Carefully remove tubes from rotor with hemostat.Remove inner nut from centrifuge tubes.
15. Put on face shield. Set up tubes in ring stand above UV transilluminator. Insert needle just above supercoiled band and bevel down to aspirate the band.
16. Pour remaining CsCl in chemical waste and wash centrifuge tube cones and nuts. The plastic centrifuge tubes are disposable but the nuts and cones are not.
17. Extract with an equal volume of H_2O saturated 1-butanol in 15 ml polypropylene tube. Saturated butanol = 40 ml butanol + 10 ml H_2O; the butanol layer stays on top.
18. Vortex ---> sit 10-60 sec @ RT. Discard top (red) layer
19. Repeat three times (total of 4 extractions). Add equal volume of H_2O-saturated butanol each time. (If begin with 1.5 ml, end with ~ 2.5 ml of solution).
20. Add 5 volumes LoTE to final volume of DNA in a 50 ml tube. Vortex, and add 2 volumes of ethanol (e.g., if 2.5 ml DNA, add 12.5 ml LoTE, mix, then add 30 ml ethanol).
21. Centrifuge 60 min @ 4200 rpm (=4800 g).
22. Wash with 75% ethanol twice. Re-spin and remove last drop of 75% ethanol. Do not speedvac.
23. Dissolve in 0.5 ml LoTE.
<This protocol was never used – I recommend the miniprep for small samples, to check sequences, and maxiprep for any preparations requiring DNA for serious manipulation (Qiagen makes good kits)>

Addendum to Viral protocol:
The protocol glosses over the most time-consuming portion of the protocol: generating the recombinant plasmids. After generating the pshuttle vectors (by first cloning the desired promoter and gene comples into some propogation vector such as TA-cloning vector, then using restriction digests and ligation to insert the promoter-gene complex into the pshuttle vectors), the pshuttle and the padeasy vectors need to be co-transformed by electroporation into the bacteria. Post transformation, there will be typically few colonies, compared to standard transformations. A few cultures should be started from each transformation. Sequencing should be performed at this point (possibly at the pshuttle if desired, but here it's much more important). Note that for the case of beta-lactamase, there is a large homologous sequence in the beta-lactamase gene and the padeasy vector, so choose primers carefully, or better yet, used a few different primers. Also note that once the padeasy recombinant has been generated, one needs to increase the number of

usable plasmids by maxiprep: this should be done in normal bacteria, not the BJ5183 cells tro prevent reverse recombination. Maxiprep will give smaller yields than normally, due to the large size of the plasmid. Use excesses for restriction digest since ethanol or chloroform/phenol extraction will lost substantial amounts of DNA.

Appendix E: Octopolar Magnetic Trap Design

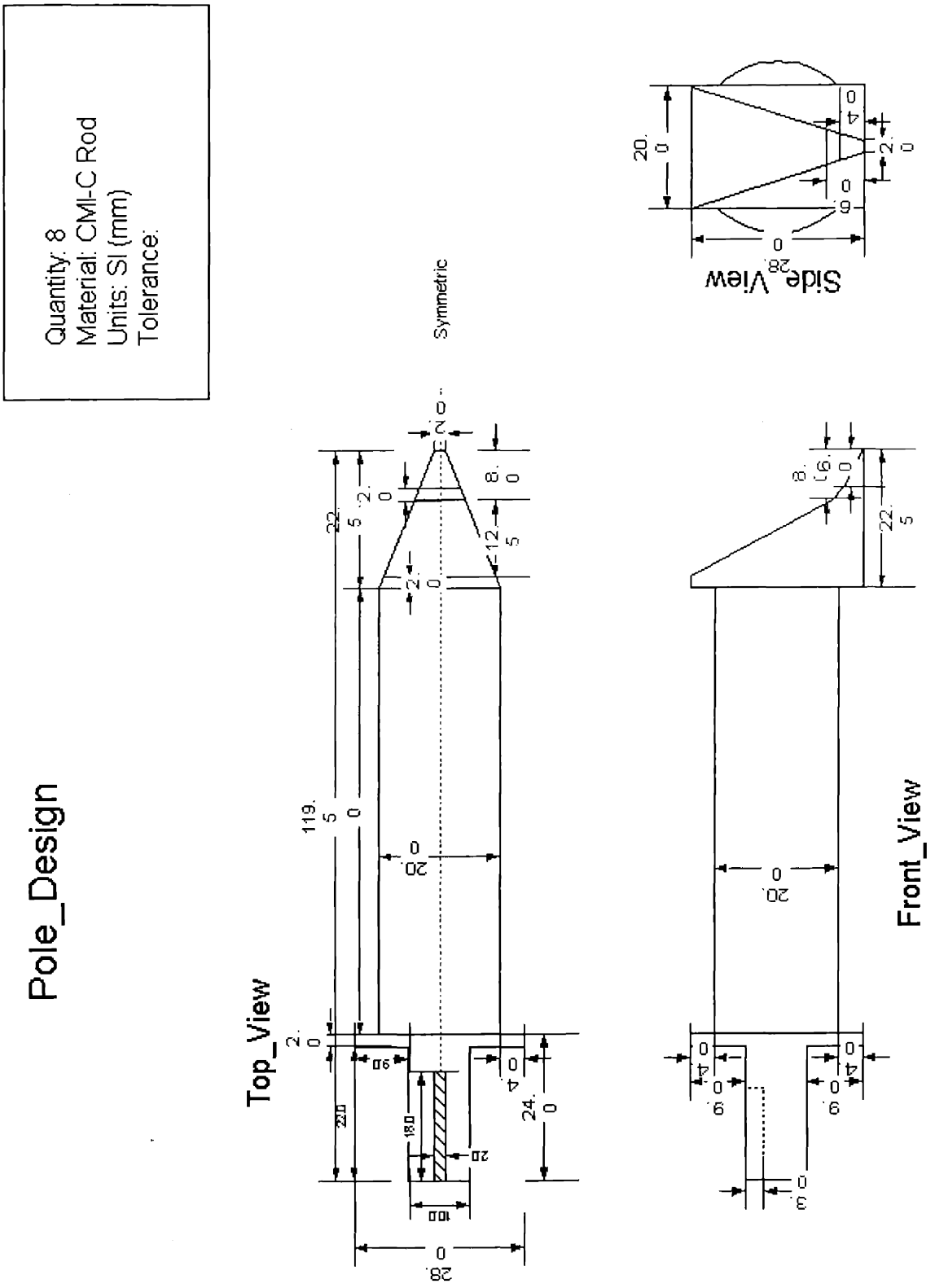

Back_Iron

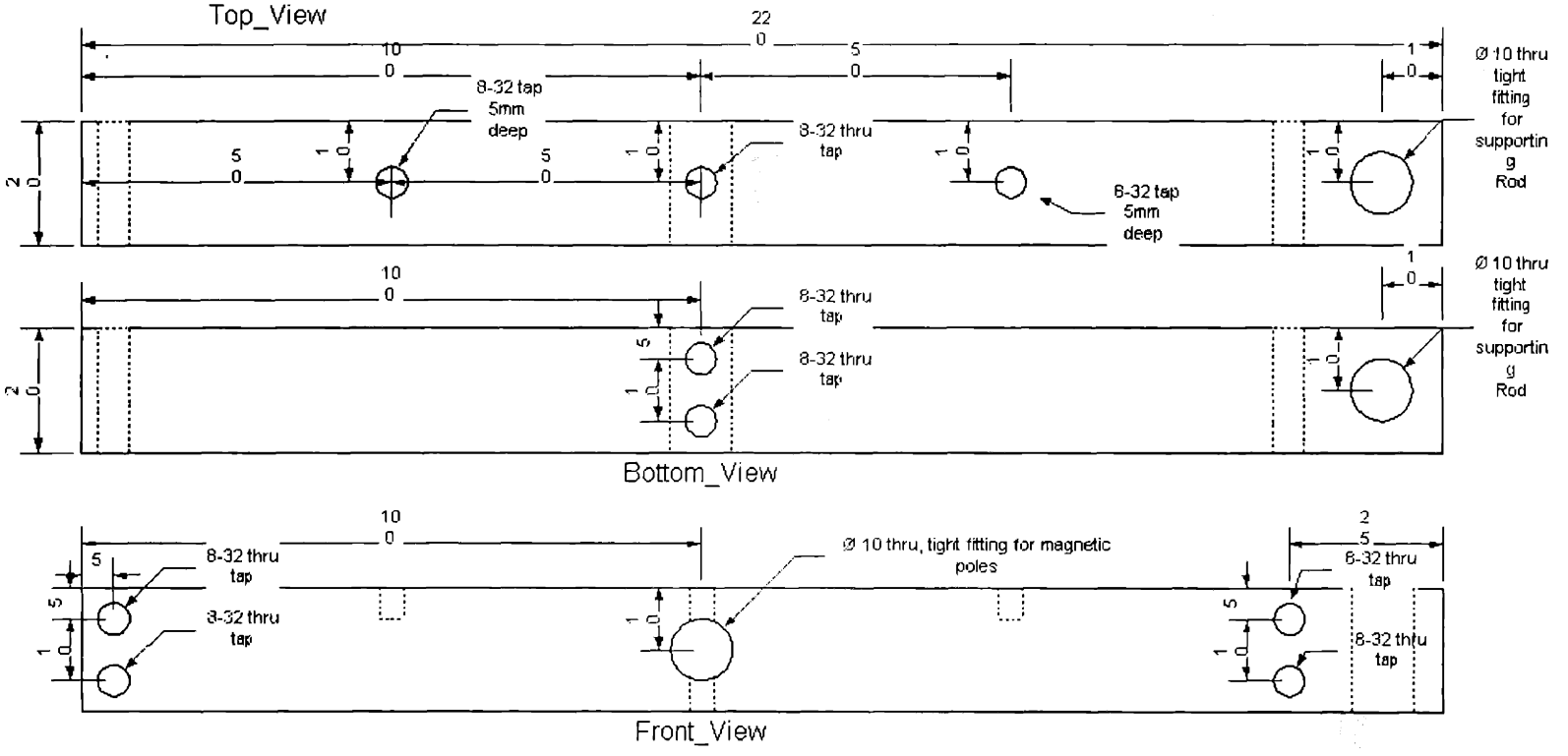

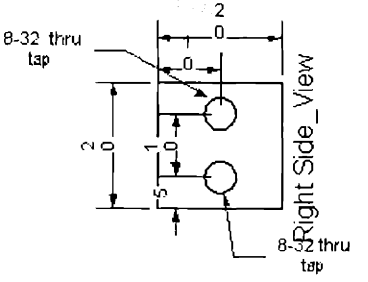

Quantity: 8
Material: CMI-C Rod
Units: SI (mm) except for the some of the holes
Tolerance: + 0.001"

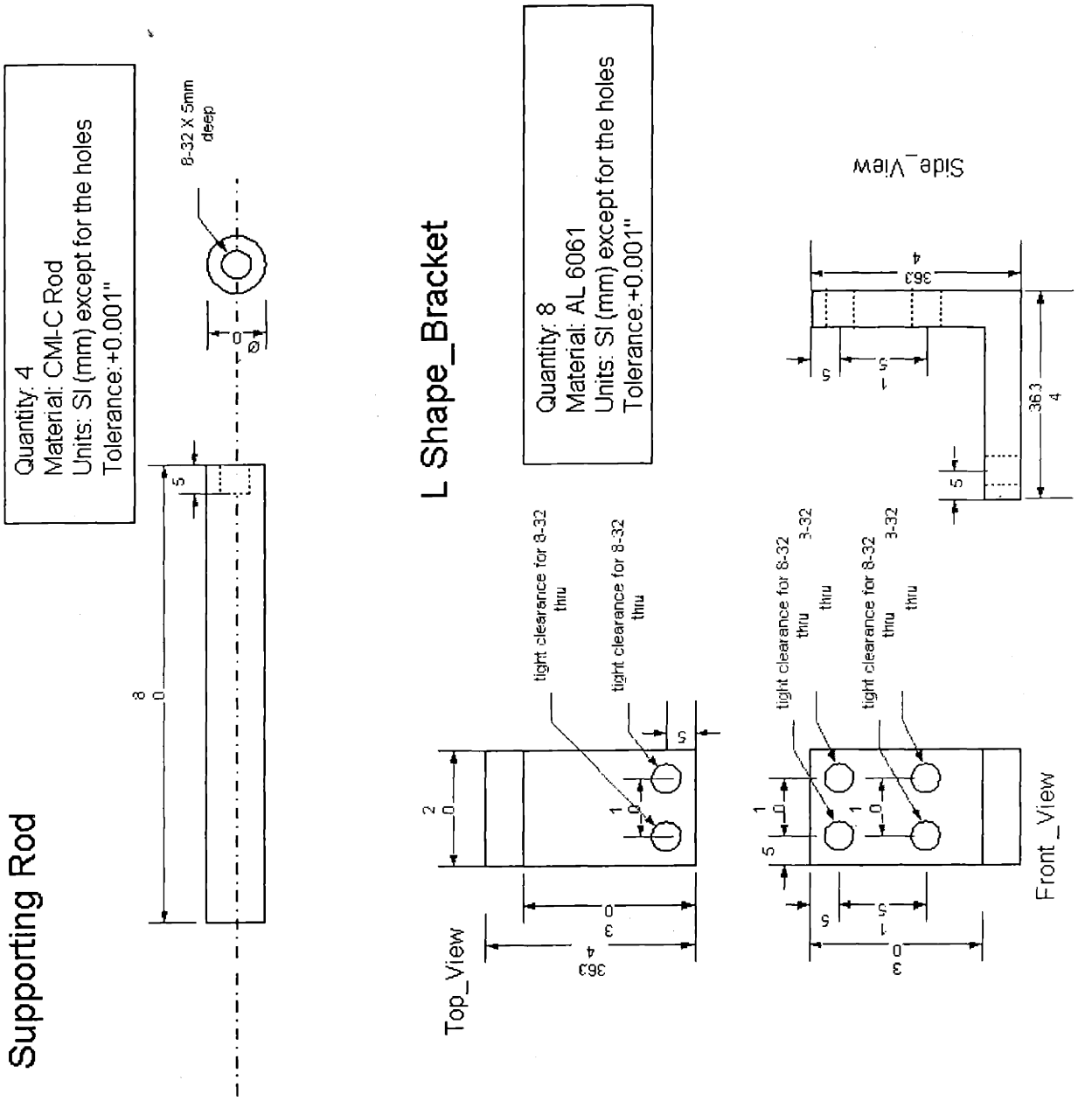

Note that the "Pole Design" is the same for both octopolar and unipolar magnetic traps. The rest of the components are for the octopolar trap only.